DATE DUE	DATE DUE	DATE DUE

A DEVELOPMENTAL STUDY OF VOLTAGE-GATED IONIC CURRENTS OF SPIRAL GANGLION CELLS OF RAT PUPS

By

Deanne B. Hall

A DISSERTATION

Submitted to
Michigan State University
in partial fulfillment of the requirements
for the degree of

DOCTOR OF PHILOSOPHY

Department of Audiology and Speech Sciences

1997

The wh

development o

spiral ganglion

mV steps from

sodium current

Peak sodium cu

$P9_1$ sodium curr

was shifted in th

outward-directed

however, continu

directed potassiu

was not a determ

applied 0.5 μM te

sodium currents.

activation for inwa

Inactivation of the

the bath. Sodium p

ABSTRACT

A DEVELOPMENTAL STUDY OF VOLTAGE-GATED IONIC CURRENTS OF SPIRAL GANGLION CELLS OF RAT PUPS

By

Deanne B. Hall

The whole cell variation of the patch clamp technique was used to investigate the development of sodium current and potassium current of rat embryonic and postnatal spiral ganglion cells (SGCs). Depolarizing pulses of 10 ms or 20 ms were applied in 10 mV steps from –80 mV to + 80 mV from a holding potential of –80 mV. Inward-directed sodium current activated at potentials more positive than –40 mV in embryonic SGCs. Peak sodium current amplitude was less than 1500 pA. In comparison to postnatal (P1 – P9) sodium currents under the same test conditions, sodium current activation voltage was shifted in the hyperpolarizing direction. Inward-directed sodium current and outward-directed potassium current amplitude increased with maturation. Some cells, however, continued to exhibit small inward-directed sodium current and large outward-directed potassium current during the maturational periods investigated, thus, cell size was not a determining factor. Postnatal sodium currents were reversibly blocked by bath applied 0.5 μM tetrodotoxin, indicating that these cells exhibit tetrodotoxin-sensitive sodium currents. Tetrodotoxin-resistant sodium currents were not observed. Rate of activation for inward-directed peak sodium current decreased with maturation. Inactivation of the sodium current was slowed in the presence of 10 μM Pb^{2+} applied to the bath. Sodium peak current amplitude, however, did not diminish following

application of P

channels that u

present prenata

structures reach

application of Pb^{2+}. Our results indicate that functional sodium channels and potassium channels that underlie the generation of the action potential of the auditory nerve are present prenatally. This development occurs before the sensory end organ and middle ear structures reach maturation, as well as before hearing commences.

This accomplishment was a blessing and is dedicated to God,
my parents, Robert and Barbara Hall,
my sister Denise and brother-in-law Leon.
Thank you for your unending love and support!

Supported in p

I wish to thank
generosity in a
the patch-clam
this method o
respectfully th
project. A he
Julia Irizarry.
Jonathan Bloc

I'd like to tha

Last, but by n
his wisdom,
program.

Romans 8:3
loved us."

Proverbs 8:
are not to be

To my sister
situations—

To all of my

ACKNOWLEDGMENTS

Supported in part by NIDCD

I wish to thank Dr. Toshio Narahashi for his insight towards my research project and his generosity in allowing me the opportunity to utilize his laboratory facilities in learning the patch-clamp technique and the specific pharmacological practices which accompany this method of research. To Drs. Chau Wu, Jay Yeh, Bill Marszalec and Ryoichi Sato, I respectfully thank each of you for your mentorship and support during this research project. A heartfelt thanks to Nayla Hasan for her never-ending assistance and patience, Julia Irizarry, and Michelle Floyd for all of their administrative support and wit and Jonathan Bloom for his expert technical assistance, both near and far.

I'd like to thank Randy Robb for his expertise and technical support.

Last, but by no means least, I wish to thank Dr. Ernest J. Moore, my major professor, for his wisdom, direction and never ending support throughout the duration of my doctoral program.

Romans 8:37 "Nay, in all these things we are more than conquerors through him that loved us."

Proverbs 8:11 " For wisdom is better than rubies; and all the things that may be desired are not to be compared to it.

To my sister in Christ, Lia Maria Haynes, thank you for <u>always</u> being there, in all situations—you have been there.

To all of my family and friends, Thank You.!@#*

TABLE OF CONTENTS

LIST OF TABLES

Figure

LIST OF FIGURES

Figure

IV-5 Single e
magnitu
1.8 um

IV-6 Single i

IV-7 Single m
postnatal

IV-8 (A) Singl
plot gener

IV-9 Single me
(P9) type I

IV-10 TTX study
and suppre
sodium cur
(C) Return
(D) Increas
of holding p

IV-11 TTX study
presence of
of 0.5 μM T

IV-12 Unidentified

IV-13 Non-inactiva
absence of sp
specific chan
of 0.5 μM TT

Figure Page

Figure

Figure Page

Figure

IV-25 Multiple
exposure
Normal s
and (D))

IV-26 Family o
sodium c
potassiur
outward-
produced
currents

IV-27 Outward
by (A) a

IV-28 Outward
postnata

KEY TO

A	A
Ach	A
AchR	A
AP	A
APV	2
Asp	A
4AP	4
Ba^{2+}	B
Ca^{2+}	C
CCh	C
Cd^{2+}	C
CDC	C
CG	C
CM	C
CMF-PBS	C
CNQX	6
CNS	C
CO_2	C
CPP	3

KEY TO SYMBOLS, ABBREVIATIONS OR NOMENCLATURE

A	Amperes
Ach	Acetylcholine
AchR	Acetylcholine receptor
AP	Action potential
APV	2-amino-5 phosphonovalerate
Asp	Aspartate
4AP	4-aminopyridine
Ba^{2+}	Barium
Ca^{2+}	Calcium
CCh	Carbamylcholine
Cd^{2+}	Cadmium
CDC	Centers for Disease Control
CG	Cochlear ganglion
CM	Cochlear microphonic
CMF-PBS	Ca^{2+} - Mg^{2+} free phosphate buffered saline
CNQX	6-cyano-7-nitroquinoxaline-2,3-dione
CNS	Central nervous system
CO_2	Carbon dioxide
CPP	3-3 (2-carboxy-piperazine-4-yl) propyl-1-phosphate

CsCl

CsOH

CVG

DB

DiCl-HQC

DMEM

DNase I

DNQX

DRG

E

EAA

EGTA

EPP

FA

FN

5HT

Gd^{3+}

Glu

GTP

gΩ

Hz

CsCl	Cesium chloride
CsOH	Cesium hydroxide
CVG	Cochleovestibular ganglion
DB	decibel
DiCl-HQC	6, 7-dichloro-3-hydroxy-2-quinoxalinecarboxylic acid
DMEM	Dulbecco's modified eagles medium
DNase I	deoxyribonuclease I
DNQX	6, 7-dinitroquinoxaline-2,3-dione
DRG	Dorsal root ganglion
E	Embryonic
EAA	Excitatory amino acid
EGTA	ethyleneglycol-bis-(b-aminoethyl ether) N,N,N,N'-tetracetic acid
EPP	End-plate potential
FA	Fast-adult
FN	Fast-newborn
5HT	Serotonin
Gd^{3+}	Gadolinium
Glu	Glutamate
GTP	guanine triphosphate
gΩ	Gigaohm
Hz	Hertz

IHC

IP_3

I_{ex}

I_{ex}

IV

K^+

KA

KCL

Kyn

M-current

$m\Omega$

$MgSO_4$

ug dl

um

MOsm

ms

mV

N_a

Na^+

NMDA

OHC

IHC	Inner hair cell
IP_3	Inositol triphosphate
$I_{to,f}$	Fast –inactivating transient outward current
$I_{to,s}$	Slow-inactivating trasient outward current
I/V	Current /voltage relationship
K^+	Potassium
KA	Kainate
KCL	Potassium chloride
Kyn	Kynurenic acid
M-current	Muscarine senstive K^+ current
mΩ	Megaohms
$MgSO_4$	Magnesium sulfate
μg/dl	micrograms/deciliter
μm	micrometer
MOsm	milliosmoles
ms	milliseconds
mV	millivolts
N_1	Negative potential 1
Na^+	Sodium
NMDA	N-methyl-D-aspartate
OHC	Outer hair cell

P

PA

Pb^{2+}

PBS

PDBu

PKC

QA

S

SGC

SPL

TEA

TEA-Cl

TTX

TTX-R

TTX-S

$V_{1/2}$

V_s

V_t

P	Postnatal
PA	picoamperes
Pb^{2+}	Lead
PBS	Phosphate buffered saline
PDBu	phorbol dibutyrate
PKC	Protein kinase C
QA	Quisqualate
S	Slow
SGC	Spiral ganglion cell
SPL	Sound pressure level
TEA	Tetraethylammonium
TEA-Cl	Tetraethylammonium chloride
TTX	Tetrodotoxin
TTX-R	Tetrodotoxin-resistant
TTX-S	Tetrodotoxin-sensitive
$V_{1/2}$	Potential at which peak current is ½ its maximum amplitude
V_h	Holding potential
V_p	Pipette voltage

Ver

modalities,

olfactory sy

developmen

and influenc

stimuli initia

cells located

specific focal

The informati

transmit infor

further proces

communicatio

by the CNS, ne

original sense c

Na^+, K^+, Ca^{2+} C

Several types of

vertebrate skelet

1992; Kandel, Sc

CHAPTER I

INTRODUCTION

Vertebrates perceive events in the environment through various sensory modalities, namely, the visual system, somatic sensory systems, the gustatory system, the olfactory system, as well as through the auditory system. External stimuli help shape the development of the central nervous system (CNS), provide warnings of existing danger, and influence learning, memory, as well as other higher cortical functioning. External stimuli initiates certain experiences which are subsequently coded neurally by receptor cells located in the periphery. The information is collected and transferred to a number of specific focal areas within the brain stem, cerebral cortex, cerebellum, and/or spinal cord. The information is transmitted to the CNS by a series of nerve fibers and cells which transmit information through electrical and/or chemical signals. The information is further processed by the CNS and is transferred to other cortical areas creating communication between collaborating brain systems. Once the information is received by the CNS, neural signals are re-directed from the CNS back to the periphery and/or the original sense organ. These electrical signals are partly conducted as ionic current (e.g., Na^+, K^+, Ca^{2+} Cl^-.) through porous membrane proteins which form ionic channels. Several types of ionic currents have been investigated and found to exist in cardiac tissue, vertebrate skeletal muscle, endocrine glands and neuronal cells, just to name a few (Hille, 1992; Kandel, Schwartz and Jessell, 1991).

arise fr

spannin

Biophys

been ext

Lin. 199

unit activ

studies ha

transducti

developm

currents, a

Developm

The

membranou

gestation. C

not occur un

ear reaches i

supports the

whether the n

transient audi

Electrophysiol

otherwise.

A key to further understanding the encoding process of auditory information may arise from investigating membrane proteins such as ionic channels. These membrane-spanning structures serve to generate action potentials as well as other electrical signals. Biophysical properties underlying the generation of action potentials from SGCs have not been extensively studied (Santos-Sacchi, 1993; Moore et al., 1996; Mo and Davis, 1997; Lin, 1997). A significant amount of information has been reported on eighth nerve single unit activity (Galambos and Davis, 1943, 1944; Tasaki, 1954; Javel, 1986), but very few studies have described ionic mechanisms of spiral ganglion neurons as part of the signal transduction process. Only one investigation (Valverde et al., 1992) has described developmental changes that occur, if any, that influence the early characteristics of ionic currents, and thus, neural coding of mammalian SGCs.

Development of the Human Auditory System

The ontogeny of the human peripheral auditory system occurs such that the membranous labyrinth of the inner ear reaches its full adult size during the third month of gestation. Complete maturation of the sensory end organ and its supporting cells does not occur until the fifth month of gestation (Northern and Downs, 1991). Thus, the inner ear reaches its full adult size by fetal midterm. Although gross, anatomical evidence supports the maturation of the cochlea by fetal midterm, the question remains, however, whether the neurophysiological mechanisms responsible for signal transduction of transient auditory cues are fully developed and capable of processing sound prenatally. Electrophysiological measures involving auditory evoked potentials would suggest otherwise.

D

indicate t

cells and

validate th

functional

be examin

Anatomic

Uni

ability to he

subsequent

(Crowley ar

old rat pup c

1000 Hz and

improved by

frequencies h

Although ma

the source of

maturation of

between P16 -

Middle ear ma

The ma

because it is re

cochlea. Witho

Developmental studies of the rat cochlea using light and electron microscopy indicate that the synaptogenetic maturation of inner hair cells precede that of outer hair cells and the development is almost complete at birth (Lenoir et al., 1980). In order to validate the presence of an auditory system which is mature and has reached its true functional capability, biophysical mechanisms in addition to anatomical maturation must be examined.

Anatomical Development of the Rat Auditory System

Unlike the human auditory system, the age at which the rat first demonstrates an ability to hear is postnatal and does not occur until P9 - P12. This is followed by subsequent improvements in auditory sensitivity and an expansion of the frequency range (Crowley and Hepp-Reymond, 1966). That is, frequency response curves show that a P8 old rat pup demonstrates an awareness to a narrow frequency band ranging between 200 - 1000 Hz and sound levels of 87 - 95 dB SPL. By P20, sensitivity to the same sounds has improved by approximately 125 dB SPL at some frequencies and the range of frequencies has expanded from 100 – 70 kHz (Crowley and Hepp-Reymond, 1966). Although maturation of the external ear and middle ear continue to mature postnatally, the source of the changes in auditory sensitivity is believed to be due to the maturation of inner ear structures. Adult sensitivity for auditory discrimination occurs between P16 - P20 (Crowley and Hepp-Reymond, 1966).

<u>Middle ear maturation</u>

The maturation of the middle ear system is important to the process of hearing because it is responsible for transmitting sound waves from the environment to the cochlea. Without the middle ear system, approximately 0.1% of the originating signal

would reach

system trans

impedance r

If on

systems and

ossicular ch

appear as a

changes tha

the fluid fill

which serve

lever ratios

the middle

accommoda

ossified and

membrane

ligaments w

Alt

sequential,

while other

birth in the

mesenchym

stage the os

continues t

would reach the cochlea, resulting in a significant hearing loss. Thus, the middle ear system transmits sound from the environment to the inner ear and eliminates the impedance mismatch which exists between the airborne sound and the cochlear fluids.

If one were to separate the middle ear from its contiguous outer and inner ear systems and view it separately, it would appear as an air filled cavity containing the ossicular chain, a series of muscles, ligaments and tendons. In other words, it would appear as a somewhat simple system, with a number of anatomical and developmental changes that it must attain before it is capable of transferring acoustical sound energy to the fluid filled cochlea. These anatomical changes give rise also to two mechanisms which serve to over come the impedance mismatch. The mechanisms are the areal and lever ratios of the tympanic membrane-ossicular chain complex and make up a portion of the middle ear transformer system. The developmental changes necessary to accommodate the areal and lever ratios include having an air filled cavity containing ossified and mature ossicles necessary for the lever ratio, a fully developed tympanic membrane which contributes to the areal ratio, and a series of tendons, muscles and ligaments which contribute to both mechanisms.

Although morphologic development of the middle ear structures are not sequential, they do mature systematically. Some middle ear structures mature rapidly while others progress at a much slower rate. Very few middle ear structures are mature at birth in the rat. In fact, when the pups are born, the bulla of the tympanum is filled with mesenchyme, a soft gelatinous mass which surrounds the soft gelatinous ossicles. At this stage the ossicles are composed mostly of water. This soft gelatinous mesenchyme continues to occupy the middle ear space and is not fully absorbed until P12.

The ty

appears as a th

to the malleus

This resonant

and pars flacci

Each area mat

like size by P1

(Zimmer et al.

lateral wall of

adult-like appe

At P3,

water content.

speckling distr

by P22, the ma

achieves 90% o

their adult-like

The ma

is the surface a

P15. The space

the stapedial foo

exceeds the area

in size to accom

The tympanic membrane develops even at a slower rate. Between P1-P3, it appears as a thin, transparent and slightly convexed membrane, except where it is fused to the malleus. Over time the membrane becomes fibrous and takes on a concave shape. This resonant membrane is made up of pars tensa, which has the greatest surface area, and pars flaccida located in the superior anterior quadrant of the tympanic membrane. Each area matures at a different rate. Pars tensa matures the earliest, reaching its adult-like size by P17. Pars flaccida reaches its adult-like state at a much slower rate at P49 (Zimmer et al., 1994). By the twelfth day, the tympanic membrane has formed the lateral wall of the now air filled bulla. By P22, the tympanic membrane has obtained its adult-like appearance.

At P3, the middle ear ossicles are soft, gelatinous and composed of a very high water content. The first signs of ossification occur around P6 and appear as diffuse speckling distributed throughout the ossicles. Although they have their bony appearance by P22, the malleus does not achieve 90% of its adult size until P36, while the incus achieves 90% of its adult-like state by P34. Thus, middle ear ossicles are slow to reach their adult-like state.

The maturation of the stapedial footplate and oval window are coincident. That is, the surface area of the oval window exceeds that of the stapedial footplate prior to P15. The space that lies between them is occupied by the annular ligament. After P16, the stapedial footplate develops to the point where the area of the stapedial footplate exceeds the area of the oval window by 5%. The annular ligament eventually decreases in size to accommodate the stapedial footplate. The areas of the oval window and

stapedial fo

continuing

All

play a very

increase the

attenuation

adult matur

not achieve

to occur in t

Inner Ear

A nu

cochlea. Th

as well as ot

functioning

mature after

stiffness and

continued de

sensitivity of

The d

basilar memb

changes withi

within the org

observations r

stapedial footplate reach 90% of their adult-like size by P13 and P17, respectively, continuing to grow in size pass P60.

All of these factors contribute to the existence of the lever and areal ratio, and play a very important part in the conductance of sound. Both the lever and areal ratios increase the force and decrease the velocity of sound, thereby, reducing the amount of attenuation that would occur due to the cochlear fluids. The areal ratio reaches 90% of adult maturity by P8. The development of the long arms of both the malleus and incus do not achieve maturity until after P30 during which time developmental changes continue to occur in both length and mass.

Inner Ear

A number of developmental changes continue to occur postnatally within the cochlea. These changes probably coincide with the improvement of cochlear mechanics as well as other cochlear functions. Some of the structures necessary for the basic functioning of the cochlea develop close to the onset of hearing, while others continue to mature after this period. The changes are numerous and involve changes in mass, stiffness and frequency representation along the length of the basilar membrane. The continued development of the cochlea is perhaps responsible for the improvement in the sensitivity of hearing (Roth and Bruns, 1992).

The development of the cochlea is incipient. The organ of Corti, including the basilar membrane, tectorial membrane and supporting border cells, all undergo specific changes within the first month of life. Very few morphological changes occur, however, within the organ of Corti between P0 and P8. For example, at P4, light microscopic observations reveal a tectorial membrane which is completely attached to the epithelial

surface an

maturation

1992). At

now detach

membrane.

1. Basilar m

Deve

cross-section

and pectinate

each area of w

reduction of th

epithelial linin

the pectinate zo

length of the co

length of the ba

the pectinate zon

P24, the basal ar

From sem

basilar membrane

Interestingly, how

for the middle (16

increase in width w

surface and a number of undifferentiated cell types. Reportedly, the most striking maturational changes in the organ of Corti do not occur until P8 - P12 (Roth and Bruns, 1992). At this stage, all extracellular fluid spaces have opened, the tectorial membrane is now detached from the epithelium and filaments can be observed in the basilar membrane.

1. Basilar membrane

Developmental changes of the basilar membrane occur in the width, thickness and cross-sectional area. At P4, the division of the basilar membrane into the arcuate zone and pectinate zone is clear. By P12, a number of specific changes have taken place in each area of which subsequent structures are dependent. Such changes include the reduction of the spiral vessel which dominates the arcuate zone, the formation of epithelial lining created by the thick tympanic layer and changes in cellular formation in the pectinate zone. At P4, the area of the pectinate zone is essentially constant along the length of the cochlear duct. By P12, there is an overall increase in the area along the length of the basilar membrane. Although there is an additional increase in the area of the pectinate zone at P24, the increase is noted predominantly in the basal region. At P24, the basal area is now more than twice as large as the apical area.

From semi-thin sections, Roth and Bruns (1992) found that the width of the basilar membrane increased from base to apex during three stages of development. Interestingly, however a distinct increase in the width of the basilar membrane was noted for the middle (166 μm - 199μm) and apical (184 μm - 229 μm) regions and only a slight increase in width was observed for the basal region.

2. Tectorial m

The te

specific areas

tectorial mem

attached fibril

main body ma

dense. By P1

to be anchored

membrane. B

membrane no

In general the

at all developm

structures, hov

P4. Between

size.

3. Supporting

The inn

sulcus cells, ph

Claudius cells,

distinguished.

on the basilar m

P12. At P12, h

sulcus disappea

2. Tectorial membrane

The tectorial membrane attaches to the epithelial cells at P4. It consists of two specific areas, namely, the marginal part and the main body. The marginal part of the tectorial membrane is the portion above the receptor cells and is characterized by loosely attached fibrils. When compared to the main body, it has a less dense appearance. The main body makes up the predominant mass of the tectorial membrane and appears more dense. By P12, the tectorial membrane is separated from the epithelial cells but continues to be anchored to the organ of Corti via marginal pillars along the length of the basilar membrane. By P24, the marginal pillars have disappeared, the marginal tectorial membrane now appears more dense and the area of the tectorial membrane has increased. In general the cross-sectional area of the tectorial membrane increases from base to apex at all developmental stages studied (Roth and Bruns, 1992). Unlike many other cochlear structures, however, the adult size reaches maturity in the basal and middle regions by P4. Between P4-P24, the area in the apical regions increases more than twice its original size.

3. Supporting cells

The inner ear of the rat has a number of supporting cells: inner border cells, inner sulcus cells, phalangeal cells and outer border cells. The latter include Hensen cells, Claudius cells, Boettcher cells and Tectal cells. At P4, the different cell types cannot be distinguished. During the early stages, the supporting cells form a single epithelial lining on the basilar membrane and spiral ligament. Minimal changes occur between P4 and P12. At P12, however, the mesenchymal cells which previously filled the inner spiral sulcus disappear and the latter is now covered by a single layer of epithelium. The

specific outer b

respective place

located betwee

layers while the

to all the other s

increase in cross

by P24 the maxi

area of the same

extend into the ap

regions of the coc

lumen of the spira

sulcus epithelium

spiral sulcus cells

4. Sensory Recept

At birth, th

from the surroundi

gradually over seve

sensory cell recepto

pear-like shape and

continue to increase

Using electr

immature IHCs and

present at the base o

specific outer border cell types can now be distinguished and are positioned in their respective places along the basilar membrane and spiral ligament. Boettcher cells are located between Hensen cells and Claudius cells. The Hensen cells now form multiple layers while the cells of Claudius are essentially localized on the spiral ligament. Similar to all the other structures discussed thus far, Hensen, Claudius and Boettcher cells increase in cross-sectional diameter between P4-P24. Development continues such that by P24 the maximum cross-sectional area towards the base exceeds the cross-sectional area of the same type of cells towards the apex. Interestingly, Boettcher cells do not extend into the apical region and are predominantly located in the basal and medial regions of the cochlea. By P24, maturation of the inner border cells is evident. The lumen of the spiral sulcus has diminished coincident with an increase in the height of the sulcus epithelium. The inner spiral sulcus is now covered by multiple layers of inner spiral sulcus cells at the base of the cochlea.

4. Sensory Receptor Cells

At birth, the sensory receptor hair cells are very immature and indistinguishable from the surrounding epithelial cells. Specific characteristics of the hair cells emerge gradually over several days. The first to appear are the inner hair cells (IHC). By P6, sensory cell receptors are more readily distinguishable. By P9, the IHC has a mature pear-like shape and by P12 three rows of outer hair cells (OHC) are present which continue to increase in length (Lenoir et al., 1980).

Using electron microscopy, Lenoir et al. (1980) observed nerve fibers under both immature IHCs and OHCs at birth. Numerous afferent and efferent nerve terminals were present at the base of the IHC. Well developed afferent synapses were characterized by

pre-synaptic v

between effere

suspected effe

level of the OH

Subsequ

at the level of t

showing post-sy

underneath OH

stage that synap

Efferent nerve e

Afferent

number of effere

level of the OHC

throughout the co

level of the IHCs

surrounded the ba

OHCs. The major

few efferent endin

fibers made contac

Developmental C

The normal

of specific structure

often times approac

pre-synaptic vesicles and post-synaptic thickenings. Only axo-dendritic synapses between efferent endings and afferent fibers were seen at those terminal endings with suspected efferent fibers. Comparatively, only afferent dendrites were observed at the level of the OHC.

Subsequent changes occurred daily. By P6, the number of afferent nerve endings at the level of the IHC has increased. IHC efferent synapses were well differentiated showing post-synaptic cisterns and presynaptic vesicles. The efferent fibers observed underneath OHCs was accompanied by axodendritic synapses. It was also during this stage that synaptic competition was evident between afferent and efferent nerve endings Efferent nerve endings were lodged between afferent dendrites and the OHC membrane.

Afferent innervation was predominant at the base of the IHC by P9, while the number of efferent endings had diminished. Synaptic competition was still evident at the level of the OHCs. Both IHCs and OHCs acquired their adult innervation patterns throughout the cochlea by P16. At this stage, the majority of the efferent synapses at the level of the IHCs were axodendritic. One to two large efferent terminals essentially surrounded the base of each OHC while very few afferent terminals made contact with OHCs. The majority of developmental changes in the cochlea occured by P25. Only a few efferent endings remained to be seen at the level of the IHC while only a few afferent fibers made contact with OHCs.

Developmental Characteristics of Rat Spiral Ganglion Cells

The normal gestational period of the rat is 21 days. The precocious development of specific structures within the auditory system and central nervous system are rapid and often times approach adult size before birth. There are some auditory structures,

however, that

postnatally.

Both s

of cells that ap

these densely p

Scarpa's gangli

The coc

apex. The coch

gestation and ha

extend well into

Electrophysiolo

The cochl

generated by the c

in the rat, the CM

that the cochlea w

which the CM cou

days later (P11-P1

The initial r

elicited prior to P8.

stimuli and stimuli f

the pup progressively

threshold progressive

threshold (20 dB) leve

however, that begin to develop during the gestational period, but continue to mature postnatally.

Both seventh and eighth cranial nerve ganglia arise as a homogeneous population of cells that appear about the 12th day of gestation. Within a day (13th gestational day), these densely packed cells can be distinguished from each other (Schwartz, 1986). Scarpa's ganglion lies laterally while the SGCs lie medially within the otocyst.

The cochlea essentially develops in an orderly fashion, namely, from base to apex. The cochlear duct develops in its spiral pattern between the 14th and 18th days of gestation and has attained its full number of coils by the 18th gestational day. The SGCs extend well into the apex by this developmental period.

Electrophysiological Responses

The cochlear microphonic (CM) is an electrophysiological response which is generated by the cochlear outer hair cells (Pickles, 1988). Uziel et al. (1981) found that in the rat, the CM could be recorded before the action potential (AP) emerged suggesting that the cochlea was functional prior to the auditory nerve. The earliest period during which the CM could be recorded was P8-P9. The AP on the other hand occurred several days later (P11-P12) coincident with the reported onset of hearing within the rat.

The initial responses of the CM were limited. No observable responses could be elicited prior to P8. Initial CM responses could only be obtained using high intensity stimuli and stimuli from a limited frequency range (0.5 to 8k Hz) (Uziel et al., 1981). As the pup progressively matured, three CM characteristics improved: (1) The CM threshold progressively decreased from high SPLs (90-100 dB) to significantly lower threshold (20 dB) levels; (2) CM amplitude increased and (3) CM responses could be

obtained fro

before.

The

1981). Alth

(Crowley an

elicited an A

an apical de

developmen

CM. That is

AP threshol

Differentiat

Hafi

SGCs from t

intermediate

during prena

and their pro

Schw

developmen

developmen

through 6; (3

During the f

homogenous

type I SGCs

obtained from a pool of stimuli having a wider frequency range (0.5 to 16k Hz) than before.

The earliest AP recordings in the rat pup occurred between P11-P12 (Uziel et al., 1981). Although the adult rat has a wide dynamic frequency range (100 - 70k Hz) (Crowley and Hepp-Reymond, 1966), only a limited band of frequencies (2-16k Hz) elicited an AP during this stage (Uziel et al., 1981). This response might suggest more of an apical developmental pattern instead of the more generally accepted base to apical developmental pattern. The development of the AP, however, was similar to that of the CM. That is, with age the AP amplitude increased, the latency of N_1 decreased and the AP threshold improved.

Differentiation of Spiral Ganglion Cells

Hafidi et al. (1993) used an immunolabeling technique to distinguish type II SGCs from type I SGCs in rat cochleas as early as P3. They found that peripherin, an intermediate filament protein, was expressed in both types of spiral ganglion cell types during prenatal development, however, it was localized to type II spiral ganglion neurons and their processes during postnatal development.

Schwartz et al. (1983) used light and electron microscopy to describe postnatal development of SGCs in the albino rat. She categorized them into one of four developmental stages: stage (1): birth through postnatal day 2; (2) postnatal days 4 through 6; (3) postnatal days 8 through 10; and (4) postnatal days 14 through 30. During the first postnatal week, Schwartz et al. (1983) stated that SGCs appear as a homogenous population of cells. Type II cells could not be readily distinguished from type I SGCs until P8. Differences between the two neuronal cell types was further

substantiated b

staining pattern

techniques. Ty

while type I SG

microscopy, a t

structures found

ultrastructural f

discovered that

different from t

and a scarcity o

type I SGCs wa

neurofilaments.

Neural Condu

The pro

length of an axo

generation of a

potassium (K^+)

movement of N

membrane. Vo

ions to pass into

depolarization o

of the action po

sensitive sodium

substantiated by light and electron microscopy. Light microscopy showed different staining patterns between the two cell types when using toluidine blue staining techniques. Type II SGCs had a darker staining cytoplasm and lighter staining nucleus, while type I SGCs had a lighter staining cytoplasm and darker staining nucleus. Electron microscopy, a technique which can be used to identify miniscule organelles and structures found in cells, was used to study the process of myelinization and the ultrastructural features that occupy the perikaryon. Through this technique, it was discovered that the cytoplasmic content of the type II spiral ganglion cell was strikingly different from that of type I cells, and contained an abundant amount of neurofilaments and a scarcity of rough endoplasmic reticulum. Once again, the cellular content of the type I SGCs was the opposite, having a large amount of Nissl substance and sparse neurofilaments.

Neural Conduction

The process of neural coding involves the transfer of signals propagated along the length of an axon. These signals are propagated in the form of action potentials. The generation of an action potential is dependent upon the presence of sodium (Na^+) and potassium (K^+) conductances. The all-or-none action potential is generated by the movement of Na^+ and K^+ ions through porous protein channels embedded in the cell membrane. Voltage-sensitive channels dispersed throughout the lipid bilayer allow Na^+ ions to pass into the cell and down its concentration gradient, causing further depolarization of the cell membrane. Sodium influx into the cell causes the rising phase of the action potential. Further depolarization results in the subsequent closing of voltage sensitive sodium channels and thus the reduction of sodium conductance, and the opening

of potassium c

mechanisms (K

Sodium Chann

Sodium

cell bodies, vert

differently at a v

initiation of actio

neurotransmitter

saltatory conduct

Sodium c

neuron (Yamaguc

SGC of the adult

have been studie

reported about th

system. Santos-S

guinea pig. Alth

sodium and potas

of guinea pigs, he

due to the differe

appears, therefore

address early dev

Sodium ch

to tetrodotoxin (T

of potassium channels. The falling phase of the action potential is the result of the latter mechanisms (Koester, 1991).

Sodium Channels

Sodium channels are found in a variety of cell populations (e.g., axons, neuronal cell bodies, vertebrate skeletal and cardiac muscle, and endocrine glands) and function differently at a variety of sites. For example, some sodium channels serve to assist in the initiation of action potentials at the axon hillock, others induce the release of neurotransmitter at cellular terminals, and still others participate in the process of saltatory conduction at the node-of-Ranvier.

Sodium channels are found within the avian embryonic cochlear ganglion (CG) neuron (Yamaguchi, 1988; Yamaguchi and Ohmori, 1990; Valverde et al., 1991) and the SGC of the adult guinea pig (Santos-Sacchi, 1990, 1993). Developmental characteristics have been studied within the avian auditory system, however, sparse information is reported about the onset of sodium channel activity found in the mammalian auditory system. Santos-Sacchi (1993) studied the properties of the sodium channel of the adult guinea pig. Although he reports the presence of some similarities in the kinetics of sodium and potassium conductances between cochlear ganglion cells of chicks and SGCs of guinea pigs, he indicates that it may be difficult to compare the two cell populations due to the differences in the levels of maturity between the two species of cells. There appears, therefore, a need to investigate ion channels from mammalian SGCs which address early developmental changes.

Sodium channels have been classified according to their toxic binding sensitivity to tetrodotoxin (TTX), a known paralytic toxin generated by the puffer fish. A sodium

channel which

as a TTX-sensi

presence of TT

The dorsal root

junction betwee

rise to afferent fi

of research has b

sodium channels

Previous

conductances of

have found diffe

sodium currents.

the isolated dors

a fast inward cur

slowly developi

the fast TTX-S i

addition, a slow

calcium channel

These same diva

current (Kostyuk

Schwartz

(S-slow; FN-fast

P5 - P8, and four

channel which is sensitive to TTX, and thus blocked by its presence externally is known as a TTX-sensitive (TTX-S) sodium channel. A channel which is unaffected by the presence of TTX extracellularly is known as a TTX-resistant (TTX-R) sodium channel. The dorsal root ganglion (DRG) is a swelling of nerve cell bodies found close to the junction between the dorsal and ventral root of the spinal cord. These cell bodies give rise to afferent fibers which control motor and sensory functions. An extensive amount of research has been conducted which describes the presence of TTX-S and TTX-R sodium channels in rat DRG neurons.

Previous studies suggest that changes occur in the characteristics of ionic conductances of sodium channels of DRG cells of young rat pups. A number of studies have found differences in the distribution of sodium channels which exhibit atypical sodium currents. Kustyuk et al. (1981) studied sodium transmembrane ionic currents in the isolated dorsal root ganglion neurons of P5 - P10 rat pups. In the absence of K^+ ions, a fast inward current was recorded in its pure form in 90% of the cells investigated. A slowly developing TTX-insensitive inward current which occurred in conjunction with the fast TTX-S inward current was identified in 10-15% of the cells investigated. In addition, a slow TTX-insensitive current was found to be unique due to its sensitivity to calcium channel blockers such as cobalt (CO^{2+}), manganese (Mn^{2+}) and cadmium (Cd^{2+}). These same divalent cations did not exert any obvious depressive effect on the TTX-S current (Kostyuk et al., 1981).

Schwartz et al. (1990) described three types of voltage-dependent sodium currents (S-slow; FN-fast newborn; FA-fast adult) in the DRG cells of rat pups, ages P1 - P3 and P5 - P8, and found that the frequency of occurrence of the current types changed with

age. The perce

DRG cells, whi

Roy and Naraha

(P3 -P7), while

Effects of Lead

The norm

extraneous influe

educators and res

Lead (Pb^{2+}) exis

and industrial pr

associated with

(Atchison and N

Reuveny and N

al., 1997) and h

Lille et al., 198

conducted by th

among the top

the Center for

risk for neuroto

µg dl (Bellinge

than 10 µg dl (

The ma

exposure, have

age. The percentage of S and mixed (S + FN) sodium currents decreased among P5 - P8 DRG cells, while the percentage of FA sodium current increased among this population. Roy and Narahashi (1992) found TTX-R current to be more common in young DRG cells (P3 -P7), while TTX-S current was more common among DRG neurons of older animals.

Effects of Lead

The normal development of the young CNS is vulnerable to a number of extraneous influences. Harmful lead levels are one such toxicant and has concerned educators and researchers for years due to its debilitating effect on learning and memory. Lead (Pb^{2+}) exists in the air, drinking water, soil, wall fixtures, dust, lead-based paints and industrial products (Singh, 1993). It is a potent environmental toxicant and has been associated with adverse neurological and behavioral disorders of both laboratory animals (Atchison and Narahashi, 1984; Oortigiesen et al., 1990a; Oortigiesen et al., 1990b; Reuveny and Narahashi, 1991; Ujihara and Albuquerque, 1992; Singh, 1993; Nagata et al., 1997) and humans (Needleman et al., 1979; Cullen et al., 1983; Bellinger et al.,1987; Lille et al., 1988; Wong et al., 1990; Deitrich et al., 1992; Otto and Fox, 1993). Surveys conducted by the Public Health Service concluded that environmental Pb^{2+} poisoning is among the top four diseases of young children (Silbergeld, 1992). Pb^{2+} is so potent that the Center for Disease Control (CDC) has had to lower its criteria of levels considered at risk for neurotoxicity several times from 60 μg/dl (Davis and Svendsgaard, 1987), to 25 μg/dl (Bellinger et al., 1987), to the current accepted level of dosage equal to or greater than 10 μg/dl (Silbergeld, 1992).

The majority of research studies which have examined the effects of Pb^{2+} exposure, have identified children exhibiting deficits within the CNS. Children exposed

to high levels o:

exhibited poore:

abilities when co

Pb^{2-} induced imp

learning and men

intense during th

period coincides

(Northern and Do

Research

young developin

(1993) reported t

to the effects of

hearing threshol

Fox, 1993) and i

in adults have be

(1983) reported

episodes of Pb^{2-}

40 µg dl to 175

were among the

Limited i

function and the

available which s

increase in the thr

to high levels of Pb^{2+} prenatally and others who were exposed to Pb^{2+} postnatally exhibited poorer scores on measures of cognitive function and central auditory processing abilities when compared to a control group of children (Bellinger, 1987; Dietrich, 1992). Pb^{2+} induced impairments are of the utmost concern because they are believed to lead to learning and memory disorders. Silbergeld (1992) reports that Pb^{2+} exposure is most intense during the first two years of life, suggesting a critical period for impairment. The period coincides with the critical period for normal speech and language development (Northern and Downs, 1991).

Researchers previously believed that Pb^{2+} exposure posed more of a threat to the young developing CNS than to the developed CNS system. However, Otto and Fox (1993) reported that the cochlear nerve and central structures were preferentially sensitive to the effects of Pb^{2+} exposure in both developing and mature systems. In fact, elevated hearing thresholds in both young children and adults (Schwartz and Otto, 1991; Otto and Fox, 1993) and increased latencies of auditory brainstem responses (Otto and Fox, 1993) in adults have been reported as a result of exposure to environmental Pb^{2+}. Cullen et al. (1983) reported 31 cases of occupationally exposed workers with acute and chronic episodes of Pb^{2+} intoxication. The highest levels of whole blood Pb^{2+} levels ranged from 40 μg/dl to 175 μg/dl with a mean of 83 μg/dl. Abdominal pain, headache and fatigue were among the many reported symptoms among the population.

Limited information is available concerning the effects of Pb^{2+} on sensory function and the mechanism(s) responsible for lead toxicity. However, sufficient data are available which support the occurrence of elevated hearing threshold levels, as well as an increase in the threshold of activation for the initiation of an action potential in the

presence of vary

have found segm

no apparent effe

voltage-gated ion

still remains, do

of lead within the

In an atte

pharmacological

release, kinetic p

Atchison and Nar

junction of rats ar

plate potential (E

solution.

Oortgiese

ion channels (Ser

two voltage-gated

induced inward cu

Comparatively, th

quantity of Pb^{2+} (

High concentratio

noninactivating in

10 μM of Pb^{2+}. H

presence of varying levels of Pb^{2+}. In addition, histological studies of auditory structures have found segmental demyelinization and axonal degeneration of the cochlea nerve with no apparent effect on the vestibular and spiral ganglia (Otto and Fox, 1993). Unlike other voltage-gated ionic channels (e.g., Ca^{2+}) and ligand-gated ionic channels, the question still remains, do SGCs exhibit normal pharmacologic and kinetic activity in the presence of lead within the mammalian auditory system?

In an attempt to identify the mechanism(s) responsible for Pb^{2+} neurotoxicity, pharmacological studies have investigated the effects of Pb^{2+} on synaptic transmitter release, kinetic properties of ionic currents and sensitivity to neuronal development. Atchison and Narahashi (1984) studied neurotransmitter release at the neuromuscular junction of rats and found that Pb^{2+} (100 μM) effectively blocked the nerve-evoked end-plate potential (EPP). Both effects were reversible when washed with normal external solution.

Oortgiesen et al. (1990a) investigated the effects of Pb^{2+} on two receptor operated ion channels (Serotonin 5-HT and neuronal nicotinic acetylcholine (ACh) receptors) and two voltage-gated ion channels (Na^+ and Ca^{2+}) of mouse neuroblastoma cells. The ACh induced inward current was blocked by nanomolar concentrations of Pb^{2+}. Comparatively, the transient inward current mediated by 5-HT receptors required a larger quantity of Pb^{2+} (1.0 μM) before a steady reduction of current amplitude was observed. High concentrations of barium (Ba^{2+}) produced a fast transient as well as a noninactivating inward current. Both types of currents were reduced in the presence of 10 μM of Pb^{2+}. However, the Na^+ current remained unaffected up to 100 μM of Pb^{2+}.

Abnorm

functional capa

important role i

exposure of rats

second messeng

intracellular sour

CNS dysfunction

The NM

learning and plas

development. U

induced currents

words, 10 μM P

however, the sa

response by 15%

Roy and

Pb^{2+}, Cd^{2+}) on

TTX-S current

to 22% by the a

but shifted in th

voltage curves

currents in the

Peak T

sensitive to Ca^{2}

Abnormalities in the movement, distribution, as well as inhibition in the functional capacity of Ca^{2+} channels in the CNS due to Pb^{2+} neurotoxicity may play an important role in neuronal development (Singh, 1993). Singh (1993) found that chronic exposure of rats to low levels of Pb^{2+} reduced the number of inositol triphosphate (IP_3) second messenger receptors and thus reduced the capacity of IP_3 to mobilize Ca^{2+} from intracellular sources. This action may alter normal cell development and thus lead to CNS dysfunction.

The NMDA glutamatergic receptor is known to be involved in the processes of learning and plasticity as well as playing a key role in the early stages of neuronal development. Ujihara and Albuquerque (1992) demonstrated that Pb^{2+} blocked NMDA induced currents of cultured hippocampal neurons in an age-dependent manner. In other words, 10 μM Pb^{2+} decreased the NMDA response by 57% during the first week, however, the same concentration of Pb^{2+} during the fourth week only reduced the NMDA response by 15%.

Roy and Narahashi (1992) investigated the response of divalent cations (Ca^{2+}, Pb^{2+}, Cd^{2+}) on both TTX-S and TTX-R sodium channels of rat DRG cells. The peak TTX-S current was reduced by 20% in the presence of externally applied Pb^{2+}, compared to 22% by the addition of 5 μM of Ca^{2+}. The activation voltage was unaffected by Ca^{2+} but shifted in the depolarized direction in the presence of Pb^{2+} (50 μM). Conduction-voltage curves showed minimal decreases in the maximal conductance of the TTX-S currents in the presence of Pb^{2+}.

Peak TTX-R currents were more sensitive to the actions of Pb^{2+} and Cd^{2+} and less sensitive to Ca^{2+} than TTX-S currents. The TTX-R current was reduced by 70.4% at a

membrane leve

membrane pote

Conductance cu

55.2% by Pb^{2+}.

the cell for 1 - 2

Pharmacology

Pb^{2+} is o

lead poisoning.

(ligands) (Klaass

such as Pb^{2+}, rea

a metal complex

chelating agents

the binding of P

formed between

reaction produc

groups of ligand

enhancing the e

Pb^{2+} poi

infrequently an

inhalation of le

adverse affects

gastrointestinal

membrane level of +10mV by 50 μM Pb^{2+}. Conductance curves were measured at membrane potentials where conductance attained 50% of its maximal values. Conductance curves were shifted 25.3 mV by Pb^{2+}. Maximal conductance decreased 55.2% by Pb^{2+}. Effects seen for both TTX-S and TTX-R were reversible after washing the cell for 1 - 2 minutes with normal external solution.

Pharmacology of Lead

Pb^{2+} is one of several heavy metals that is toxic to the body and found to cause lead poisoning. It exerts its toxic effect by combining with one or more reactive groups (ligands) (Klaassen, 1996) essential for normal physiological functions. Heavy metals such as Pb^{2+}, react in the body with ligands containing oxygen and nitrogen. This creates a metal complex formed by a coordinate bond. Heavy metal antagonists known as chelating agents are designed to reverse the binding of Pb^{2+} to body ligands by blocking the binding of Pb^{2+} to the ligands. Klaassen (1996) defines a chelate as a complex formed between a metal and compound that contains two or more potential ligands. This reaction produces a heterocyclic ring. Chelating agents are designed to compete with the groups of ligands for the metal, thereby, preventing or reversing the toxic effects and enhancing the excretion of the metal.

Pb^{2+} poisoning can be either acute or chronic. Acute Pb^{2+} poisoning occurs infrequently and typically results from ingestion of acid-soluble lead compounds or inhalation of lead vapors. Chronic Pb^{2+} poisoning also known as plumbism, can have adverse affects involving one or any combination of the following systems: gastrointestinal system, neuromuscular system, CNS, hematological and renal systems.

The abs

and the gastroi

(vapor vs. parti

nine percent of

Inorganic Pb^{2+} i

It is later found r

Only small amou

Pb^{2+} found in gra

The Problem

The mech

membrane displa

which initiate au

replete with stud

events involving

auditory nerve)

in vivo and sing

however, have n

Voltage-

conductances an

are for the most

use the whole-c

embryonic CG

of the N-methyl

The absorption of Pb^{2+} into the body enters by two major routes, the respiratory and the gastrointestinal tract. Absorption of inhaled Pb^{2+} depends upon the form of Pb^{2+} (vapor vs. particles) ingested as well as the concentration of the ingested Pb^{2+}. Ninety nine percent of Pb^{2+} absorbed into the blood stream binds to hemoglobin in erythrocytes. Inorganic Pb^{2+} is initially distributed in soft tissue organs such as the liver and kidneys. It is later found redistributed and deposited in bone, teeth (seen as lead lines) and hair. Only small amounts of inorganic Pb^{2+} accumulate in the brain, with most of the deposited Pb^{2+} found in gray matter and the basal ganglia.

The Problem

The mechanics of the peripheral auditory system (e.g., traveling wave, basilar membrane displacement, shearing action, hair cell motility, etc.) are cochlear events which initiate auditory neural signal transduction. The available literature is rather replete with studies which describe these mechanical processes. Electrophysiological events involving auditory neural coding and transduction beyond the cochlea (i.e., of the auditory nerve) have been described, but the majority of these studies consist of recording in vivo and single-unit auditory nerve activity. Investigations at the in vitro level, however, have not been clearly defined and thus require further investigation.

Voltage-gated patch clamp studies have been used to describe various ionic conductances and receptor types of CG chick neurons. Although relevant, these studies are for the most part incomplete and few in number. Yamaguchi (1988) was the first to use the whole-cell voltage-clamp technique to study Na^{+} and Ca^{2+} ionic currents in the embryonic CG cell. In the same study he provided data also that supported the presence of the N-methyl-D-aspartate (NMDA) subtype glutamate receptor. Shortly thereafter,

several studie

activation ina

work revealed

Valverde et al

(Yamaguchi ar

(Yamaguchi, 1

1992), glutamat

Nakagawa et al

(Yamaguchi an

only one study

characteristics

There a

mammalian au

to study the ex

SGC. Using g

D-aspartate (N

mammalian SG

transient ionic

guinea pigs. I

Sacchi found t

and taste syste

these findings,

several studies followed in order to further characterize the kinetic properties (e.g. activation/inactivation) and antagonistic blocking characteristics found in the CG. The work revealed the existence of outward going K^+ current (Yamaguchi and Ohmori, 1990; Valverde et al., 1992; Sheppard et al., 1992), the TTX-sensitive sodium current (Yamaguchi and Ohmori, 1990; Valverde et al., 1992), Ca^{2+} sensitive currents (Yamaguchi, 1988; Yamaguchi and Ohmori, 1990; Valverde et al., 1992; Sheppard et al., 1992), glutamate receptor subtypes (Yamaguchi, 1988; Yamaguchi and Ohmori 1990; Nakagawa et al., 1991) and the carbamylcholine (CCh-sensitive) current in CG neurons (Yamaguchi and Ohmori, 1993). Although the embryonic CG cell was used in all cases, only one study described the developmental onset, kinetic activity and ionic channel characteristics in these auditory cells (Valverde et al.,1992).

There are studies which describe the ionic characteristics of the SGC of the mammalian auditory system. Nakagawa et al. (1991) used the mature guinea pig in order to study the excitatory amino acid (EAA) responses produced within the dissociated SGC. Using glutamate (Glu) and its agonist quisqualate (QA), kainate (KA), N-methyl-D-aspartate (NMDA) and aspartate (Asp), he found that the Glu receptor of the mammalian SGC was the non-NMDA subtype. Santos-Sacchi (1993) defined the rapid transient ionic conductive properties of Na^+ current and K^+ current of the adult SGCs of guinea pigs. In comparing his results with those of several other investigators, Santos-Sacchi found that the channel kinetics of the cells from the mammalian visual, olfactory and taste systems were comparatively slow to that of the mammalian SGC. Based on these findings, he postulated that the rapid transient kinetic responses demonstrated by

SGCs posse

characteristi

Moc

postnatal ra

other mamn

blocked by

than -50 m

inactivation

with a fast a

as early as

Unli

information

understandi

of data is av

In as

coding and t

structures, th

which to det

evident from

describes the

inactivation

applied toxica

SGCs possessed the timing properties necessary to faithfully code temporal characteristics present in auditory signals.

Moore et al. (1996) recorded both sodium current and potassium current from postnatal rat type I SGCs. The activation-inactivation kinetic properties were similar to other mammalian preparations. Sodium current activated rapidly and were reversibly blocked by 0.5 μM TTX. Channels were activated at membrane potentials more positive than -50 mV and reversed at approximately +30 mV. $V_{1/2}$ for sodium channel inactivation occurred at approximately -83 mV. Recovery from inactivation occurred with a fast and slow time course. Peak sodium current began to recover from inactivation as early as 0.8 ms and continued to recover with a time constant of 7.5 ms.

Unlike the information presented above about DRGs, there is a lack of information about ionic characteristics of SGCs. These facts provide clues to a better understanding of the process of auditory neural coding. However, only a cursory amount of data is available which describe ionic characteristics of the mammalian SGC.

In asking the question, are the underlying nerve fibers which are responsible for coding and transferring auditory information present and develop parallel to anatomical structures, the patch-clamp technique provides an investigative scientific method in which to determine the presence or absence of sodium currents in SGCs. What should be evident from the information presented above is the lack of physical evidence that describes the developmental stages of sodium ionic expression, normal activation and inactivation kinetics. Furthermore, ionic expression in the presence of an externally applied toxicant such as Pb^{2+} of young mammalian SGCs is lacking.

In

propose th

(1)

(2)

(3)

(4)

(5)

In order to further investigate the kinetics of the mammalian spiral ganglion cell, I propose the following research questions:

(1) Are sodium channels and potassium channels present in the embryonic rat SGCs?

(2) Do postnatal (P2 – P9) SGCs exhibit TTX-S and TTX-R sodium channels?

(3) Are there differences in the kinetics of activation and inactivation of sodium currents between embryonic and postnatal SGCs?

(4) Are there changes in the current amplitude and gating characteristics of SGCs in the presence of externally applied Pb^{2+}?

(5) Do postnatal (P2 – P9) SGCs exhibit delayed rectifying outward-going potassium currents?

Voltage-Gated

Earlier p

the very small ti

membrane, an e

resistance serve

originating from

Improved patch

serve to reduce

with resistances

debris, and whe

resistance seals

noise and impro

Accordi

attachment of th

the giga-seal lea

forming a gigaol

inside-out patch

CHAPTER II

REVIEW OF THE LITERATURE

Voltage-Gated Patch-Clamp Technique

Earlier patch-clamp studies involved the formation of "megaohm seals". When the very small tip of a heat polished glass pipette is pressed against a small patch of cell membrane, an electrical seal results creating a high resistance (circa 50 MΩ). This high resistance serves partly as a mechanism which ensures that most of the current originating from within the membrane patch flows into the pipette (Hamill et al., 1981). Improved patch-clamp techniques now allow the formation of "gigaohm seals" which serve to reduce background noise and data contamination. Tight pipette membrane seals with resistances between 10 – 100 GΩ can be obtained when the pipette surface is free of debris, and when negative suction is applied to the pipette's interior. These high resistance seals are called "gigaohm" seals and are key to reducing unwanted background noise and improving the recordings of ionic currents.

According to Hamill et al. (1981), gigaohm seals are mechanically stable. The attachment of the pipette to the cell membrane can be partly disrupted without destroying the giga-seal leaving a cell-free membrane. Four recording configurations can result after forming a gigaohm seal: (1) cell attached, (2) whole-cell, (3) outside-out patch, and (4) inside-out patch (See Figure II-1). Cell attached, outside-out and the inside-out patch are

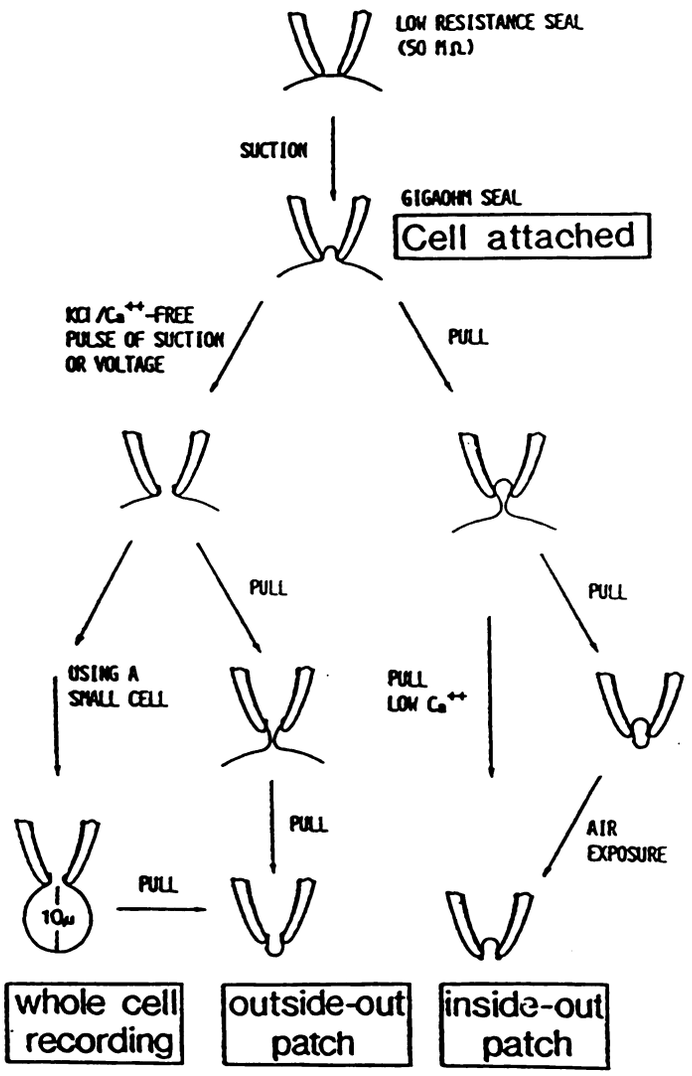

Figure II-1. Four recording configurations utilized while recording voltage-gated ionic currents from various preparations (Hamill et al., 1981)

techniques use

conformation.

from multiple

used on a varie

inactivation, ga

cell patch-clam

Voltage-Gate

The firs

technique to re

Yamaguchi (19

cochlear gangl

dependent ioni

excitatory ami

Yamag

internally with

activated at m

course of char

peak amplitud

25 mV and 0.

monotonicall

-25 mV and 0

occurred at -6

techniques used for recording single channel currents. The cell attached pipette conformation, like that of the whole-cell patch clamp technique can be used to record from multiple channels. The four pipette-membrane seal conformations listed have been used on a variety of cell preparations to study the kinetic characteristics (e.g., activation, inactivation, gating, etc.) of various ionic channels and their conductances. The whole-cell patch-clamp configuration is utilized in the present research project.

Voltage-Gated Patch Clamp Studies of Acoustic Ganglia

The first reported account of using the whole-cell voltage-gated patch-clamp technique to record cellular activity of cultured acoustic ganglion neurons was that of Yamaguchi (1988). He studied specific biophysical properties inherent within embryonic cochlear ganglion (CG) neurons of the chick and observed the activity of three voltage dependent ionic channels. He observed current flow also in response to several excitatory amino acids.

Yamaguchi (1988) isolated the sodium current by blocking potassium channels internally with CsCl and TEA-Cl externally. TTX-sensitive sodium currents were activated at membrane potentials more positive than -35 mV. Conventionally, the time course of channel activation is measured as the time it takes a current to reach 1/2 of its peak amplitude, $T_{1/2}$. The $T_{1/2}$ decreased with depolarization, where $T_{1/2}$ was 0.7 ms at -25 mV and 0.3 ms at +10 mV. The time constant for inactivation also decreased monotonically with depolarization and had times similar to those of activation, 0.8 ms at -25 mV and 0.3 ms at +10 mV. Half-inactivation of embryonic cochlear ganglion cells occurred at -65 mV.

demonst

noninact

potentia

inactivat

could be

type of -

mV. resp

resistant

noninacti

shifted in

mV for V

T

properties

Activatio

Yamaguc

activating

membran

and inacti

time that

the sodiu

by 1.0 μV

Two types of calcium currents were identified in the CG neurons which demonstrated different activation and inactivation characteristics. The first type, the noninactivating type, when held at a holding potential of -50 mV activated at membrane potentials more positive than -40 mV and did not inactivate. The second type, the inactivating type, occurred when held at a more negative holding potential of -90 mV and could be stimulated at a more negative step voltage command than the noninactivating type of -65 mV. Half-inactivation and complete inactivation occurred at -85 mV and -50 mV, respectively. Both types of calcium channels were permeable to Ba^{2+} and Sr^{2+} and resistant to nifedipine (2.0 μM). The time constants for activation and inactivation of the noninactivating Ca^{2+} current were dependent upon the presence of Ba^{2+}, Sr^{2+} or Ca^{2+}, and shifted in the depolarized direction by approximately 13-14 mV for activation and 12-13 mV for $V_{1/2}$ in the presence of Ca^{2+}.

Two years later, Yamaguchi and Ohmori (1990) studied the electrophysiological properties of sodium channels present in cultured embryonic cochlear ganglion neurons. Activation and inactivation characteristics were similar to those in the previous work of Yamaguchi (1988). This work further confirmed the voltage dependency of CG neurons, activating at potentials more positive than -40 mV and half inactivation occurring at membrane potentials more positive than -64 mV. The time constants of both activation and inactivation decreased monotonically. That is, as the cell was depolarized further the time that it took for the cell to activate or inactivate decreased systematically. Similar to the sodium currents observed by Yamaguchi (1988), these were also reversibly blocked by 1.0 μM TTX.

T

responses

of potassi

inward di

embryoni

potentials

The time

hyperpola

potassium

potassium

Va

exhibited

chicks. As

compared

both cochl

forming th

transforms

current exp

the inward

in isolation

appear in c

Occasionall

absence of

There are a variety of voltage-gated potassium channels which exhibit differing responses to pharmacological agents. Excitable cells use a combination of different types of potassium channels to carry out specific functions (Hille, 1992). In addition to the inward directed sodium current, Yamaguchi and Ohmori (1990) observed that the embryonic CG neurons possessed an outward directed current which activated at potentials more positive than -66 mV when measured at a holding potential of -94 mV. The time constant for inactivation ranged between 2 - 20 ms and was accelerated upon hyperpolarization. Visually, the current did not appear as the characteristic A-type potassium current, but had characteristics which closely resembled the delayed rectifying potassium channel.

Valverde et al. (1992) were the first to investigate developmental patterns exhibited by sodium and potassium currents in the embryonic type I CG neurons of chicks. As one might expect, these embryonic cells were physiologically immature compared to postnatal CG cells and showed very little activity before E6. Anatomically, both cochlea and vestibular ganglia appear at E2 - E3 as a conglomerate cell mass forming the cochleovestibular ganglion (CVG). The CVG proceeds to develop and transforms into distinct cochlea and vestibular ganglia by E4 - E5. The sequence of ionic current expression is such that the outward potassium current appears first followed by the inward sodium current by E6 and E8, respectively. The sodium current never appears in isolation. That is, without the benefit of ionic blocking strategies, sodium currents will appear in conjunction with other ionic currents, such as the potassium current. Occasionally, Valverde et al. (1992) found cells which generated outward currents in the absence of detectable inward currents.

neuron

E14 re

"inflec

not pr

expres

mV at

reflect

neuron

neuron

curren

E8. fa

increa

not di

transi

these

curre

chara

thres

neur

Current clamp data revealed the presence of spike activity in E8 cochlear ganglion neurons. By E10, these underdeveloped spikes were easily distinguishable but small. By E14 regenerative action potentials were clearly developed and characterized by an "inflection/hump" in the falling phase and a distinct afterhyperpolarization, which was not present during the earlier stages. The "inflection/hump" was believed to reflect the expression of Ca^{2+}.

As cochlear ganglion cells matured, resting membrane potentials shifted from -40 mV at E7 to -61 mV at E16. Input resistance decreased during the same time period, reflecting the change in cell size and channel density.

Under specific experimental conditions, both K^+ and Na^+ currents appeared in CG neurons. Of the two, voltage-gated K^+ currents appeared first. At E6, cochlear ganglion neurons produced weak outward-directed K^+ currents. Shortly afterwards, however, K^+ currents were clearly present from E7-E14 showing changes with maturation and age. By E8, fast transient inward currents accompanied the outward directed currents which also increased in magnitude with maturation. Between E12-E14, the basic current patterns did not differ significantly from that of an adult.

In fully developed neurons (E16), depolarizing step commands induce fast transient inward currents that had a threshold of activation of -40 mV. Activation of these currents was very fast, occurring between 0.1 to 1.0 ms. Although the potassium current appeared first, it seems as though the Na^+ current acquired some of its adult characteristics early on. For example, unlike their accompanying outward K^+ current, the threshold for activation, -40 mV, remained the same for both young and mature CG neurons. With a holding potential of -80 mV, maximum peak sodium current was

reach

unch

peak

pA) a

in cel

youn

curre

outwa

work

curre

curre

inacti

speci

than

non-i

more

61 m

Reco

much

inact

cons

reached at a membrane potential of -20 mV. Steady-state inactivation also remained unchanged throughout development. Sodium currents produced a threefold increase in peak sodium currents such that the current magnitude increased between E7- E11 (200 pA) and E14- E16 (600 pA). This change in peak amplitude perhaps reflects the increase in cell membrane size and sodium channel density due to cellular maturation. Cells as young as E8.5 generated inward currents that were reversibly blocked by 1.0 μM TTX.

Sheppard et al. (1992) further characterized two distinct transient outward currents in developing CG neurons and classified them as (1) fast inactivating transient outward currents ($I_{to,f}$) and (2) slow inactivating outward currents ($I_{to,s}$). Similar to the work reported by Valverde et al. (1992), the response characteristics of the outward current featured three identifiable components. (1) fact activating and inactivating current, (2) a slowly relaxing current and (3) a portion of the current which was non-inactivating. Isolation of the fast transient outward current was accomplished by a specially designed pre-pulse protocol.

The slow outward-current had clearly different activation and inactivation kinetics than it's faster counterpart which was present in much younger CG neurons. The slower non-inactivating outward current generated from an E9-11 ganglion neuron had a much more positive activation threshold of -34 mV than the faster transient outward current (-61 mV), but possessed a similar mean half-inactivation membrane potential of -67 mV. Recovery from inactivation differed between the two current types as well and occurred much faster (100 ms) in the $I_{to,f}$ than the $I_{to,s}$ current (1 sec). The time constant for inactivation of $I_{to,f}$ was minimally influenced by membrane potential, however, the time constant for inactivation of $I_{to,s}$ clearly showed an increase with depolarization. It should

be noted that

period for the

young $I_{to,s}$ CG

neuron exhibit

Two kn

used to further

transient curren

reduced the ste

outward curren

Both peak and

more than stea

The act

-10 mV which

presented in th

"hump" sugge

Pharmacologic

current of E14

reportedly occ

curve for $I_{to,f}$.

presence of Ca

current was fo

not found to be

be noted that in my opinion, the change in activation thresholds and faster recovery period for the $I_{to,f}$ may reflect a change in cellular maturity that is not present in the young $I_{to,s}$ CG neuron. Valverde et al. (1992) in a comparison analysis found that the CG neuron exhibited the $I_{to,s}$ with less frequency in older CG neurons.

Two known pharmacological compounds, TEA and 4-aminopyridine (4AP), were used to further identify the current type. Interestingly, TEA did not block the fast or slow transient currents. However, in an E16 neuron which exhibited a slow component, TEA reduced the steady-state current without showing a significant change in the transient outward current. A diminishing effect was clearly found on $I_{to,f}$ using 4 AP (0.5 - 2 mM) Both peak and steady-state outward currents were reduced, with peak current influenced more than steady state current. $I_{to,s}$ was unaffected by 4AP.

The activation curve consistently revealed a "hump" occurring between -20 mV to +10 mV which was more apparent in the conductance vs. potential plot (Figure III/2D presented in their article). Sheppard et al. (1992) go on to explain the significance of this "hump" suggesting that the inflection was related to the presence of Ca^{2+}. Pharmacological experiments found that the removal of extracellular Ca^{2+} suppressed $I_{to,f}$ current of E14-E16 cochlear ganglion neurons in a voltage dependent manner. Inhibition reportedly occurred in the voltage range which corresponded to the "hump" in the I/V curve for $I_{to,f}$. Suppression of $I_{to,f}$ was mimicked by solutions containing Co^{2+} in the presence of Ca^{2+}, a known calcium channel blocker. Therefore, the fast transient outward current was found to be Ca^{2+} dependent whereas the slow transient outward currents was not found to be Ca^{2+}-dependent. 4-aminopyridine (0.5 - 2.0 mM) effectively blocked the

$I_{m,f}$ but shov

the expressi

Yam

studied the a

olivocochlea

neurons of cu

hydrolysable

slowly outwa

atropine (3.0

CCh-sensitive

μM) did not r

supports the p

mediate the pr

characterize th

protein and fou

during the proc

by ACh have b

Yamaguchi and

CCh sensitive

μM) and phorb

current to a sim

phorbol (2.0 μM

μM), a specific

$I_{to,f}$ but showed no effect on $I_{to,s}$. From the results, Sheppard et al. (1992) concluded that the expression of two distinct transient outward currents were present in CG neurons.

Yamaguchi and Ohmori (1993) using whole-cell voltage-clamp techniques studied the action of the efferent innervation of the afferent terminal (the lateral olivocochlear system) through the direct action of acetylcholine (ACh) on afferent neurons of cultured CG neurons. Using carbamylcholine (CCh) (30-100 μM), the non-hydrolysable form of ACh, they were able to demonstrate the reversible suppression of a slowly outward directed current. In the presence of a known muscarinic blocker such as atropine (3.0 μM) and a blocker of the M_1 muscarinic receptor, pirenzepine (3.0 μM), the CCh-sensitive current suppression was blocked, while bath applied D-tubocurarine (3.0 μM) did not reduce the CCh response. These results provide strong evidence which supports the presence of a muscarinic AChR, probably an M_1 type receptor that may mediate the process leading to suppression of the potassium current. To further characterize the properties of this receptor, they investigated the involvement of a G-protein and found that GTP-γ-S, the non-hydrolysable analogue of GTP, was activated during the process of suppression of the slow outward current. Protein kinases activated by ACh have been suggested to suppress the muscarine-sensitive K^+ current (M-current). Yamaguchi and Ohmori (1993) found that while protein kinase A had no effect on the CCh sensitive current, protein kinase C (PKC) such as phorbol dibutyrate (PDBu) (2.0 μM) and phorbol 12-myristate 13-acetate (PMA) (1.0 μM), reduced the slow potassium current to a similar extent as that caused by CCh (30 μM). A non PKC activator, 4-phorbol (2.0 μM) did not suppress the slow outward current. When sautrosporine (30 μM), a specific inhibitor of PKC was applied internally, CCh failed to reduce the slow K^+

current. These results support the idea that the activation of the M_1 muscarinic receptor suppresses the slow K^+ current in CG neurons through the activation of PKC.

The first synapse of the auditory system is peripheral and occurs at the level of the hair cell and primary afferent. Glutamate (Glu) has been suggested to be the chemical neurotransmitter signal at this junction. As stated above, Yamaguchi (1988) and Yamaguchi and Ohmori (1990) used voltage-gated patch-clamp techniques to study the induced responses of Glu receptors using various excitatory amino acids in non-mammalian CG cell preparations. Controversy exists in the literature with reference to the subtype of Glu receptors present within the mammalian SGC of the guinea pig. Nakagawa et al. (1991) used the patch-clamp technique to study the physiological and pharmacological properties of excitatory amino acid induced responses in the mammalian isolated SGCs of mature guinea pigs. Glu and aspartate (Asp) are reported to be the most abundant transmitter class in the CNS (Vander et al., 1990).

Nakagawa et al. (1991) investigated the subtype Glu receptor of SGCs using various excitatory amino acids and their agonists. Glu and the agonists quisqualate (QA) and kainate (KA) induced inward currents in a concentration dependent-manner. NMDA and Asp, another intrinsic excitatory amino acid did not elicit any type of a response. The NMDA response is suppressed in the presence of extracellular Mg^{2+}, and glycine is thought to be necessary for activating NMDA receptors. NMDA and Asp still had no effect on SGCs under these conditions.

Kynurenic (Kyn) acid and its derivatives diCl-HQC are known competitive antagonists for EAAs. Quinoxalinediones (CNQX and DNQX) are known non-NMDA receptor antagonists in CNS neurons. The antagonists mentioned above blocked the

current

phosph

are ant

QA an

recepto

ganglio

NMDA

current

respons

conclus

while t

charact

pigs. T

that un

that the

myelin

along t

1990; S

(1993)

These c

currents induced by all of the agonists in a concentration-dependent manner. 2-amino-5-phosphonovalerate (APV) and 3-3(2-carboxy-piperazine-4-yl) propyl-l-phosphate (CPP) are antagonist of NMDA receptors. They had no effect on responses activated by Glu, QA and KA suggesting that the Glu receptors in SGCs did not contain NMDA preferring receptors (Nakagawa et al., 1991).

Yamaguchi (1988) studied the EAA induced currents from cultured cochlear ganglion cell ectomized from chickens. Twenty eight cells responded to Glu, KA, QA, NMDA and Asp. APV and Mg^{2+} partially suppressed the peak component of the inward current induced by Glu but had little effect on the steady-state component. The NMDA response was almost fully suppressed by APV and Mg^{2+}. Nakagawa et al. (1991) concluded that the non-NMDA subtype Glu receptor was present in SGCs of guinea pig while the mixed type of Glu receptors was present in CG cells of chickens.

Santos-Sacchi (1990, 1993) used the whole-cell voltage-clamp technique to characterize the ionic conductances of SGCs removed from the inner ears of adult guinea pigs. The purpose of his research was to explain the uncharacterized neuronal influences that underlie the generation of auditory nerve single fiber activity. He proposed the idea that the myelinated spiral ganglion cell acted as an internode along the course of the myelinated eighth nerve fiber serving to enhance the conduction of neuronal impulses along the length of the auditory afferent nerve fiber.

Similar to the findings of others (Yamaguchi, 1988; Yamaguchi and Ohmori, 1990; Sheppard et al., 1992; Valverde et al., 1992) in embryonic CG cells, Santos-Sacchi (1993) identified both outward K^+ currents and fast inward TTX-sensitive Na^+ currents. These cells had an average resting membrane potential of -67.3 mV. Although the

average cell diameter (19.01 μm) of the guinea pig spiral ganglion neurons were comparable in size to the embryonic CG neurons (15-20 μm at E17), these mammalian SGCs exhibited faster kinetic activity which may reflect the difference in maturation between the two cell populations.

The slowly developing voltage dependent outward K^+ currents displayed rapid onset kinetics with little or no inactivation. At -43 mV, activation began within 360 μs after stimulus onset. Above -50 mV outward currents reached half-maximal amplitude within 1.5 ms which was faster than the times reported for embryonic CG neurons by Yamaguchi and Ohmori (1990). Again, this may reflect differences in maturation. Removal of external Ca^{2+} resulted in the reversible reduction of K^+ currents, while Gd^{3+} (50 μM) blocked the outward K^+ current, a reflection of perhaps stretch-activated channels.

In addition to the outward K^+ current, Santos-Sacchi observed two additional inward currents, one which had rapid onset kinetics and the other which exhibited slower onset kinetic activity with no inactivation. TTX-sensitive (0.1-0.3 μM) sodium currents were present in the SGCs of guinea pig and varied in their current densities. TTX-R currents were not reported (Moore et al., 1996). The guinea pig SGCs had a very rapid onset with a maximum peak current occurring within 400 μs between a voltage range of -10 and 0 mV and inactivation within 4 ms. Inactivation was also voltage dependent and ranged between 0.8 ms at -23 mV to 0.3 ms at +25 mV. The time constant of recovery

from

holdi

-70 m

inacti

sustai

curren

Santos

rates. s

fibers

Sacchi

activity

capabl

rat SG

activat

than -5

showed

differen

the basi

of under

from inactivation was 2.16 ms when the command pulse was stepped to -10 mV from a holding potential of -80 mV.

A slower voltage dependent inward current activated at membrane potentials near -70 mV and had an activation time constant of several milliseconds. The current did not inactivate during sustained depolarizations. A concentration of 50 μM Cd^{2+} reduced the sustained current and its associated tail current and 50 μM Gd^{3+} completely blocked the current. Co^{2+} (2.0 mM) in the absence of extracellular Ca^{2+} also blocked the current. Santos-Sacchi (1993) suggested that this current appears to involve a Ca^{2+} component.

Stimulus frequency and intensity coding involves firing patterns and high firing rates, some rates reaching 2000 spikes per second (Javel, 1986). Therefore, eighth nerve fibers must faithfully detect and process hair cell activity at a tremendous pace (Santos-Sacchi, 1993). In consideration of the voltage-dependent characteristics and fast kinetic activity displayed by SGCs, Santos-Sacchi (1993) suggested that these cells are thus capable of faithfully transmitting high frequency acoustic information to the CNS.

Moore et al. (1996) characterized the sodium and potassium currents of postnatal rat SGCs. With a V_h of -80 mV, these TTX-S (0.5 μm) neurons demonstrated rapid activation and inactivation kinetic properties and activated at potentials more positive than -50 mV. It was clear that these bipolar cells produced sodium currents which showed differences in their inactivation properties (e.g. fast, slow, steady-state). These differences in inactivation characteristics may result from their place along the length of the basilar membrane. On the other hand, these differences may account for the shaping of underlying auditory nerve activity such as temporal or frequency cues.

and

outw

mV

pres

obta

outw

in th

norm

gang

1997

to ex

distin

length

had a

types

demon

neuron

eighth

rostral

Voltage-gated potassium currents were also identified in SGCs in the presence and absence of TTX and appeared to be of the delayed rectifier type. These often robust outward directed potassium currents were activated at potentials more positive than -40 mV with a V_h of -80 mV. Surprisingly, these currents were only suppressed in the presence of 25 mM of TEA-CL and not completely blocked. On a few occasions after obtaining adequate seals, spiral ganglion neurons were found which produced only outward directed potassium currents in the absence of TTX or robust potassium currents in the presence of diminished sodium currents. It was not clear whether this was the normal activity produced by a healthy cell or the results produced by an unhealthy spiral ganglion neuron.

Several investigators (Davis, 1993, 1996; Lin, 1996; Mo and Davis, 1997, Lin, 1997, Zun-Li, M. and Davis, R. L., 1997) have used single channel recording techniques to examine the firing patterns of SG neurons. Lin (1996) observed the activity of two distinctly different potassium channels that were characterized by their conductance and length of burst opening states. As seen in other studies, one potassium channel clearly had a larger conductance (112$\pm$ pS) than the other (57$\pm$ pS). Both potassium channel types showed very little inactivation during a 750 ms test pulse. The channel which demonstrated the smaller conductance was also less dependent upon calcium.

Davis (1996) examined potassium channel activity within the primary-auditory neurons of goldfish. The saccular nerve is comparable to the auditory component of the eighth cranial nerve. Its peripheral innervation pattern is made up of two branches, the rostral saccular macula and the caudal macula. Using single channel patch clamp

techniques, she found physiological differences between neurons which innervated the rostral and caudal epithelium. The internodal membrane of these primary-auditory neurons revealed a number of different potassium selective channel types. The three most commonly observed K^+ channels in both rostral and caudal sacular neurons were characterized based upon their conductance and subconductance states and were identified as $K_{(32)}$, $K_{(19)}$, and $K_{(12)}$. These three voltage-dependent potassium channels were found in both somatic and axonal membranes of the sacular nerve. Interestingly, $K_{(12)}$ showed differential channel activity when compared to its faster conducting channel counterparts. The $K_{(12)}$ channel flickered rapidly throughout depolarizing step protocols and was noninactivating. A fourth potassium channel, $K_{(Ca)}$, was observed and found to exist exclusively in the neurons that innervated the caudal sensory epithelium. According to Davis (1996) multiple potassium channel types have been shown to exist in the internodal regions of peripheral myelinated axons. Although uncertain as to the specific role these four potassium channels play in coding auditory stimuli, she was able to identify four different potassium channels in the somatic and axonal regions of primary-auditory neurons found in goldfish

Mo and Davis (1997) characterized the endogenous firing patterns of neonatal mouse spiral ganglion neurons. Using current-clamp patch-clamp measures, they were able to identify postnatal SG neurons which produced differing neuronal firing patterns. Frequency histograms representing the maximum number of fired action potentials showed that neurons could be classified as either slowly adapting or rapidly adapting. The larger percentage of neurons were found to be rapidly adapting. Rapidly adapting

neurons fired one or only a few APs in response to a constant depolarizing current injection while slowly adapting neurons fired multiple APs in response to the same stimulus. These firing patterns were dependent upon the holding potential such that at a holding potential of -60 mV, the neurons produced a larger number of APs than when held at a holding potential of -80 mV for both neuronal types. Other measures found differences between the two cell types which further categorized their specific attributes. Namely, input resistance, spike amplitude decrement, instantaneous firing frequency, and inward rectification all showed different patterns between rapidly and slowly adapting neurons. The investigators concluded that mouse neonatal SG neurons possessed the intrinsic firing patterns that regulate the number of fired APs and timing characteristics necessary for neuronal signal coding.

Lin (1997) investigated the excitability of cultured SGCs from early (P0 – P1) postnatal gerbils using whole-cell patch-clamp techniques and found that young postnatal SGCs were capable of generating APs long before hearing commenced. Investigation of the kinetic properties of APs were carried out through the use of current-clamp protocols utilizing various frequency patterns and stimulus durations in addition to voltage-gated studies using specific channel blocking strategies.

Frequency of AP generation and amplitude were dependent upon the frequency and duration of the current pulses. Single depolarizing pulses of long durations elicited only single APs. When SGCs were excited by a train (50 Hz) of short current pulses, successive APs fired at lower amplitudes, broader durations and delayed peak times. Limited success was accomplished in obtaining APs using pulse trains at higher

frequencies while APs at 20 Hz and lower had similar amplitudes to those obtained at 50 Hz.

TTX-S sodium current, potassium current and dihydropyridine-sensitive L-type calcium current were identified through voltage-gated techniques. Lin (1997) characterized the kinetic properties of each specific current and discussed their contribution towards the generation of the AP and neuronal excitability in postnatal (P0 – P1) gerbil SGCs.

The review presented above shows the progress that has been made thus far in a sensory system that remains to a large extent still uncharacterized. Although much is known about the anatomy of the auditory system and to a great extent, the physiology of the auditory system, we still have not uncovered the neuronal mechanism(s) responsible for the normal processing of auditory information. Among the numerous scientific techniques used in neuroscience research, the whole-cell voltage-gated patch clamp technique offers a means through which we can further identify and characterize the activity occurring at the single neuronal level. As described above, most of the patch clamp studies involving the spiral ganglion cell have: (1) been conducted within the avian auditory system; (2) described the occurrence of a variety of outward potassium currents to a greater extent than the inward sodium current; (3) provided support for the subtype of Glu receptor present in the SGCs of guinea pig vs. cochlear ganglion of embryonic chicks, and (4) described the mechanisms responsible for ACh suppression of outward currents.

CHAPTER III

METHODS AND PROCEDURE

Dissociated Cell-Culture

Sprague-Dawley rat pups (E18, P2 – P9) were anesthetized with methoxyflurane (Metofane) and rapidly decapitated. Right and left bullae were opened to expose the cochlea. The bony labyrinth of the cochlea was mechanically removed exposing the modiolus. SGCs were removed, isolated and incubated in trypsin (2.5 mg/ml, type XI, Sigma Chemical Co., St. Louis, MO) in a Ca^{2+}/Mg^{2+}-free filtered phosphate-buffered saline (PBS) for 25 - 30 min at 37° C. Cells were rinsed and centrifuged twice in PBS supplemented with D^{+} glucose. The enzymatic treatment was interrupted by the addition of six drops of a mixture of DNase I (1.5 mg/ml, Sigma) and $MgSO_4$ (2.5 mg/ml, Matheson, Coleman and Bell, Norwood, Ohio). Prior to trituration, two ml of filtered Dulbecco's Modified Eagles Medium (DMEM) (Gibco BRL, Grand Island, NY) supplemented with HAM's F12 (50 ml, Gibco BRL), glutamine (0.5 ml, Sigma), 10% heat-inactivated fetal calf serum (R. H. Lurie Cancer Center, Chicago, IL) and antibiotics (20 U penicilin/20 ng streptomycin/ml) was added to the cell suspension. The cells were gently dissociated mechanically by pipetting the media using fire-polished Pasteur pipettes. The cells were plated onto cover-slips (12 mm, Costar, Cambridge, MA) that had been previously coated with collagen (0.01%) and placed in plastic 6 or 24 well cell

culture clusters filled with 1.0 ml or 2.0 ml of culture media, respectively. The cells were kept in culture for as long as they survived without granularity.

Materials and Methods

A. Auditory Spiral Ganglion Neuron Preparation

Spiral ganglion cells are located within the modiolus of the inner ear which is located medially within the cochlea. The isolation of the myelinated bipolar cells was accomplished in three steps: (1) removal of the neuronal cell bodies from the encapsulated cochlea, (2) enzymatic treatment to remove unwanted and problematic myelin, and (3) trituration and plating of cells onto the previously coated collagen-treated glass cover slips. Upon completion, cells were stored in a controlled incubated environment (i.e., 95% Humidity; 5% CO_2; Temperature, 34.7° C) until time of use. SGCs were then used within a twenty four hour period for patch-clamp voltage-gated studies

1. Removal of Neuronal Spiral Ganglion Cells

Rat fetuses were rapidly removed from the mother by cesarean section and placed in a petri dish filled with PBS. Each fetus was removed from its sac and subsequently decapitated. Cochlea from both right and left sides were isolated. Isolation of SGCs followed the same procedure discussed below for postnatal SGCs.

Prior to each experiment, a P2 – P9 pup was anesthetized by methoxyflurane (Metofane) respiration. Pups were gently placed in a sealed glass receptacle filled with Metofane until they were anesthetized. When responses to a pinched tail ceased and the respiratory pattern slowed, pups were doused in 70% ethanol and rapidly sacrificed by

decapitation. The head was mounted so that its ventral surface faced the lens of the phase contrast microscope (see Figure III-1). Using iris scissors, a longitudinal incision was made separating the left and right sides of the epidermis which was further separated into quadrants (See Figure III-1B, III-1C). The tissue located deep to the epidermis was cut away until the dense white ring of the tympanum was exposed bilaterally (Figure III-1D). The ring served as an essential landmark for identifying the cochlea and was characterized by a dense white ring surrounding a more opaque bulla. Once the ring was identified, it was carefully cut away, ensuring that the cochlea located deep to this structure was not damaged. Once the covering was removed, a gelatinous mesenchyme filler which covered the cavity and protected the cochlea was removed, leaving the cochlea surrounded by the shell of an empty cavity. The bony shell of the cochlea was mechanically removed exposing the 2 1/2 coils around which the organ of Corti spiraled. The organ of Corti was removed with ultra-fine forceps, and discarded, while the modiolus was removed and stored on ice in a petri dish filled with Ca^{2+} and Mg^{2+} free phosphate buffered saline (CMF-PBS).

2. Enzymatic Treatment of Spiral Ganglion Tissue

A Pasteur pipette was used to transfer the SGCs into a 15 ml centrifuge tube containing trypsin (7.5 mg) and PBS (6.0 ml). The centrifuge tube was placed in a water bath and incubated for 20 - 25 minutes at 37° C. After removal of the centrifuge tube from the water bath, the SGCs which characteristically formed into a mass of tissue at the bottom of the tube now appeared somewhat translucent. Trypsin was removed from the centrifuge tube by a micropipette and replaced by 5.0 ml of CMF-PBS. Immediately

Surgical Technique

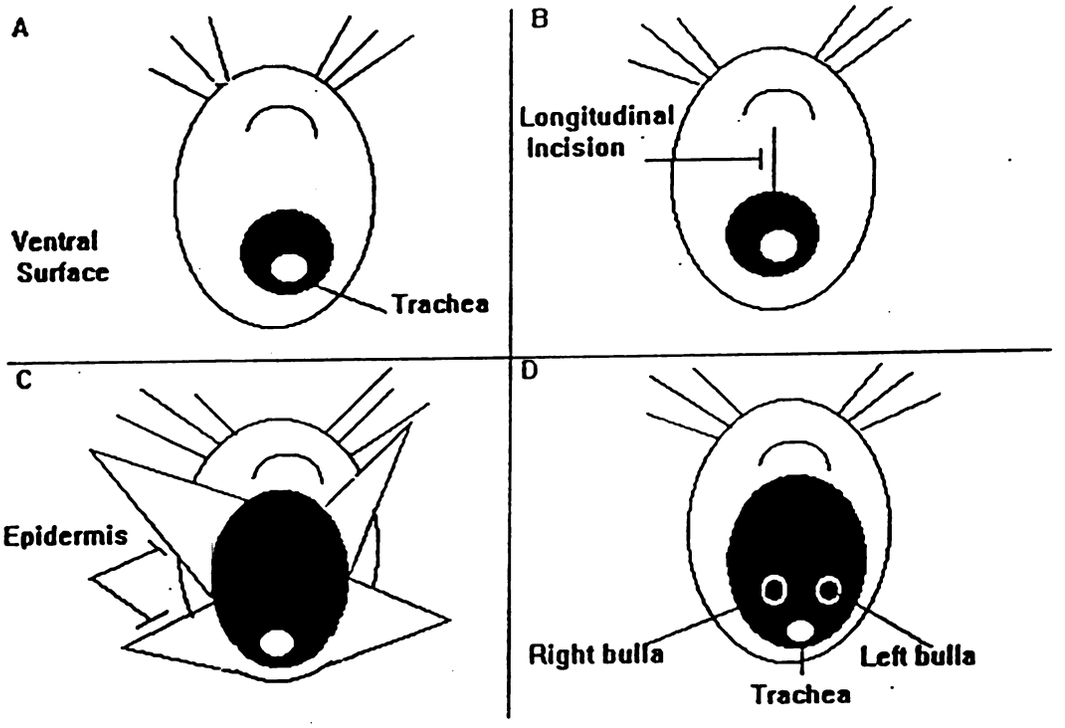

Figure III-1. Schematic illustration highlighting tissue isolation technique. (A) Ventral surface following decapitation, (B) Medial longitudinal incision, (C) Removal of outer epidermal layers, and (D) Exposure of right and left bulla.

following this procedure, the cells were centrifuged for 5 minutes at 5000 rpm. The cell suspension was rinsed twice with CMF-PBS. Following the second and final rinse, the CMF-PBS was removed and 6 - 8 drops of a mixture was added (1.5 mg Dnase, 2.5 mg $MgSO_4$, 1 ml CMF-PBS) .

3. Trituration and Plating of SGCs

The spiral ganglion tissue was triturated in order to free the neuronal ganglion into isolated SGCs. One ml of Dulbecco's Modified Eagle Medium (DMEM) (supplemented with 50 ml HAMS F-12, 50 ml heat-inactivated fetal bovine serum, 1.5 ml glutamine and 1.0 ml penicillin) was added to the centrifuge tube which contained the DNase mixture. The cell suspension was gently drawn into and out of a heat polished Pasteur pipette approximately 20 times. Pipettes having graduating internal diameters were used throughout the trituration process. The internal diameter of the first pipette was not reduced and therefore allowed the mass of tissue to pass through the lumen with ease. The passage of the SGCs into and out of the tip continued until a transparent mixture resulted in a cloudy cell suspension. A portion of the resulting cell suspension was evenly distributed over 5 to 10 collagen-coated glass cover slips (12 mm, Costar, Cambridge, MA) in a twenty four or six well cluster containing 1.0 ml of culture media. One ml of culture media was added to the remaining undissociated cells which remained within the centrifuge tube and was again triturated with a Pasteur pipette having a smaller internal diameter as compared to the first pipette. Trituration continued until a cloudy cell suspension resulted and cells were evenly distributed among the same 5 to 10 cover slips. The cell cluster was then placed in an environmentally controlled incubator

(Humidity, 95%; CO_2, 5; Temperature 34.7° C) until time for use in an experiment. Cells were typically not used earlier than two hours nor later than 24 hours after plating.

B. Electrophysiological Recording

1. Pipette Preparation

Voltage gated ionic currents were obtained using the whole cell variation of the patch clamp technique as described by Hamill et al. (1981). Suction pipettes made of borosilicate glass capillary tubes, having an internal diameter of 1 - 1.5 mm (Kimble Products, Vineland, NJ) were pulled to have resistances between 1 - 3 MΩ. To accomplish this, a vertical microelectrode puller (PP-83, Narashige, Tokyo, Japan) was used which involved two separate pulls. During the first pre-pull, a platinum-iridium heating coil was adjusted to 12 A which supplied enough current to cause the capillary to drop and reduce the diameter of the tube over a specific length (e.g., 7 - 10 mm). Ten seconds were allowed to pass between the first and second pull. Within that time period, the heating coil was repositioned approximately 3 mm in the downward direction. The setting for the current during the second pull was adjusted to 9.6 A which resulted in the final drop and consequently the breaking off of the thinned portion of the tubing, resulting in two pieces, the pipette, and a portion which was discarded. All electrodes were stored in a clean glass jar until time of use.

To smooth the rough edges present at the electrode tip as well as to improve the membrane pipette seal, the tips of the electrodes were heat polished using a microforge (Narashige, Model 9-28 Kasuya 4-Chome, Tokyo, Japan). Electrodes were placed in an electrode holder and slowly lowered until it was in close proximity to a V-shaped

platinum-iridium filament. Through the use of a hand switch, the filament was heated until an orange-red glow was produced. Slight shrinkage of the electrode tip and darkening of the tip walls indicated polishing of the electrode rim. New electrodes were pulled and subsequently heat polished daily.

2. Solutions

External and internal solutions were prepared which approximated the natural extracellular and intracellular environments and were designed to produce specific voltage-gated ionic currents. The external solution used to record both sodium and potassium currents contained (in mM): NaCl 140, KCL, 5.0, $CaCl_2$ 2.5, HEPES-Acid 5.5, HEPES-Na 4.5 and Glucose 10. Modifications to the extracellular solution are noted for specific currents. When necessary the pH was adjusted to 7.4 with NaOH. The osmolarity was maintained close to 300 mOsm at all times and was measured using an osmometer (Precision System, Model 5004, Natick, MA). In those instances where the osmolarity was too low, it was increased by the addition of sucrose. Tetrodotoxin (TTX, 0.5 μM) a known paralytic toxin and specific Na channel blocker, was used to suppress the Na^+ current.

Lead acetate was dissolved in 100 ml of distilled H_2O to create a stock solution. When performing lead studies, various concentrations of stock solution (0.1 μM, 0.3 μM 1.0 μM, and 3.0 μM 10 μM) was diluted into 100 ml of the external solution. The solution was allowed to flow for 2 minutes prior to initiating the stimulus protocol and the recording of current traces.

The internal solution used to record both sodium and potassium currents contained (in mM): KCL 140, NaCl 10, MgCl 2.0, HEPES Na 10, EGTA 2.0, and Glucose 5.0. When necessary, the pH was adjusted to 7.4 with KOH and the osmolarity was maintained at $\leq$ 20 mOsm of the external solution. All solutions were filtered prior to use to eliminate unwanted particles and/or contaminants.

The external solutions used specifically to isolate Na currents thus blocking K^+ current contained (in mM): NaCl 140, TEA-CL 25, $CaCl_2$ 2.5, HEPES-Acid 5.5 and HEPES Na 4.5. The internal solution used to isolate the Na current included (in mM): CsCl 110, NaCl 10, $MgCl_2$ 2.0, HEPES Na 10, EGTA 2.0, and Glucose 5.0. As described above, the pH was adjusted to 7.4 when necessary with 1N CsOH while the osmolarity for the external solution was maintained close to 300 mOsm. All experiments were conducted at room temperature of between 22 - 25° C.

3. Sealing Procedures

In order to fill the tip of the microelectrode, it was placed in a 1.5 ml Eppendorf tube that contained internal solution. The solution was drawn into the tip of the electrode by a syringe which was attached to the opposite end. The remaining body of internal fluid was inserted by backfilling with a fine tipped plastic syringe. The microelectrode was placed in the Axopatch system's electrode holder and mounted into the Axopatch 201 CV headstage (Axon Instruments, Foster City, California). Gross manipulations were used to position the electrode into the bath. Positive pressure was applied to the electrode as the electrode broke the surface of the external fluid and entered the bath. This positive pressure was used to remove or prevent debris from interfering with obtaining a gigaohm

seal between the surface of the plasmalemma and the electrode tip. Once the electrode tip was placed in the external bath, adjustments were made using the micromanipulator until the pipette tip was positioned over the center of the cell. The resistance, created when the electrode enters the bath increases once the tip of the electrode touches the surface of the cell membrane (See Figure III-2). Once contact had been made between the tip of the electrode and the cell membrane, slight negative pressure was used to form a tight gigaohm seal (Hamill et al.,1981). According to Hamill et al. (1981), the high resistance of a gigaohm seal helps to reduce background noise and ensures that most of the ionic current originating in a small membrane patch flows into the pipette and from there into the current measurement circuitry. In order to eliminate the residual transient resulting from the electrode capacitance after obtaining a gigaohm seal, adjustments were made using the electrode capacitance compensation, fast tau control and fast magnification control. In some instances, however, the transient was not adjusted in order to conserve time. After reducing the capacitive transients, sharp negative pressure was applied to rupture the cell membrane. This would then allow the internal solution to mix with the cell's interior creating a continuous electrical circuit between the pipette and whole cell membrane (Roy, 1992). Further adjustments were made to reduce the capacitive transients created by the rupture of the cell.

With the exception of a few cells, the majority of the cells were held at a holding potential of -80 mV. After obtaining a successful patch-clamp and membrane rupture, a depolarizing voltage step protocol from -100 mV to +80 mV was introduced to the cell.

Patch-clamp Recording Configuration

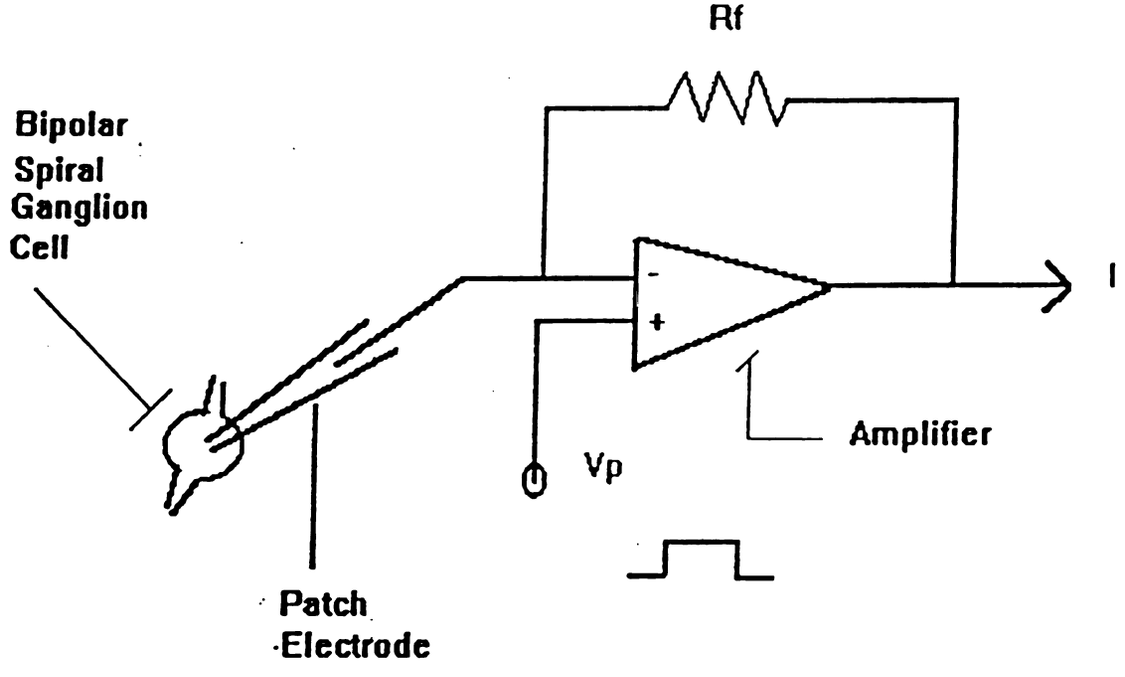

Figure III-2. Patch-clamp recording configuration. The amplifier is used as a current to voltage converter. The pipette voltage (Vp) is clamped by the voltage command signal and maintains agreement between the voltage across the membrane and the designated potential (Roy, 1992).

Electrical Recording

The whole-cell variation of the patch clamp technique was used to record ionic currents under voltage-clamp conditions (Hamill et al.,1981). Suction pipettes made of borosilicate glass capillary tubes (0.8 - 1.1 mm i.d., Kimble Products, Vineland, NJ) were pulled to have resistances between 1 - 3 MΩ. Inverted voltage clamp command pulses were applied through the pipette and a pellet/3.0 M KCL-agar bridge was used as a reference electrode. Membrane currents passing through the pipette were recorded by a current-to-voltage converter consisting of a 500 MΩ feedback resistor and an amplifier (Axopatch 1B, Axon Instruments, Burlingam, CA). Data were stored on disks using a computer (PDP 11/73, Digital Equipment Corp., Maynard, MA)/micro-computer (Zenith Z-466x+, St. Joseph, MI) patch-clamp work station. Leakage and capacitive currents were digitally subtracted using the P + P/4 protocol (Bezanilla and Armstrong, 1977). Currents were sampled at a rate of 2 - 50 K Hz with a 14 bit A/D converter and filtered with a 8-pole Bessell filter from DC - 5 K Hz. Figure III-3 is a schematic design illustrating the complete research work space.

Laboratory Work Space

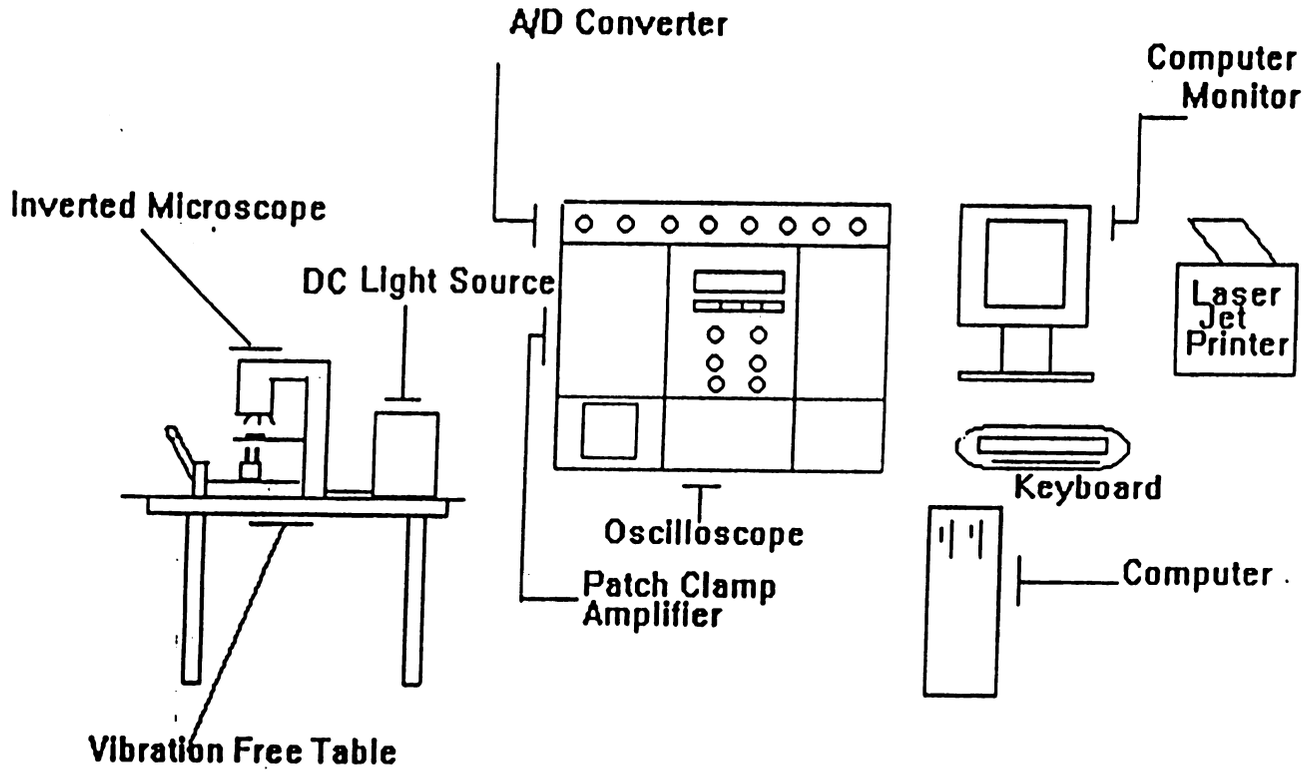

Figure III-3. Schematic illustrating complete research work space including rig, Axopatch system and computer system.

(

(

(

(

(S

ob

et

use

dur

dep

wer

mV

reco

CHAPTER IV

RESULTS

The following research questions were proposed and serve as the focus of the results that follow.

(1) Are sodium channels and potassium channels present in embryonic rat SGCs?

(2) Do postnatal (P2 - P9) SGCs exhibit TTX-S and TTX-R sodium currents?

(3) Are there differences in the kinetics of activation and inactivation of sodium currents between embryonic and postnatal SGCs?

(4) Are there changes in the current amplitude and gating characteristics of SGCs in the presence of externally applied Pb^{2+}?

(5) Do postnatal (P2-P9) SGCs exhibit delayed rectifying outward-currents?

In order to answer the questions listed above, sodium and potassium currents were obtained using a variation of the whole-cell voltage-gated patch clamp technique (Hamill et al., 1981). The patch-clamp technique is an electrophysiological recording method used to study the kinetics of various whole-cell and single-cell membrane ionic currents during pharmacological studies. The protocols used for this study consisted of depolarizing step commands lasting 10 ms or 20 ms in duration. The command pulses were applied in 10 mV steps from various holding potentials (e.g., -70 mV, -80 mV, -100 mV) which are indicated (see Figure IV-1). The protocol in Figure IV-1 was used to record from both embryonic and postnatal rat SGCs. The data obtained represents

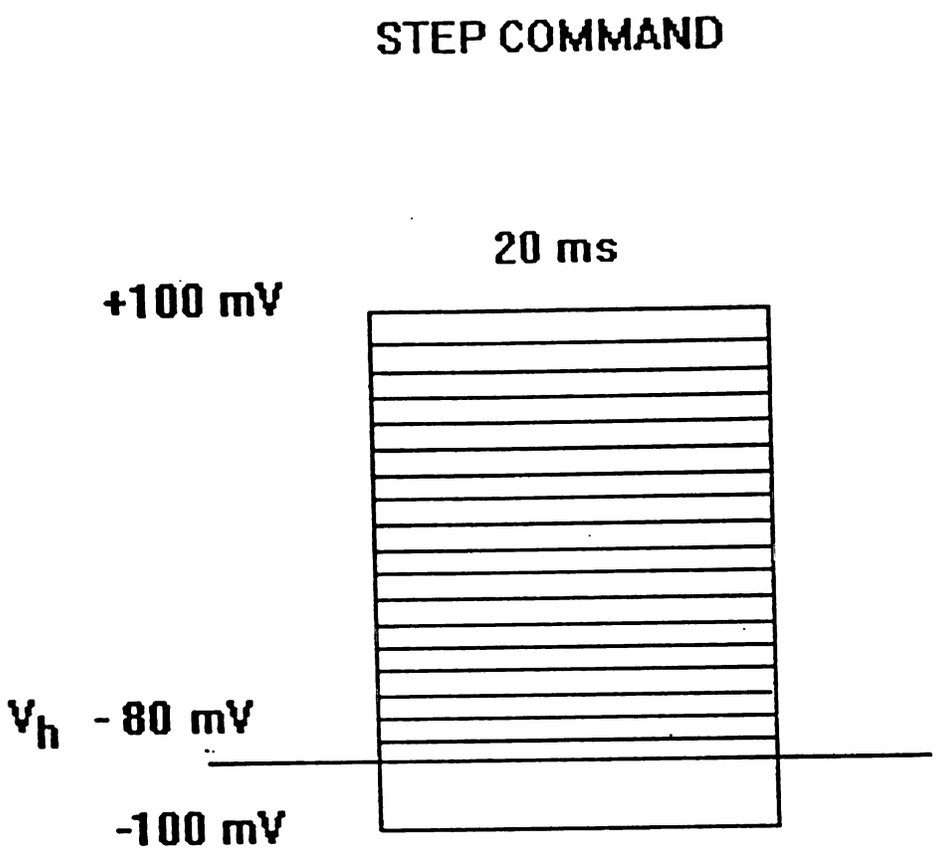

Figure IV-1. Pulse protocol used during voltage-gated patch-clamp embryonic and postnatal studies. Controlled recordings were obtained using 10 ms or 20 ms voltage commands stepped from -80 mV to +80 mV in 10 mV steps, with the exception of the first command step, which was hyperpolarized to -20 mV. Cells typically were held at a holding potential of -80 mV.

normal ionic channel activity in the absence of specific channel blockers as well as ionic channel activity in the presence of known channel blockers.

Immunocytochemistry

To identify spiral ganglion neuronal cell bodies, immunocytochemical studies were conducted which included both toluidine blue staining and labelled streptavidin-biotin (LSAB) techniques. These studies were completed using postnatal SGCs and showed specific staining of cell bodies. Type I SGCs stained with toluidine blue showed the characteristic darker-staining cytoplasm and lighter staining nucleoplasm. The LSAB studies produced specific binding of antigens which were evident by the intense staining of dissociated cell bodies. Both studies clearly identified the SGCs as bipolar spherical cells. In some instances, the perikaryon was oval while the majority of cells were spherical

Q1: Are sodium channels and potassium channels present in embryonic rat SGCs?

Description of embryonic spiral ganglion cells

Figure IV-2 shows a histogram representative of the cross-sectional cell diameter of seventy two acutely dissociated embryonic rat SGCs at one day in culture. Cell cultures typically produced a high yield of cells which appeared healthy based on their smooth somatic surface and lack of granularity. The cross-sectional diameter of embryonic SGC was variable and ranged between 9.5 μm and 16.25 μm. SGCs appeared to show the greatest variability at E17, exhibiting cells with cross-sectional diameters as small as 9.5

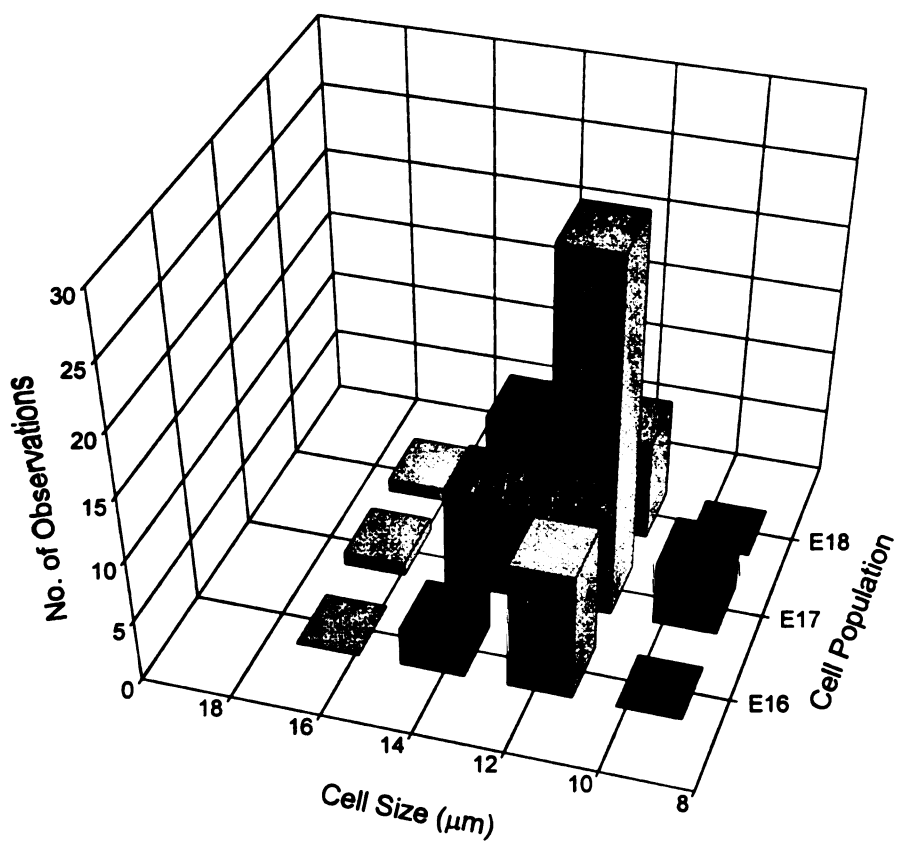

Figure IV-2. Histogram showing the distribution in cell size diameter in three embryonic populations (E16, E17, E18)

μm to cells having cross-sectional diameters as large as 16.62 μm. The average cross-sectional diameter of an E17 SGC was 12.15 μm. The average cross-sectional diameter of an E16 SGC was 12.41 μm. E16 SGCs were fewer in number and also showed variability in cell size diameter. Spiral ganglion cells cultured from E18 rat pups were larger and had very few cells with cross-sectional diameters equal to or less than 9.5 μm. The average cross-sectional diameter of an E18 SGC was 13.27 μm.

The perikaryon of the embryonic SGCs appeared spherical when viewing cells positioned beneath a phase contrast microscope. The cell surface was concave and at times made it difficult to secure a gigaohm seal due to the drift of the electrode across the surface of the cell membrane. The movement of the electrode across the cell membrane ("electrode drift") could, at times, be minimized by making various adjustments to the equipment in order to stabilize the electrode drift. The majority of the SGCs were bipolar which was evident by neurite outgrowth at either pole. Neurite extensions could be seen projecting from the cell body as early as four hours during cell culture

Figure IV-3A exhibits the plasmalemma of a single embryonic spiral ganglion neuron. There are a few neurons of equal or smaller size located in the upper left section of the panel. Axons within the peripheral nervous system of mammals are covered by layers of myelin sheath. This lipid-rich material is produced by Schwann cells and functions to assist in conducting neural signals rapidly along the length of the axon. When viewing the SGCs under the microscope, darker outer concentric rings could be

Figure IV-3A. Single embryonic (E18) spiral ganglion neurons at one day in culture.

Figure IV-3B. Undissociated embryonic (E18) spiral ganglion cell at one day in culture

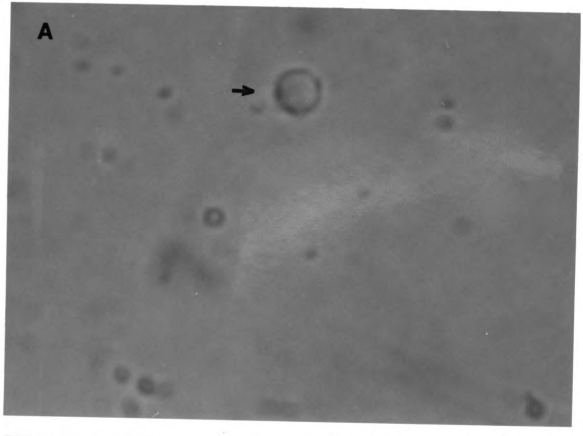
A

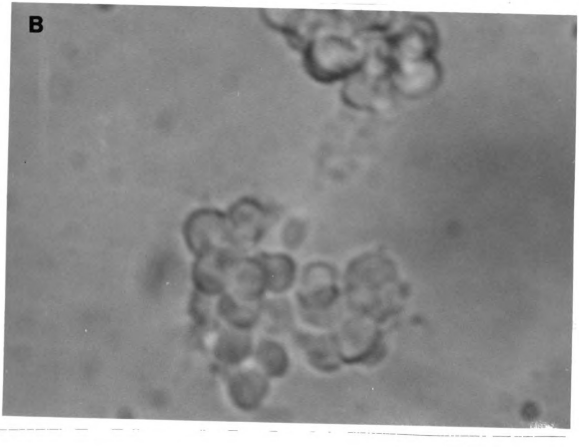
B

seen toward the periphery of most cells. These rings comprise the layers of loose myelin which characteristically surround most type I SGCs. The myelin sheath surrounding the cultured SGCs did not always shed from the cell body during the incubation process. The presence of myelin during the embryonic stage of development offers further support to suggest that several underlying mechanisms responsible for delivering auditory information from the periphery to the central nervous system are in place at this stage of development (E18).

During cell culture, masses of ganglia were dissociated into isolated ganglion via Pasteur pipettes. On occasion, however, SGCs did not always dissociate completely although gentle trituration was employed. These undissociated cells remained cohesively attached as clusters of cell bodies (Figure IV-3B) and were not subsequently influenced by the separation of neighboring ganglions. Morphological preservation was maintained and there were no visible signs of cell death. Longevity of the clusters appeared to be consistent with that of the isolated SGCs. Although these clusters were sustained, they were not used in the present investigation to record membrane ionic currents.

Isolation of voltage-gated ionic currents of embryonic spiral ganglion cells

In the absence of specific channel blockers, embryonic (E17 - E18) rat SGCs possessed functional voltage-gated ionic channels. Figure IV-4A illustrates a family of both inward-directed Na^+ currents and outward-directed K^+ currents from an E18 spiral ganglion neuron with a cross-sectional diameter of 14.25 μm. Depolarizing step pulses with a duration of 10 ms were applied in 10 mV steps from a holding potential of -80 mV

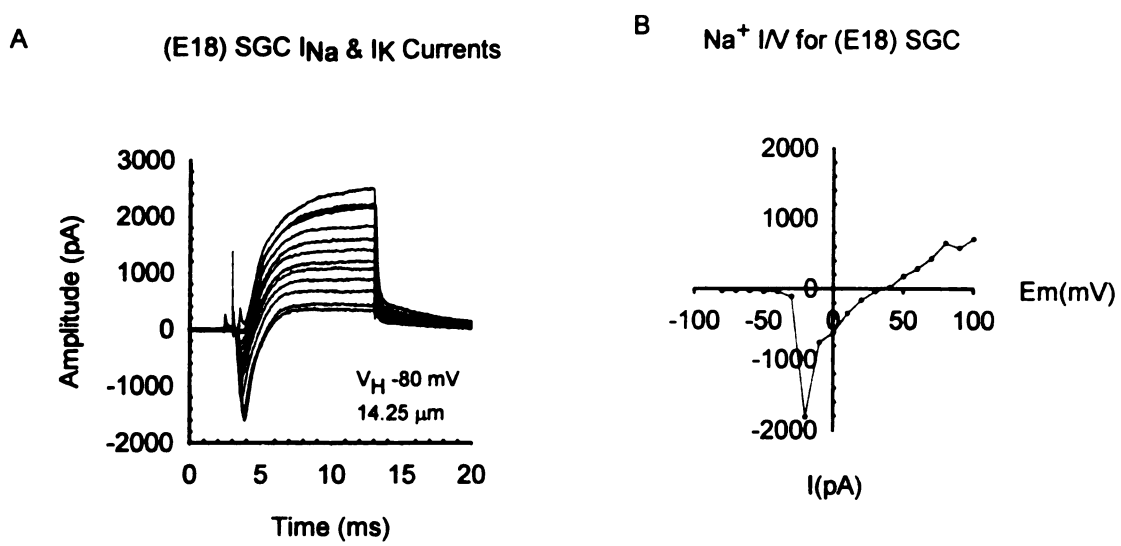

Figure IV-4A. Family of embryonic sodium currents and potassium currents.

Figure IV-4B. Current-voltage (I/V) relationship for embryonic peak sodium currents for Figure IV-4A.

to +100 mV. Peak sodium currents activated and inactivated rapidly and were followed by delayed rectifying potassium currents. Peak sodium current for this embryonic SGC did not exceed 1500 pA. The current-voltage (I/V) relationship for peak sodium current is depicted in Figure IV-4B. Channel activation occurred at a membrane potential more positive than -40 mV. The reversal potential for the peak sodium current occurred close to +40 mV.

Embryonic peak sodium currents were generally small, on the order of 1500 pA or less (n = 5). Cell diameter was not a reliable indicator of peak current magnitude. Figure IV-5A illustrates a single membrane ionic current generated from an E17 SGC in response to a depolarizing voltage step command. The cross-sectional diameter was 14.25 μm, the most frequently observed cell size for postnatal SGCs. The peak sodium current for this particular cell reached -539 pA. Outward-directed currents generated by potassium channels were always present regardless of the presence or absence of sodium currents for both embryonic and postnatal SGCs. Embryonic potassium currents were uncharacteristically small. Figure IV-5A shows a very small outward-directed potassium current in the absence of any specific channel blockers.

Figure IV-5B shows a current generated from a different SGC from the same rat pup. The cross-sectional diameter of this cell measured 11.87 μm. Using the same protocol described above, the peak sodium current generated by this cell measured -1039 pA and comparatively, produced a noticeably larger current in response to a 10 ms depolarizing command stepped to +10 mV. The outward-going potassium current

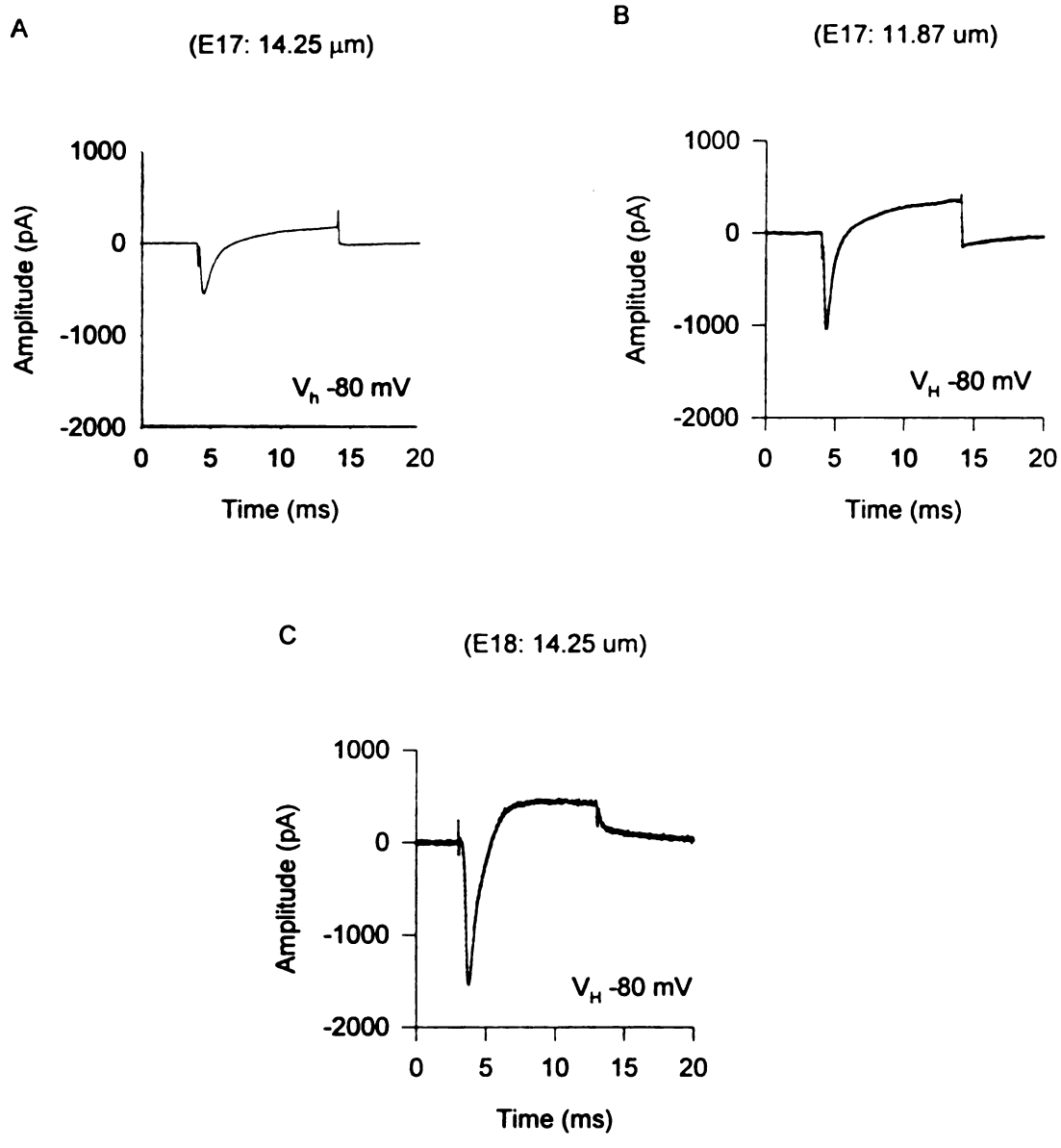

Figure IV-5. Single embryonic current traces showing variability in peak current magnitudes (irrespective) of cell size. (A) E17, 14.25 μm; (B) E17, 11.87 μm; (C) E18, 14.25 μm.

generated by this cell was also noticeably larger than the potassium current observed in the larger cell.

The peak sodium current observed for an E18 SGC approached 1500 pA (Figure IV-5C) showing an even larger current magnitude than either of those observed for the E17 SGCs in (Figures. IV-5A and IV-5B). The cell size diameter was 14.25 mm. The potassium current did not show any significant changes in magnitude when compared to currents generated by E17 SGCs (Figure IV-5A and 5B).

These data clearly show that embryonic SGCs possess functional inward directed sodium currents as early as E17. Likewise, outward-directed potassium currents are present also in these neurons. Cell size diameter, however, is not a reliable indicator for sodium peak magnitude nor potassium peak magnitude, although both peak sodium current and potassium current magnitudes exhibited an increase with maturation.

Q2: Do postnatal (P2 – P9) SGCs exhibit TTX-S and TTX-R sodium currents?

Description of postnatal spiral ganglion cells

At one day in culture, postnatal SGCs were either spherical or oval in shape. Following a five hour incubation time-period, neurite extensions could be found extending from either pole of the cell, giving these sensory neurons their characteristic bipolar classification. Similar to the embryonic SGCs, postnatal type I SGCs showed also signs of myelination which was evidenced by the presence of an outer layer of myelin which appeared as a shadow around the periphery of the cell.

In order to systematically study the development of membrane ionic currents exhibited by SGCs, postnatal cells were divided into three developmental stages: early (P2-P4); intermediate (P5-P7) and differentiated (P8-and older). Early SGCs (P1 - P4) showed the same rapid transient activity as the embryonic SGCs, showing fast activation and inactivation kinetics (See Figure IV-6A and 6B). Non-inactivating currents were not observed for any of the cells tested. Peak current magnitudes remained small for both sodium currents and potassium currents when compared to older SGCs. Thus, minimal maturational changes were observed between embryonic SGCs and P1 SGCs. P3 SGCs, on the average, had larger cross-sectional diameters and were found to have larger sodium and potassium currents (n = 5) as compared to P1 SGCs.

Intermediate SGCs (P5 - P7) showed obvious changes in current magnitude. What is clearly evident among the SGCs during this stage of development is the variability in peak sodium current irrespective of cell-size diameter. Figure IV-7A illustrates the results of P5 spiral ganglion cell. When compared to embryonic and early (P1 - P3) neurons, a significant increase in peak sodium current magnitude is noted. Figure IV-7B shows two separate currents generated by SGCs obtained from two different rat pups (P6). The cells were clamped to the same holding potential of -80 mV, but had different cell size diameters. The peak sodium current for the larger SGC was significantly smaller, once again showing the variability in peak sodium current among cells at the same developmental stage. Figure IV-7C shows two single current traces generated by two different SGCs obtained from two different older (P7) rat pups. The

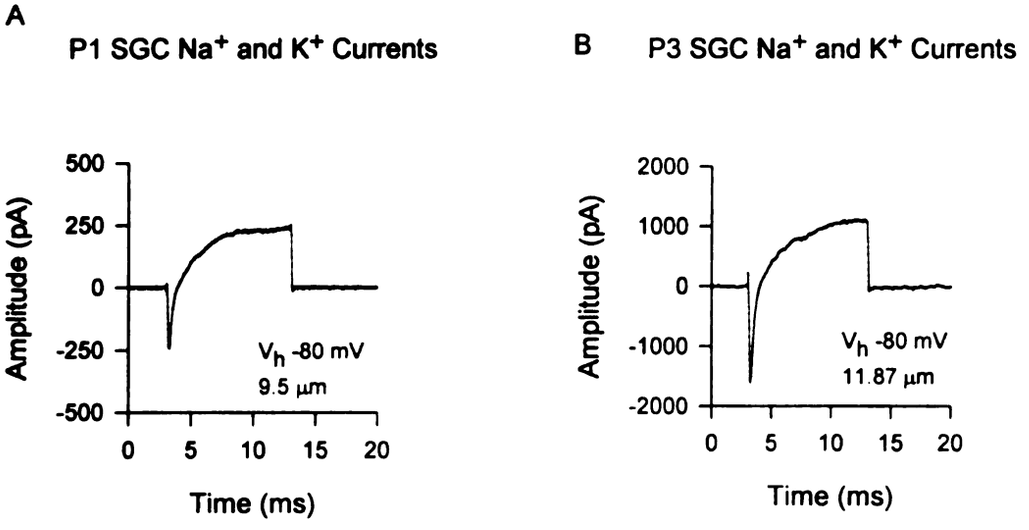

Figure IV-6. Single membrane ionic currents produced by early (P2 and P4) postnatal SGCs.

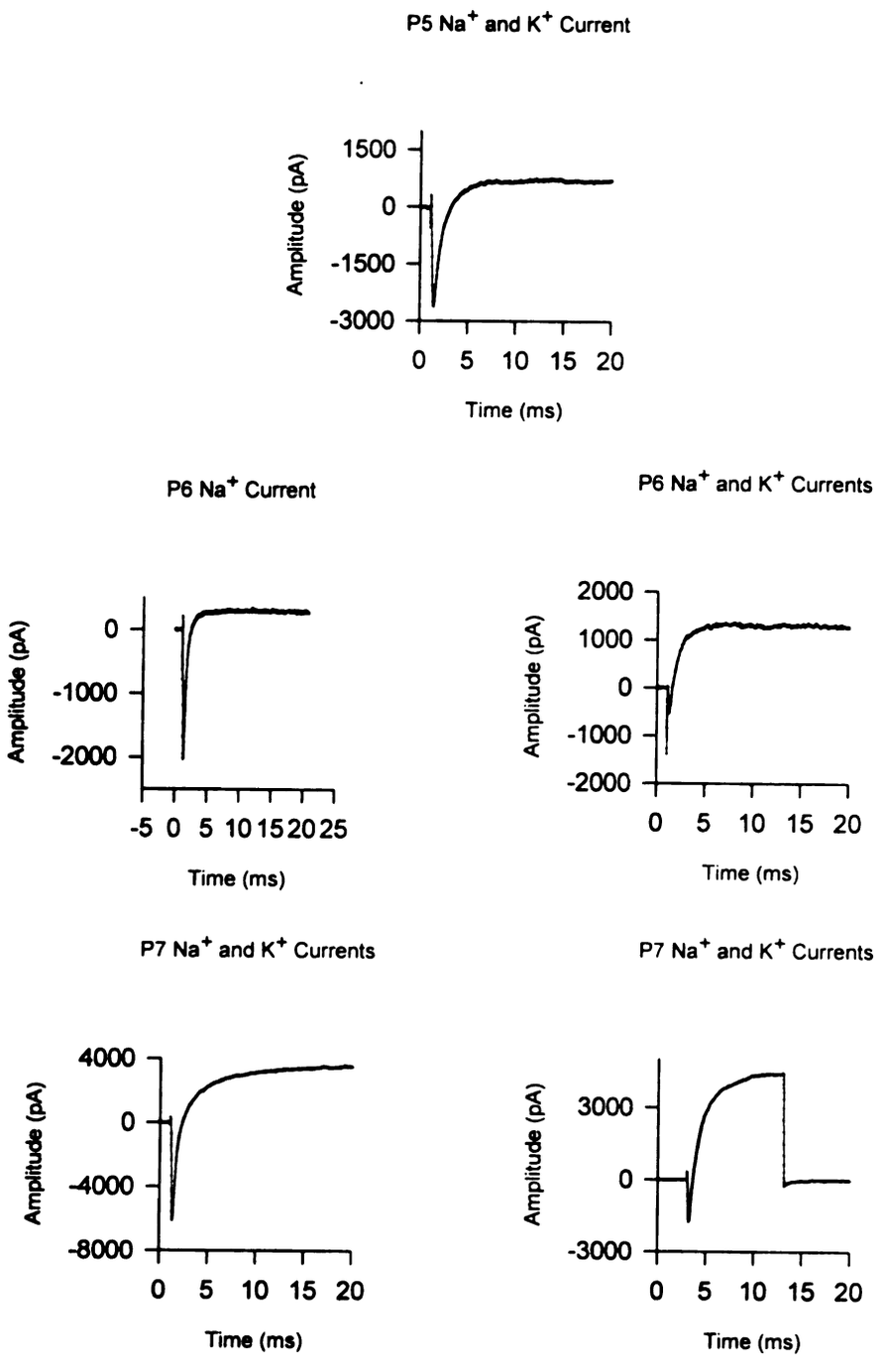

Figure IV-7. Single membrane ionic currents produced by intermediate P5 - P7 postnatal SGCs.

sodium currents generated by the larger SGC had a magnitude which was larger than the peak sodium current generated by the smaller SGC.

Mature SGCs are comprised of two cell types, type I and type II. The differentiation between the two cell types does not occur until P8. After this period, type I SGCs can be differentiated from type II SGCs, typically by their cell size and cytoplasmic content. Figure IV-8A shows a single membrane ionic current generated by a P8 SGC. Activation and inactivation kinetics were rapid (and did not change significantly from rates observed in younger cells). The rate of activation for the inward directed sodium current was 0.4 ms. Fig IV-8B shows a family of membrane ionic currents generated by the same cell. Peak sodium current approached -4657 pA. Both inward-directed and outward-directed membrane ionic currents were generated following a 20 ms depolarizing step command. The cell was stepped by 10 mV commands to +80 mV from a holding potential of -80 mV. Figure IV-8C depicts the current/voltage relationship for this cell. Mature type I SGCs activated at potentials more positive than -50 mV. The reversal potential occurred close to +30 mV.

Figure IV-9A shows a single current generated by a cell having a large cross-sectional diameter of 23.7 μm. The magnitude of the inward peak sodium current approached -8000 pA. Figure IV-9B shows ionic currents produced by a P9 SGC with a smaller cross-sectional diameter. The peak sodium current approached -2000 pA. Once again, however, the peak sodium current observed in the older (P9) SGC with a smaller cross sectional diameter generated a smaller sodium current.

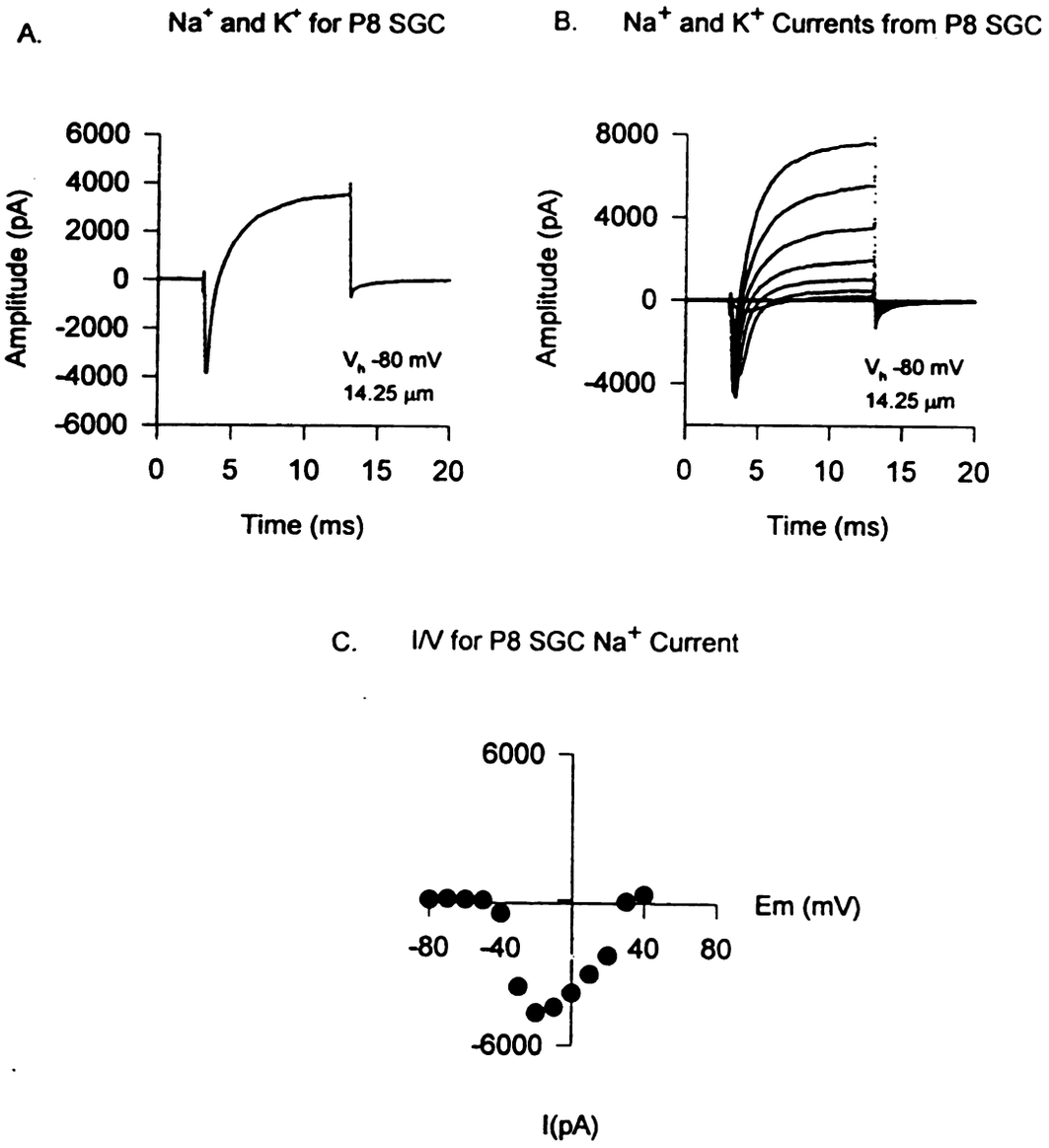

Figure IV-8. (A) Single current, (B) Family of currents and (C) Current-voltage plot generated for a mature type I SGC.

A.

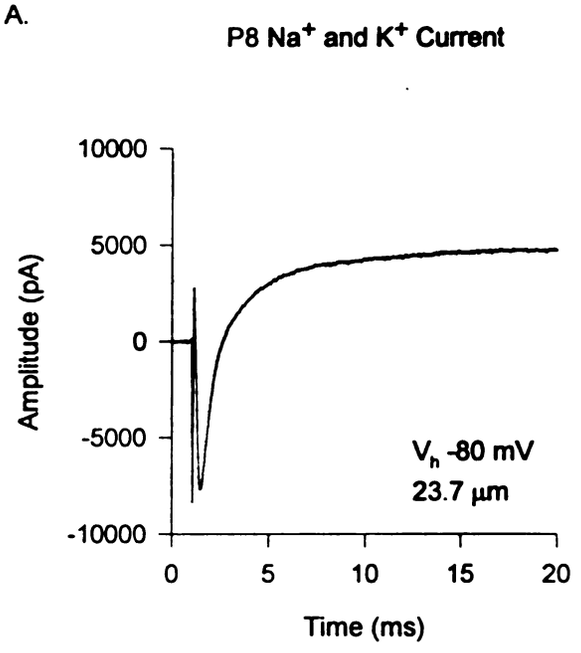

B.

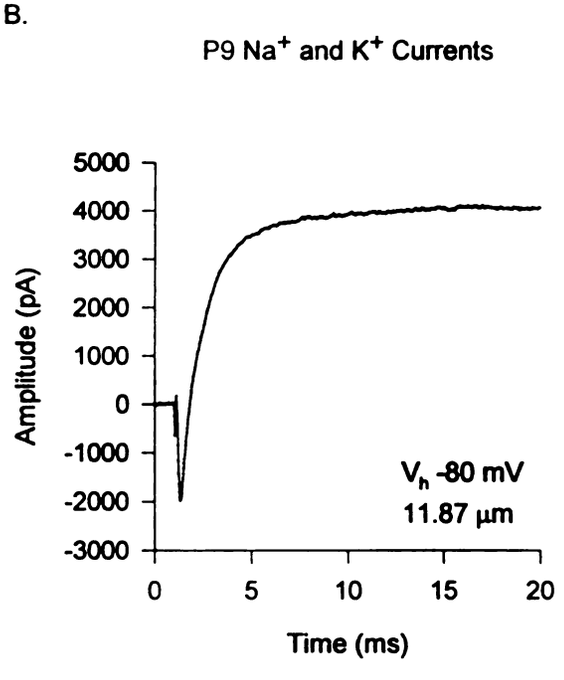

Figure IV-9. Single membrane ionic currents generated by differentiated (P8) and (P9) type I SGCs.

Responses of sodium channels to TTX

Figure IV-10A depicts a family of membrane ionic currents generated in the presence of one-half sodium (70 mM NaCl) and 68.4 mM TMA applied externally. A solution of 110 mM CsCl was introduced to the internal cytoplasm through the pipette. The cell was held at a holding potential of -90 mV. Depolarizing 10 mV step commands with a duration of 20 ms were delivered to the cell. Sodium currents activated at potentials more positive than -50 mV (I/V curve not shown). The reversal potential for this cell occurred at +30 mV. Note that the outward-going potassium current, which is typically very robust, is suppressed in the presence of externally applied (68.4 mM) TMA and internally applied (110 mM) CsCl. In the presence of 0.5 μM TTX, the sodium current generated from a P6 SGC was blocked (Figure IV-10B). The potassium current was not affected by the presence of externally applied TTX, but remained suppressed. The blockage of the sodium current in the presence of externally applied TTX, a known sodium channel blocker, suggests the presence of a TTX-sensitive sodium current.

In all of the TTX experiments conducted, there were no instances where the sodium current remained in the presence of TTX, thus, rendering cells TTX-resistive. Following a two minute rinse, the sodium currents returned to 50% of the initial current magnitude (Figure IV-10C) and thus, the blocking effects of the TTX was reversible. The currents activated at potentials more positive than -50 mV and the reversal potential was maintained at +30 mV. When the holding potential was increased to -100 mV (Figure IV-10D), the inward directed sodium currents increased in magnitude.

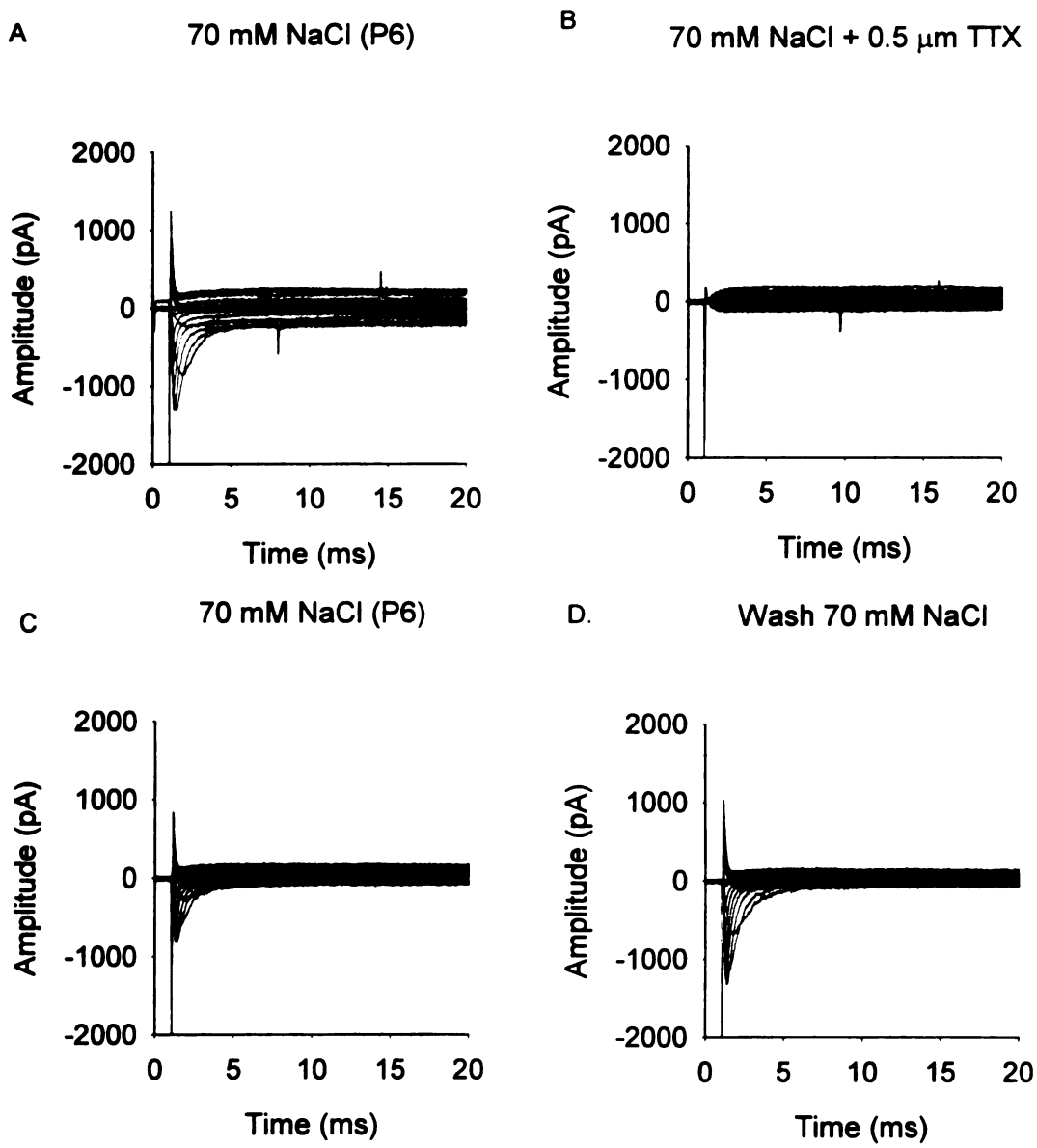

Figure IV-10. TTX study of a P6 SGC. (A) Family of inward-directed sodium current and suppressed outward-directed potassium currents. (B) Inward-directed sodium currents shown above blocked in the presence of 0.5 μM TTX. (C) Return of sodium current following rinse with normal solution. (D) Increase of peak sodium current following - 10 mV hyperpolarization of holding potential.

Figure IV-11A illustrates a family of ionic currents generated from a type I SGC of a P9 rat. The cell diameter was14.25 μm. From a holding potential of -80 mV, a series of 10 mV depolarizing commands were stepped from -100 to +80 mV. The duration of the voltage-gated pulse was 20 ms. In the presence of the following external solution [(in mM) 140 NaCl, 5 KCl, 2.5 CaCl, 10 Glucose, 5.5 HEPES Acid, and 4.5 HEPES Na+] and internal solution [(in mM) 140 KCl, 10 NaCl, 2 MgCl2, 10 HEPES Na, 2 EGTA 5 Glucose], inward-directed sodium currents and outward-directed potassium currents were generated. Inward-directed sodium currents activated and inactivated rapidly. Outward directed potassium currents were consistent with the currents generated by delayed rectifying potassium channels. In the presence of 0.5 μM of TTX , applied externally, the inward directed sodium current was abolished (Figure IV-11B).

Unknown Inward Voltage-Gated Currents

Currents which were initially thought to be possible leak currents appeared frequently following initiation of the test protocol. These currents would only activate following the onset of the depolarizing test stimulus and would remain activated throughout the duration of the test pulse. Thus, the currents appeared as non-inactivating inward-directed voltage-gated currents. Figure IV-12 A-C shows a family of non-inactivating inward-directed voltage-gated currents from the same cell. The cell size diameter was 14.25 μm. Three successive episodes are shown. Cells were bathed in the standard solutions where the main charge carriers consisted of 140 mM NaCl in the external solution and 140 mM KCl in the internal solutions.

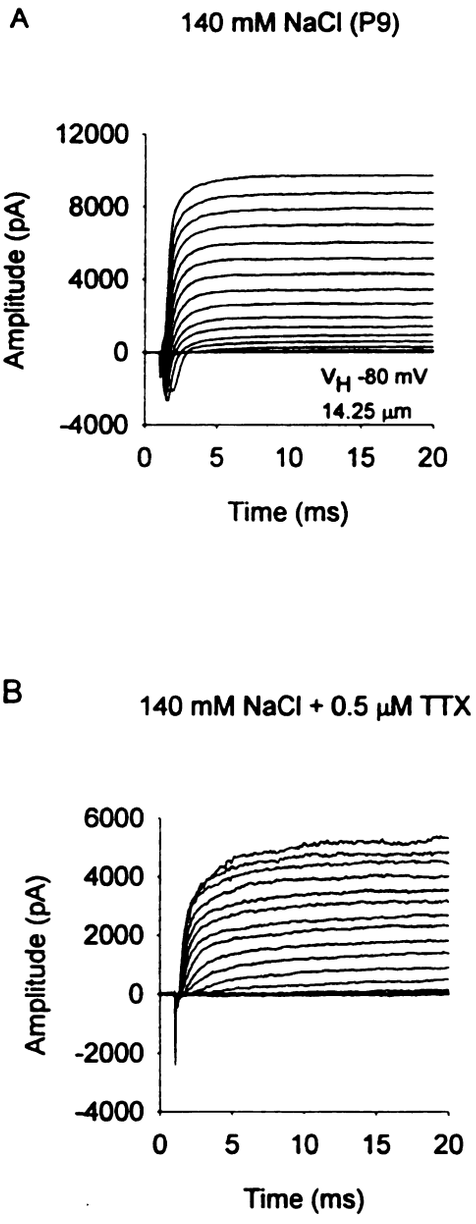

Figure IV-11 TTX study of a P9 SGC. (A) Family of membrane ionic currents in presence of 140 mM NaCl. (B) Blocked sodium current in the presence of 0.5 µM TTX.

Non-inactivating Inward-Directed Current (P5)

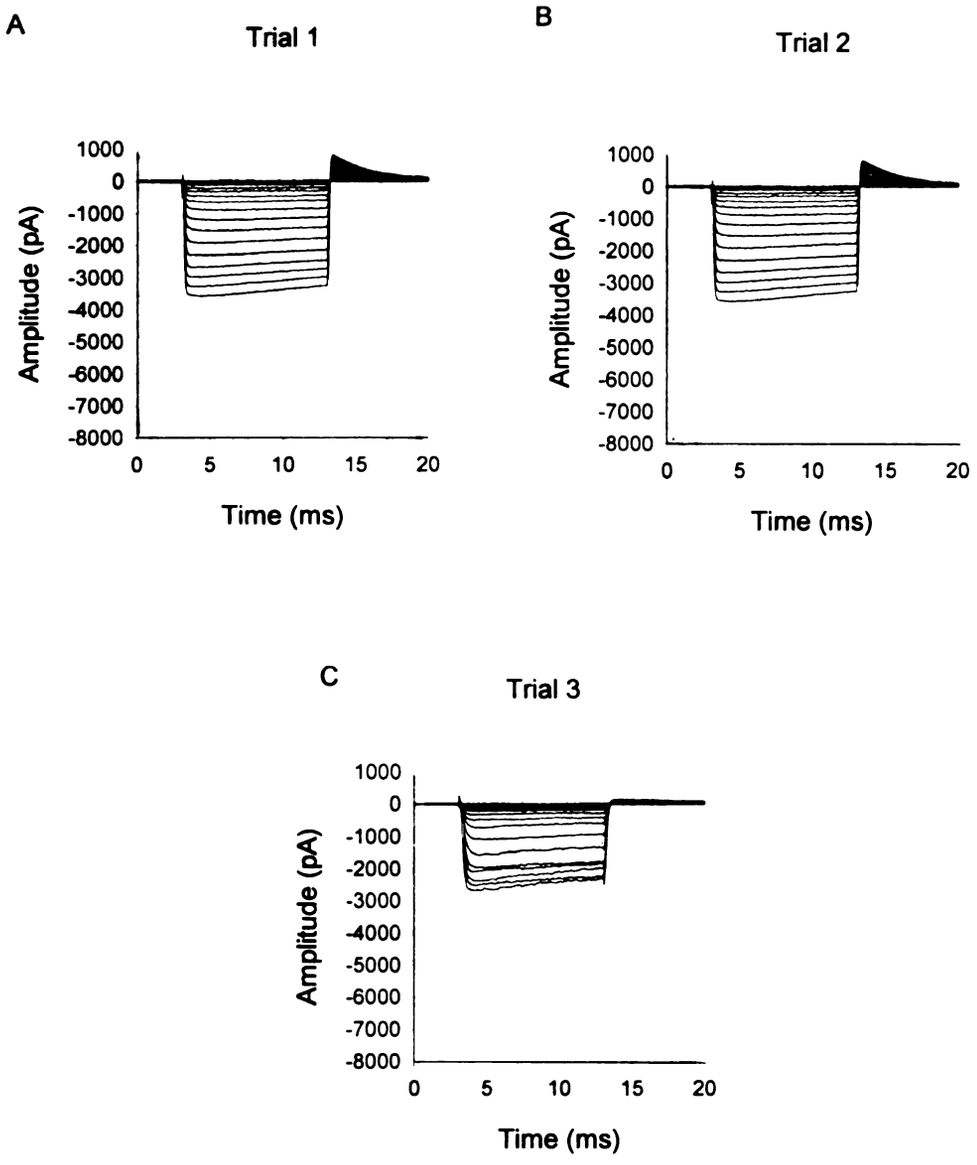

Figure IV-12. Unidentified inward-directed voltage-gated current.
(A) Initial response to 10 ms depolarizing test pulses.
(B) Second response to 10 ms depolarizing test pulses.
(C) Third response to 10 ms depolarizing test pulses.

A P5 SGC produced a current also with the same kinetic characteristics shown in Fig IV-12A, showing rapid activation following the onset of a depolarizing test pulse and slow to no inactivation throughout the duration of the test pulse (Figure IV-13A). Peak current magnitudes approached -1500 pA. Figure IV- 13B produced the same type of response following re-initiation of the test protocol. In the presence of externally applied TTX (0.5 μM) the inward current was abolished. The SGC was exposed to TTX for one minute prior to introducing the test protocol for a second trial. Non-inactivating currents returned following a two minute wash with 140 NaCl. Currents did not, however, recover completely.

Figure IV-14A depicts a family of non-inactivating inward-directed currents generated by a P9 SGC. Cell diameter measured 11.87 μm. Following a 10 ms depolarizing voltage command, non-inactivating currents appeared and remained activated throughout the duration of the test pulse. Tail currents are shown which indicate re-opening of the channels. In the presence of 1.0 μM Pb^{2+} (Figure IV-14B) applied externally for two minutes prior to initiating a depolarizing step command, the previously viewed inward-directed current was predominantly abolished. Following a two minute wash using normal (140 mM NaCl) solution, a noisy non-inactivating current returned suggesting a reversible effect in the presence of 1.0 μM Pb^{2+} (Figure IV-14C).

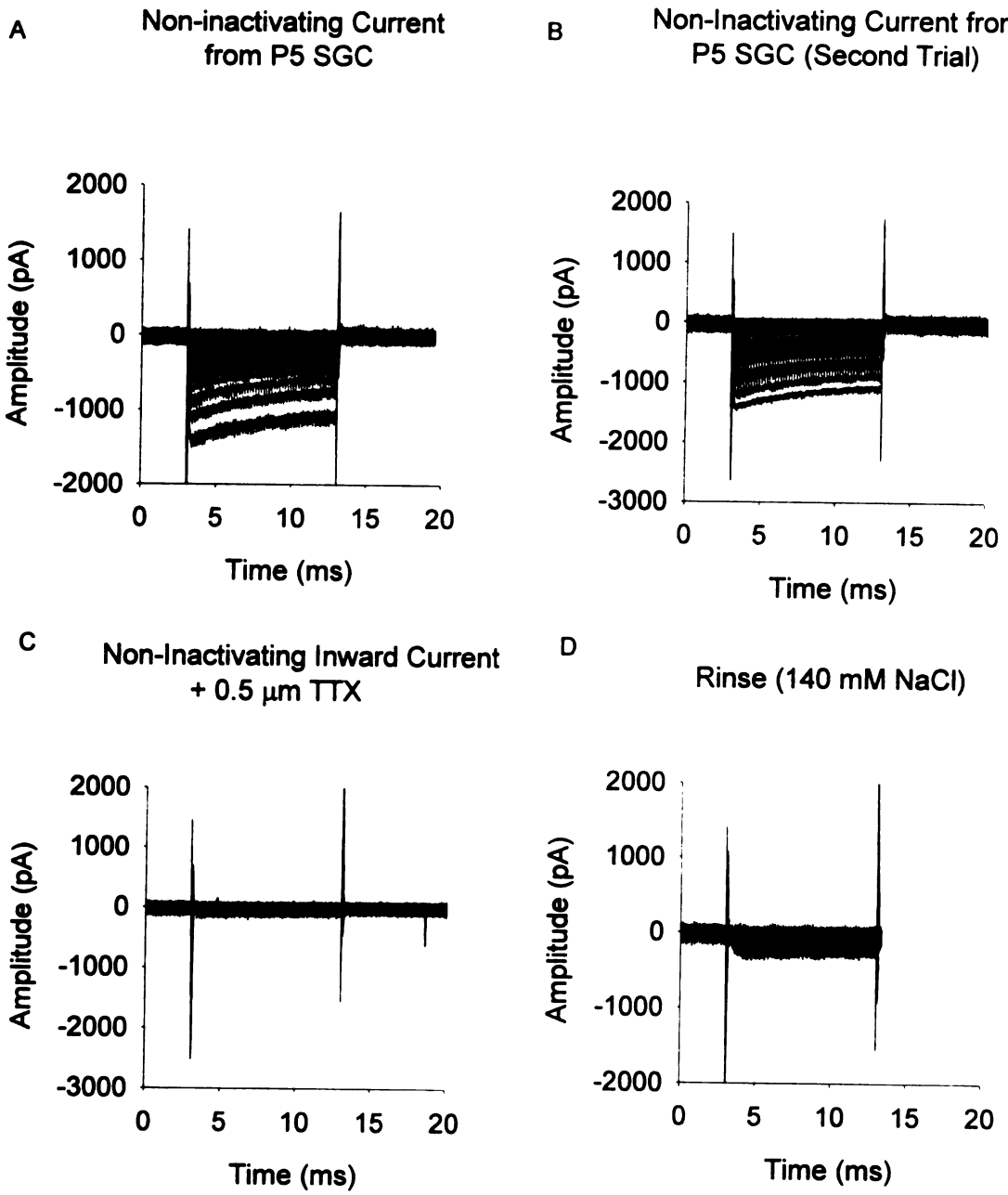

Figure IV-13. Non-inactivated current produced by a P5 SGC. (A) Initial trial in absence of specific channel blockers. (B) Second trial in the absence of specific channel blockers. (C) Abolished inward current in presence of 0.5 μM TTX.

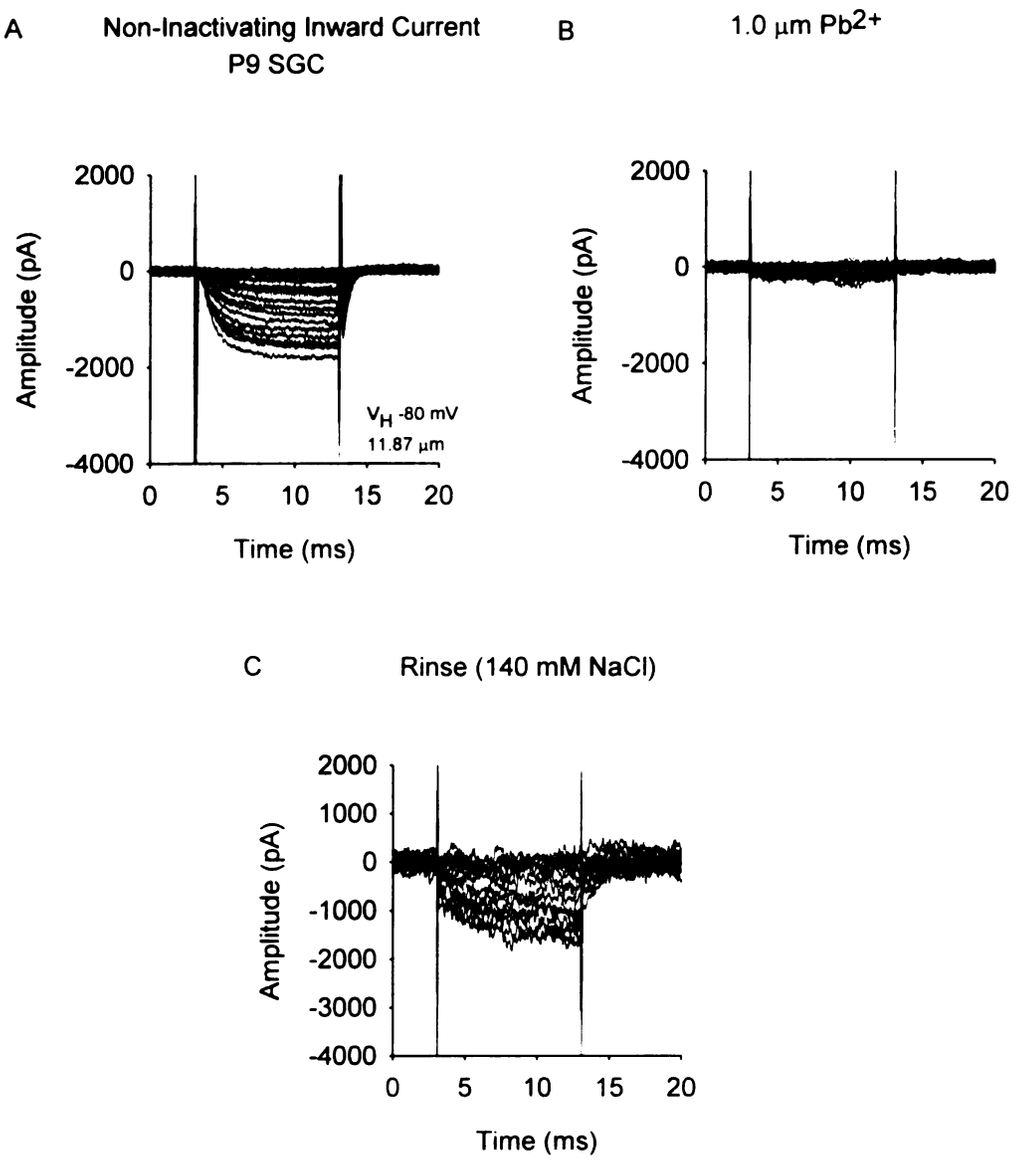

Figure IV-14. Non-inactivating inward-directed current produced by a P9 SGC. (A) Family of inward-directed non-inactivating currents in response to 10 ms depolarizing voltage step command. (B) Blockage of currents by 1.0 μM Pb^{2+} seen in Fig. IV-15A. (C) Noisy reversible inward-directed current following rinse with normal solution (140 mM NaCl).

Q3: Are there differences in the kinetics of activation and inactivation of sodium currents between embryonic and postnatal SGCs?

The characteristics of membrane ionic currents are often described by their rates of activation, inactivation and recovery from inactivation. Depolarization has two effects on the sodium current: activation and inactivation. Activation is the point where there is an increase in the conductance of the sodium current from a point of rest. Inactivation develops more slowly and results from the closing (or turning off) of sodium channels.

Activation of SGCs

Table I shows the rate of activation for embryonic SGCs and postnatal SGCs. Measures were taken from the point of onset to the peak sodium current. Overall, embryonic SGCs revealed longer activation rates when compared to the activation rates of postnatal SGCs. Activation rates decreased while peak sodium current amplitudes increased among postnatal SGCs.

Steady-state Inactivation of SGCs

Steady-state inactivation of the sodium channel was measured from three postnatal SGCs. Potassium currents were suppressed by application of 25 mM TEA-Cl. A protocol implementing depolarizing prepulses were used to study steady-state inactivation. Following 1 s pre-pulses to various potentials in 10 mV steps, sodium currents were generated by depolarizing pulses to 0 mV. Figure IV-15 shows peak sodium current amplitudes plotted as a function of pre-pulse potentials. Test pulses were normalized to the maximal value at -100 mV. The data are fitted with curves calculated

TABLE I

Rates of Activation for Embryonic and Postnatal SGCs

Age	Cell Size (μm)	Onset (ms)	Peak (ms)	Peak-Onset Delta (ms)	Peak Amplitude
Embryonic					
E17	11.87	4.00	4.56	0.56	-81.05
E17	11.87	3.88	4.44	0.56	-1071.00
E17	14.25	3.88	4.48	0.60	-548.75
E18	14.25	3.00	3.60	0.60	-255.62
E18	11.87	3.00	3.64	0.64	-219.37
Postnatal					
P3	11.87	3.00	3.32	0.32	-1865.00
P3	14.25	3.00	3.80	0.80	-131.83
P3	14.25	3.00	3.52	0.52	-391.35
P4	14.25	3.96	4.36	0.40	-1458.75
P4	16.62	3.96	4.40	0.40	-701.25
P5	14.25	3.00	3.32	0.32	-387.50
P7	11.87	3.00	3.32	0.32	-2143.10
P8	14.25	3.00	3.48	0.48	-4656.90
P8	14.25	3.00	3.36	0.36	-1203.12

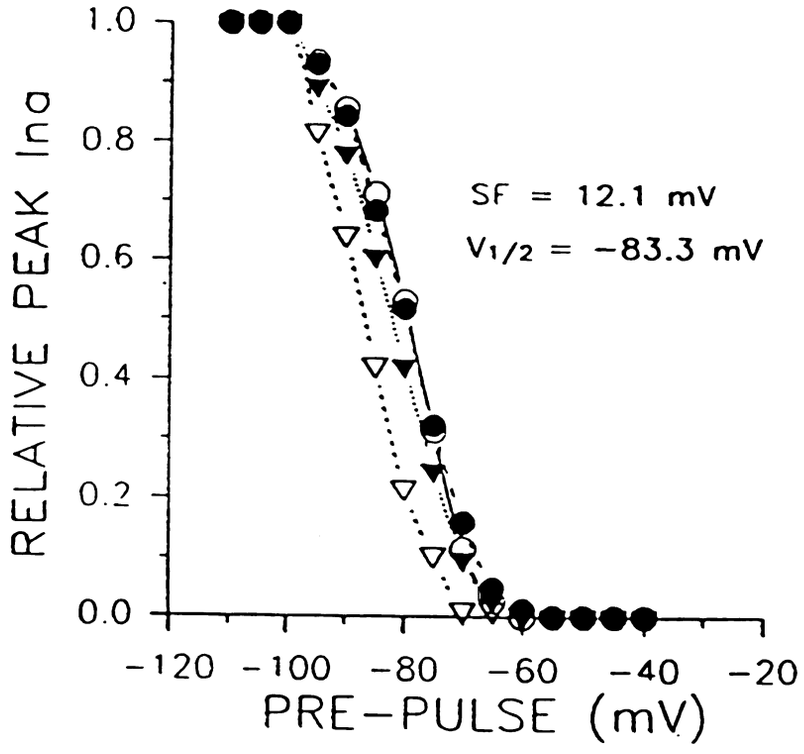

Figure IV-15. Steady-state inactivation curves for three cells normalized to the maximal value at -100 mV and plotted as a function of the pre-pulse potentials.

by the equation: I/Imax = 1{1+exp[(Vh - V1/2)/k]} where V_h is the holding potential, $V_{1/2}$ is the potential at which peak sodium current is one-half maximum and k is the slope factor. The half-inactivated potential was estimated to be -83 mV, and the slope factor was 12 mV.

Rate of Recovery from Inactivation

The rate of recovery from inactivation occurs at a very rapid rate and is shown in Figure IV-16. Measures were obtained from a postnatal (P7) SGC with a cell diameter of 14.25 mm. The rate of recovery for sodium channel inactivation was measured using a two-pulse protocol where the interpulse interval was the independent variable. A 10 ms conditioning pulse from a holding potential of -80 mV to 0 mV was followed by a test pulse to 0 mV at various intervals. Figure IV-17 shows three current records obtained at interpulse intervals of 2 ms, 10 ms and 50 ms. The recovery from inactivation proceeded with a fast and slow time course. The peak sodium current began to recover from inactivation as early as approx. 0.8 ms and continued to recover with a time constant of 7.5 ms. Recovery from inactivation was complete by approximately 50 ms.

Q4: Are there changes in the current amplitude and gating characteristics of SGCs in the presence of externally applied Pb^{2+}?

Various concentrations of Pb^{2+} (0.1 μM, 1.0 μM, 3.0 mM, 10 μM) were used to study its effects on the current of voltage-gated sodium channels of embryonic and postnatal spiral ganglion neurons. Figure IV-18 shows the response of a

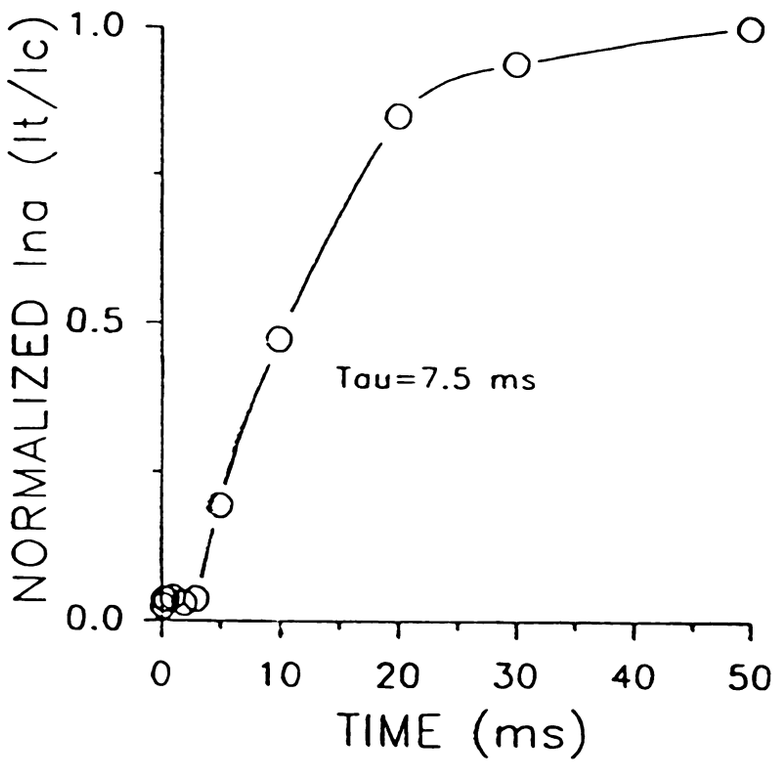

Figure IV-16. Rate of recovery from inactivation for peak sodium current to various interpulse intervals.

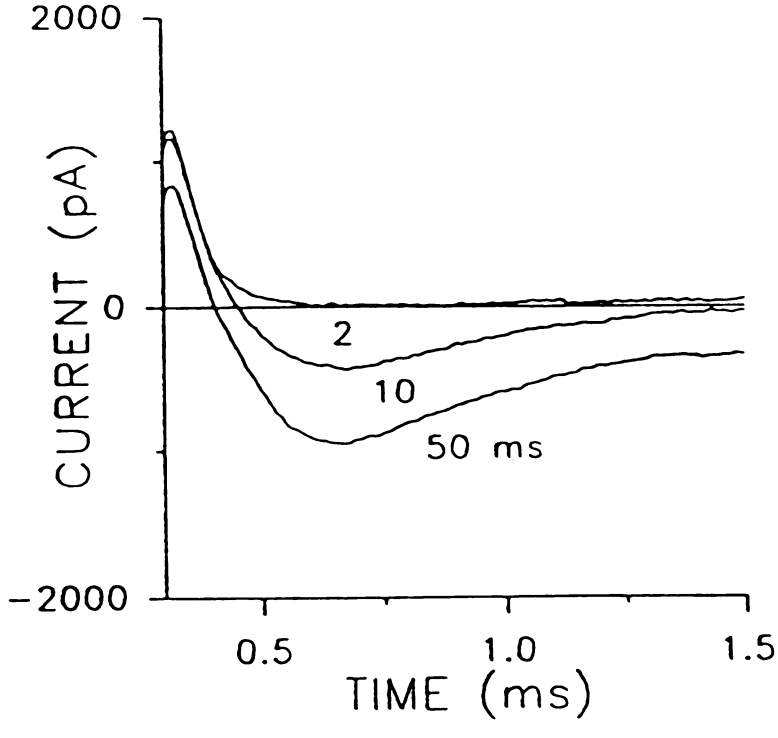

Figure IV-17. Peak sodium currents to interpulse intervals of 2 ms, 10 ms and 50 ms.

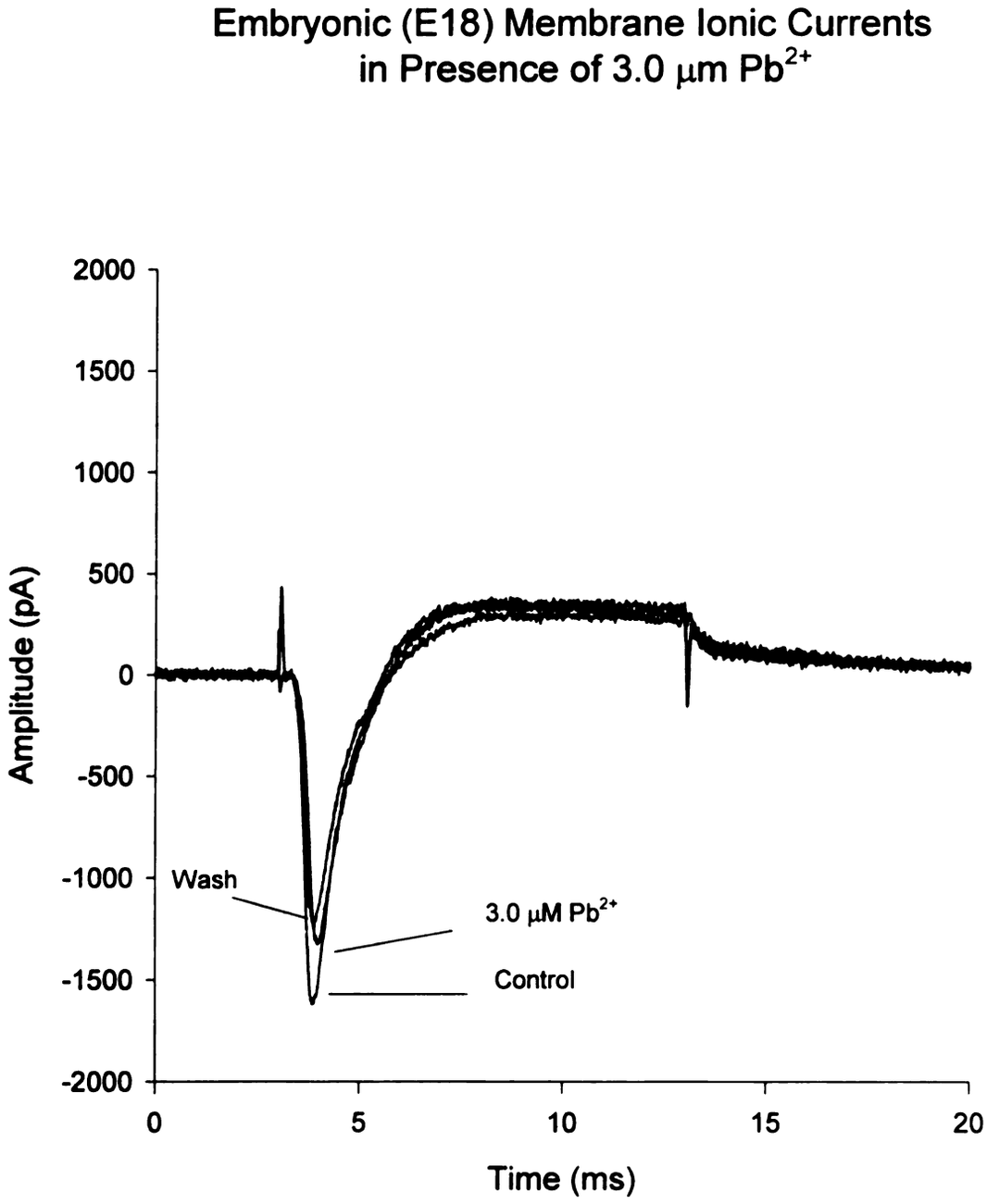

Figure IV-18. Voltage-gated sodium current in the presence of normal solution (140 mM NaCl) and externally applied (3.0 μM) Pb2+.

voltage-gated sodium current in the presence of 3.0 μM Pb^{2+} from an E18 SGC. The cross-sectional diameter of the cell was 14.25 μm. A holding potential of -80 mV was used while administering a 10 ms depolarizing voltage step command in 10 mV steps to the neuron. The transient sodium current exhibited a magnitude of -1600 pA. The external solution was (in mM:) 140 NaCl, 5 KCl, 2.5 CaCl , 10 Glucose, 5.5 HEPES Acid and 4.5 HEPES Na. The pipette solution was (in mM:) 70 CsFl, 40 CsCl, 10 NaCl, 2 MgCl, 10 HEPES Na , 2.0 EGTA. The cell was exposed to 3.0 μM of Pb^{2+} for two minutes following the recording. The inward-directed sodium current was not completely blocked by the presence of externally applied Pb^{2+}, but did show a decrease in peak magnitude (-1300 pA). Inactivation was not affected by the presence of Pb^{2+} and appeared consistent with the rate of inactivation of the control sodium current. The effect which occurred in the presence of Pb^{2+} did not reverse following a two minute wash in the lead-free solution. The peak magnitude decreased further to approximately -1250 pA.

In the absence of specific channel blockers (Figure IV-19A), both an inward-directed sodium current and an outward-directed potassium current from a postnatal (P5) SGC in response to a 10 ms depolarizing voltage step command occurred. The holding potential was -60 mV. A very small inward sodium current resulted following a depolarizing step command which displayed a peak current of -250 pA, while the outward-directed potassium current was +1700 pA. Activation and inactivation of the sodium current was rapid. The cell was exposed for two minutes to an external solution which contained 1.0 μM of Pb^{2+} prior to initiation of the test protocol. No significant

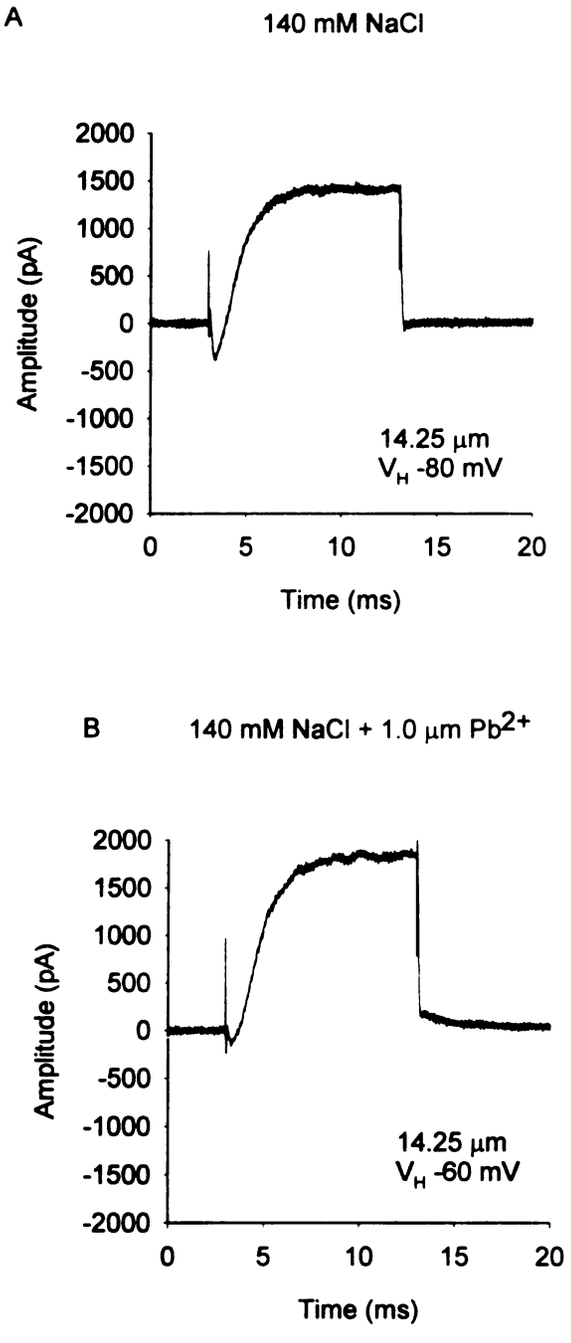

Figure IV-19. Single current trace from a postnatal (P5) SGC in normal (140 mM NaCl) and in the presence of externally applied 1.0 µM Pb^{2+}.

changes were observed in the peak sodium current following exposure to Pb^{2+} for four minutes (Figure IV-19B). Figure IV-20 is a superimposed illustration of the same two currents in Figure IV-19. There were no changes in the activation kinetics of inward peak sodium currents, and minimal changes observed for the peak sodium current magnitude. An increase was noted, however, in the peak potassium current magnitude following exposure to 1.0 μM Pb^{2+}.

The sodium current is voltage dependent and highly sensitive to the holding potential. Peak sodium current magnitudes increased as the holding potential becomes more negative. Figure IV-21 is an illustration showing the effects of holding potential on the inward sodium current magnitude from a P6 SGC. These effects were observed for several cells. The effect was seen for the Pb^{2+} study discussed above. When the cell was clamped at a holding potential of -60 mV, a very small inward current resulted (Fig IV-22A). In the presence of externally applied lead (1.0 μM), a minimal change in current magnitude was noted. No significant increase in peak current magnitude was noted following a wash in lead-free solution. When the holding potential was increased to -80 mV, the peak sodium current increased to -1000 pA. There were no significant changes noted in the peak potassium current as the holding potential changed. The holding potential has an effect on the magnitude of peak sodium current without showing much of an effect on the potassium currents.

Figure IV-23 illustrates the effect of 1.0 μM Pb^{2+} when the cell is held at a holding potential of -80 mV. Fig IV-23A shows the peak sodium current in the absence of Pb^{2+} following a depolarizing voltage step command. The peak current magnitude approached

Control + 1.0 μm Pb^{2+}

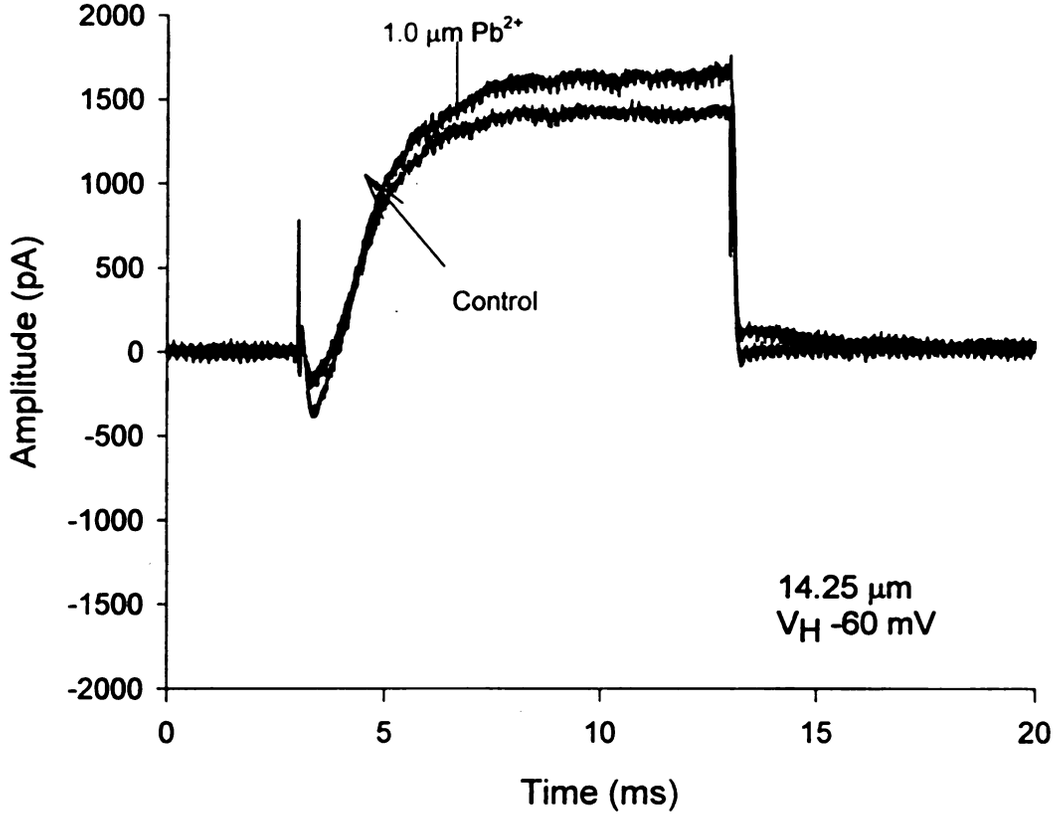

Figure IV-20. Superimposed ionic currents shown in Figure IV-19.

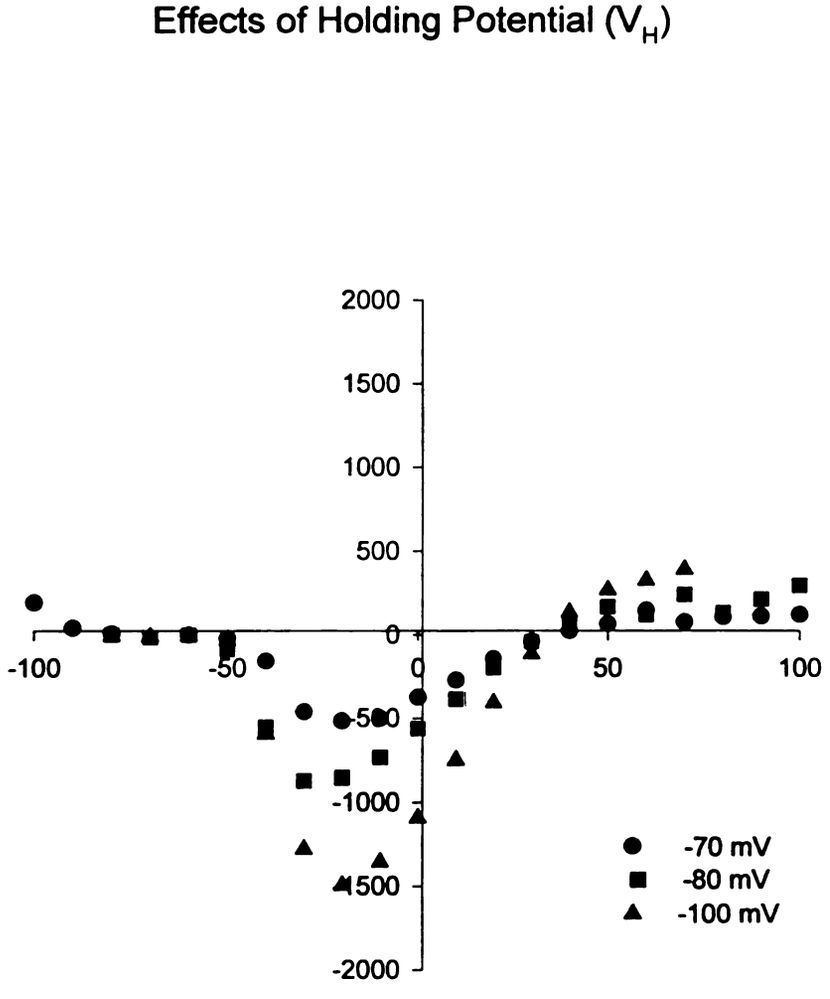

Figure IV-21. Effects of holding potential on the inward-directed peak sodium current magnitude.

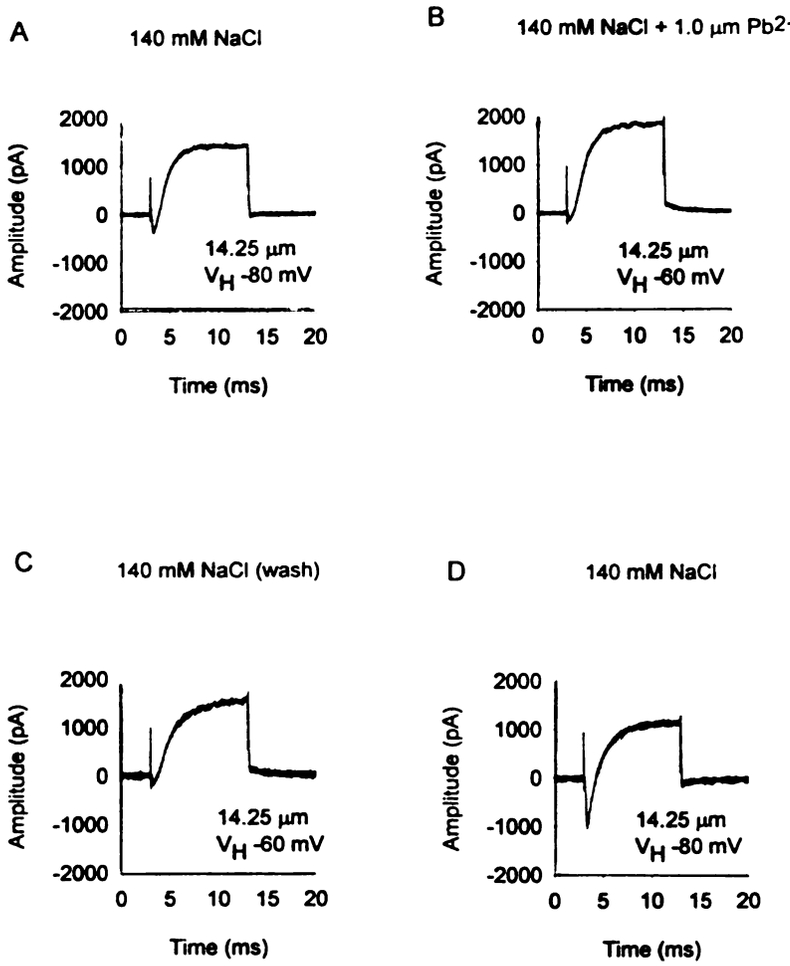

Figure IV-22. Effects of 1.0 μM Pb^{2+} and change in V_h for peak current magnitude in a P5 SGC.

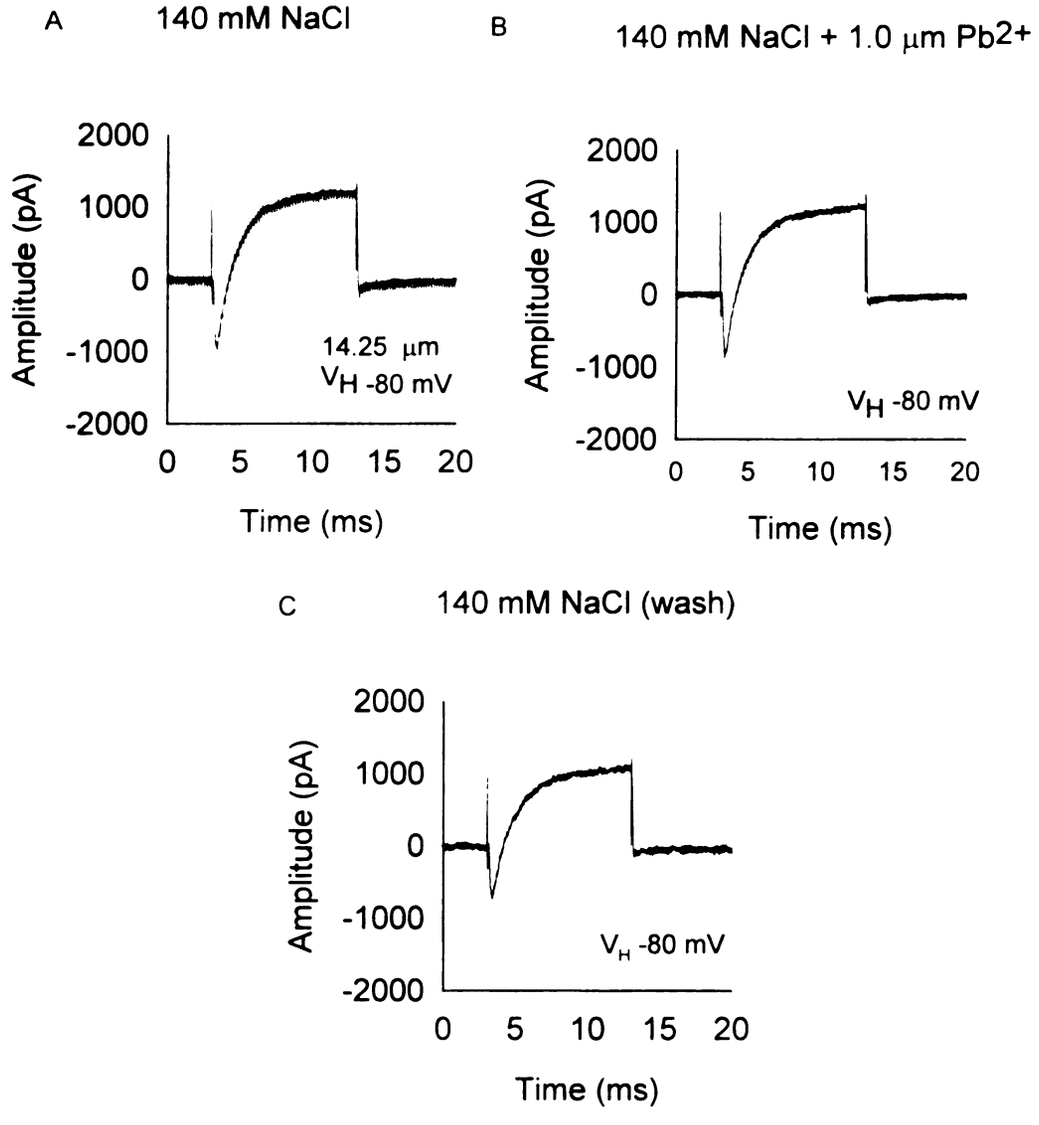

Figure IV-23. (A) Single membrane ionic current (B) Single membrane ionic current in presence of 1.0 μM Pb2+ and (C) Rinse with normal (140 mM NaCl) solution.

-1000 pA. Figure IV-23B illustrates the peak sodium current in the presence of 1.0 μM Pb^{2+}. A negligible change in peak sodium current was observed following a four minute exposure to 1.0 μM Pb^{2+}. Figure IV-23C shows the effect of what appears to be run down of the SGC following a two minute wash in the lead-free solution. Figure IV-24 illustrates the response of the three single traces shown above in Fig IV-23. There was only a minimal difference noted between the control peak sodium current and the peak current generated following the exposure to lead (1.0 μM). The greatest change in peak sodium current is observed following the two minute wash which is believed to be the result of run down.

Figure IV-25 depicts the response of a P9 SGC in the presence of 10 μM Pb^{2+} The cross-sectional diameter of the cell was 14.25 μM. The cell was clamped at a holding potential of -120 mV prior to the initiation of 10 mV step commands. Inward-directed sodium currents were produced following depolarizing step commands. Fig, IV-25A shows the responses of four successive single sodium currents in response to depolarizing voltage potentials. Sodium currents activated and inactivated rapidly. Peak sodium currents were very small, approaching only -150 pA. In the presence of 10 μM Pb^{2+} sodium currents continued to activate and inactivate. Following the application of 10 μM Pb^{2+} peak sodium currents had a magnitude of -150 pA. However, the inactivation of the sodium appeared to be prolonged (Figure IV-25B) Figure IV-25C shows the continued application of lead exposure for the same cells. However, following a four minute rinse in lead-free solution, the original kinetic activity of the sodium

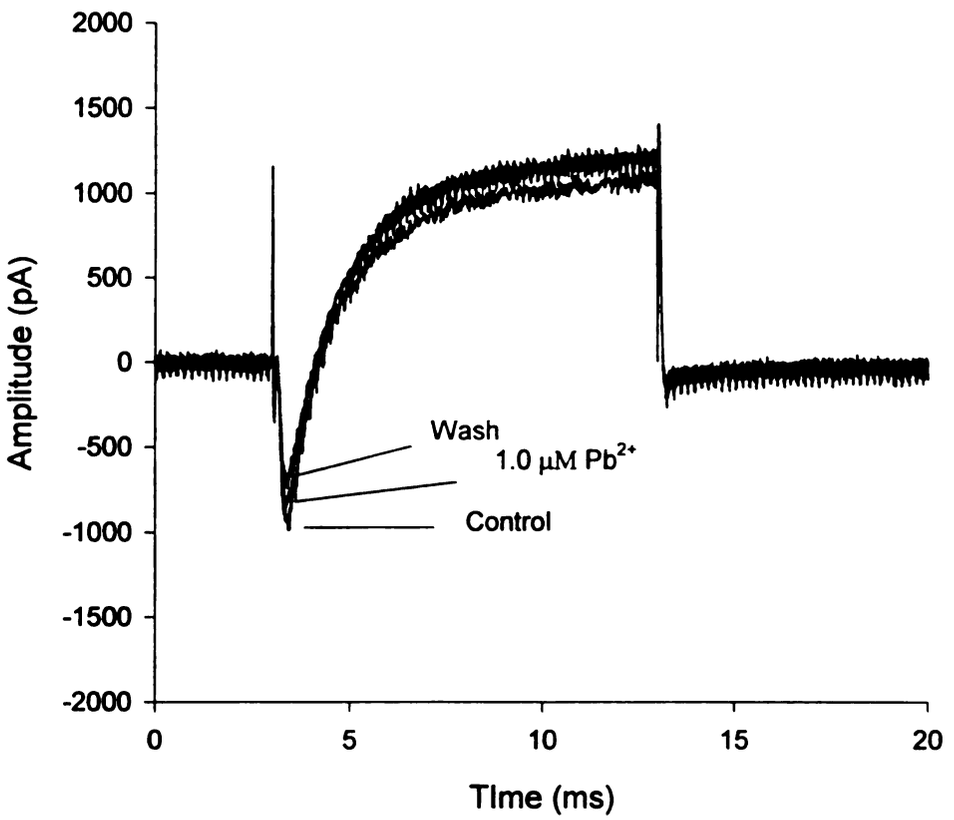

Figure IV-24. Superimposed single membrane ionic currents exposed to 1.0 μM Pb^{2+} shown in Figure IV-23.

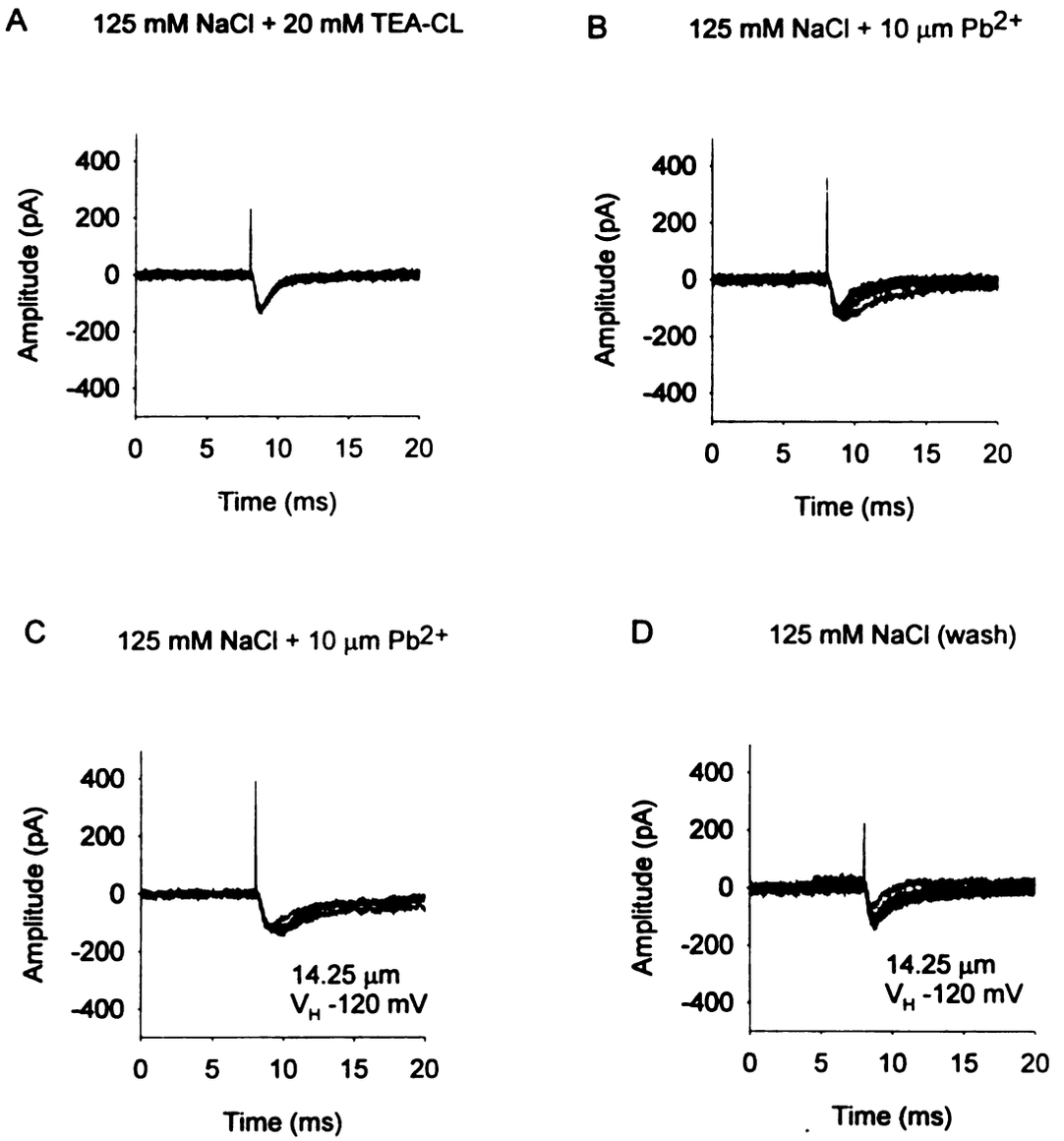

Figure IV-25. Multiple single sodium currents generated by P9 SGCs following exposure to 10 μM Pb^{2+} (A) Normal (125 mM CaCl) solution, (B) Normal solution + 10 μM Pb^{2+}, (C) Normal solution + 10 μM Pb^{2+} and (D) Normal solution (125 mM NaCl).

currents shown in Figure IV-25A reappeared (Figure IV-25D)and the prolonged inactivation disappeared. Table II shows the change in rates of activation and peak current amplitudes for SGCs exposed to 10 μM Pb^{2+} and lead-free solution. Thus, as the SGCs are exposed to Pb^{2+} the rates of activation increased and gradually decreased following a rinse with normal (140 mM NaCl) solution.

Q5: Do postnatal (P2 – P9) SGCs exhibit delayed rectifying outward going currents?

In the absence of specific channel blockers such as TEA or CsCl, potassium currents were consistently present in both embryonic SGCs and postnatal SGCs. There were several experiments, however, during recordings of both embryonic and postnatal SGCs in which only outward-directed potassium currents were present, in the absence of the specific sodium channel blockers TTX. When present, potassium currents were typically very large, with peak magnitudes reaching 15,000 pA in some cases. Potassium currents typically did not inactivate following activation, but remained activated throughout the duration of the stimulus. The delayed onset indicated that the currents generated by voltage-gated potassium channels present in SGCs are of the delayed-rectifier type.

Figure IV-26A shows a family of both inward-directed sodium currents and outward-directed potassium currents generated by a P6 SGC (diameter 14.25 μm). The membrane holding potential was -80 mV and was depolarized from - 100 mV to +80 mV by 10 mV voltage-step commands lasting 20 ms. Channels activated rapidly and remained activated throughout the duration of the stimulus protocol. Bath application of

TABLE II

Comparison of Traces showing Rates of Activation for Lead-free and 10 μM Pb^{2+}

Experiment I

Trace	Rate of Activation (ms)	Peak Current Amplitude (pA)
Lead-free		
(1 – 4)	1.04	-134.37
10 μM Pb^{2+}		
5	0.96	-121.35
6	1.04	-125.83
7	1.20	-119.79
8	0.88	-112.18
9	1.44	-130.52
10	1.52	-147.70

Experiment II

Trace	Rate of Activation (ms)	Peak Current Amplitude (pA)
7	2.08	-150.31
2	2.00	-123.64

Table II cont.

Trace	Rate of Activation (ms)	Peak Current Amplitude (pA)
3	1.44	-110.31
Lead-free		
4	1.52	-120.31
5	1.20	-126.14
6	1.28	-118.33
7	1.04	-120.41
8	0.96	-117.70
9	1.12	-103.02
10	0.88	-74.58

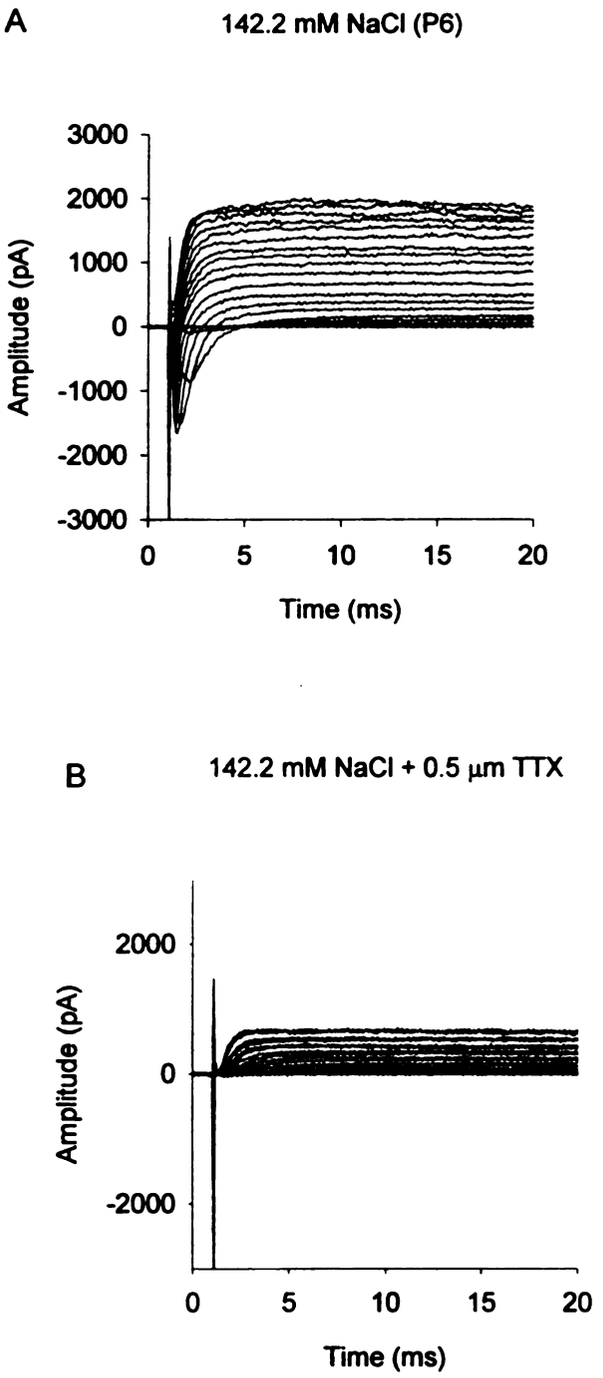

Figure IV-26. (A) Family of outward-directed potassium current and inward-directed sodium currents generated by a P6 SGC. (B) Sustained delayed rectifying potassium currents following application of 0.5 μM TTX. (C) Family of outward-directed potassium current and inward-directed sodium current produced by a P9 SGC. (D) Remaining delayed rectifying potassium currents following application of 0.5 μM TTX.

C

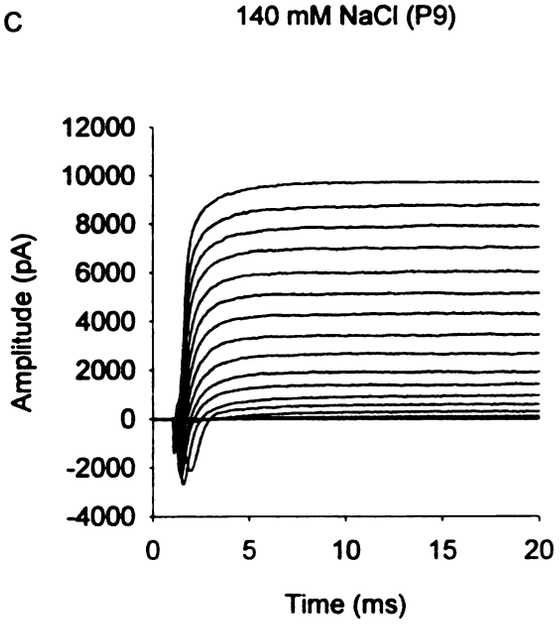

D

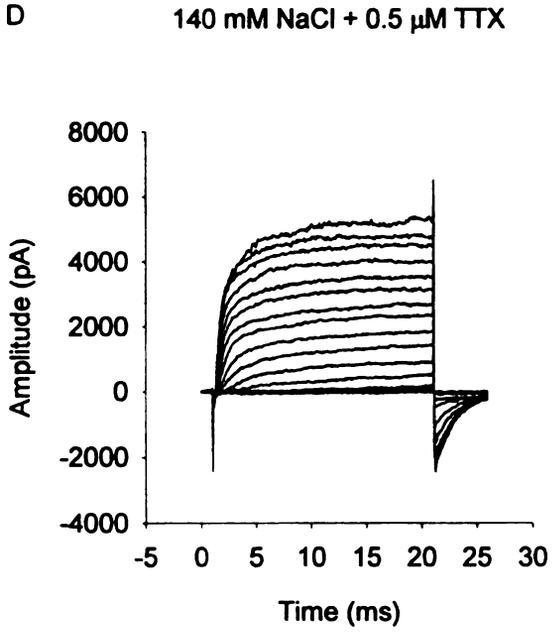

Figure IV-26

0.5 μM TTX blocked the TTX-S sodium channels revealing uncontaminated potassium currents (Figure IV-26B).

The same effect was observed for a fully differentiated P9 SGC. Figure IV-26C reveals a family of inward-directed sodium currents and outward-directed potassium currents (diameter 14.25 μm) under the same test conditions listed above. Inward-directed sodium currents and outward-directed potassium currents were revealed following initiation of a depolarizing pulse protocol. Rapid potassium currents were exhibited following depolarizing voltage step commands which reached a peak magnitude of +9000 pA. Bath application of 0.5 μM TTX completely eliminated the inward-directed sodium currents leaving uncontaminated delayed rectifier potassium currents (Figure IV-26D). These delayed rectifying potassium currents activated to step depolarizations more positive than -40 mV.

Figure IV-27A shows the response of a family of outward-directed potassium currents produced by an embryonic (E18) SGC in response to 10 mV depolarizing voltage-gated step commands lasting 10 ms. The cross-sectional diameter of the cell was 14.25 μm. The cell was held at a holding potential of -80 mV and stepped from -100 mV to +80 mV in 10 mV steps. Inward-directed sodium currents were not present. That is, in the absence of the specific sodium channel blocker TTX , only potassium current appeared.

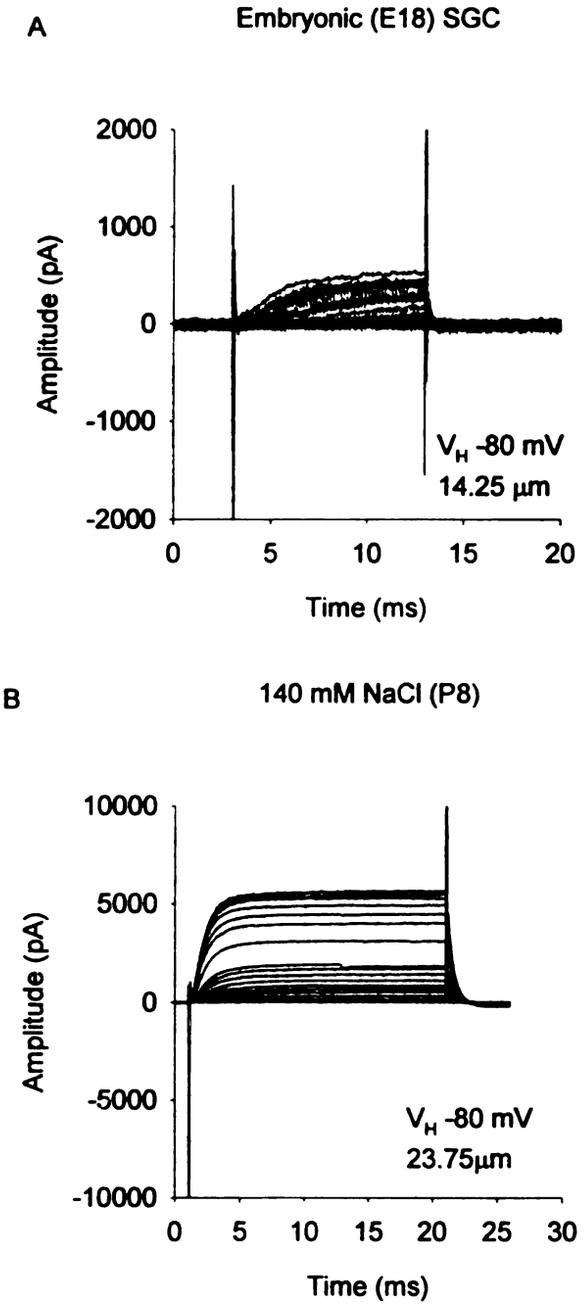

Figure IV-27. Outward-directed potassium currents in the absence of TTX generated by (A) an embryonic SGC and (B) P9 SGC.

A similar response was noted in postnatal SGCs as well. Fig IV-27B shows a family of outward-directed potassium currents produced by a P8 SGC in the absence of TTX. The cross-sectional diameter of the cell was 23.75 μm. The cell was clamped at a V_h of -80 mV. Ten mV depolarizing voltage commands lasting 20 ms were introduced to the cell. When compared to the embryonic response, the postnatal cell activated faster. It activated at potentials more positive than -80 mV and remained activated throughout the duration of the stimulus. The outward-directed potassium current reached a peak current magnitude of +5000 pA.

Potassium currents were produced by embryonic SGCs and postnatal SGCs from each maturational group described above, i.e., early (P2-P4), intermediate (P5-P7) and differentiated (P8 and older)). Overall, peak potassium current magnitudes observed in embryonic SGCs were weak and produced very small currents in comparison to the current magnitudes produced by the older more mature SGC (Figure IV-28 A-G).

Embryonic K^+ Currents

A

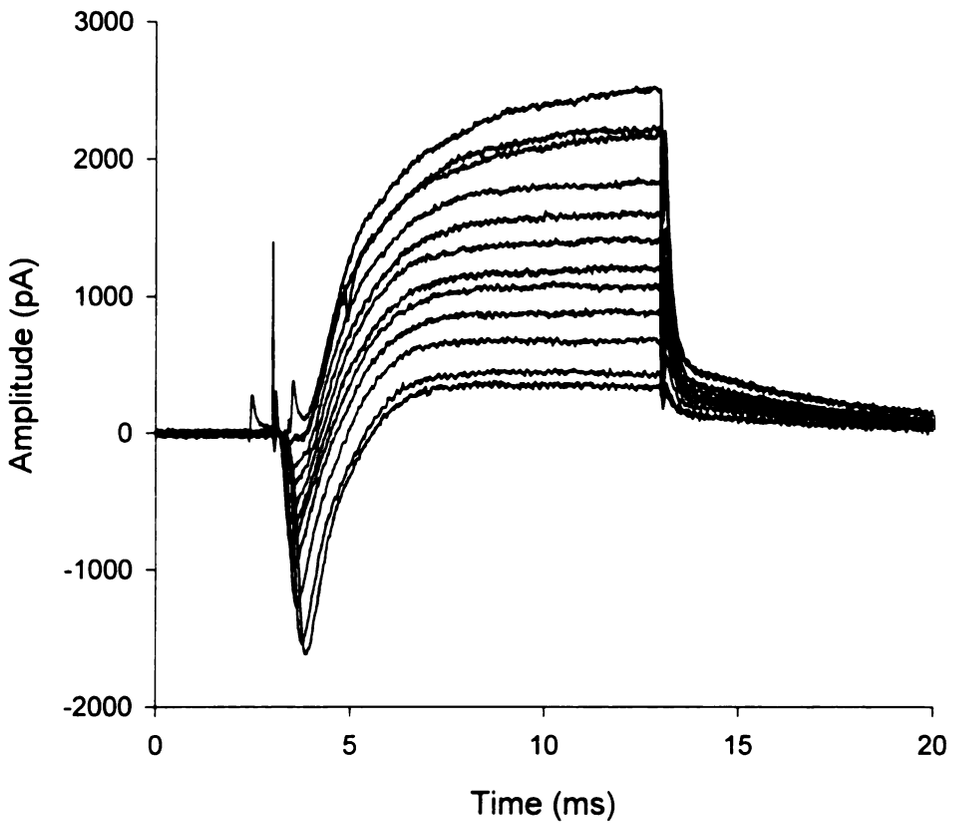

Figure IV-28. Outward-directed potassium currents for embryonic (IV - 28A) and postnatal (P1 - P8) (IV - 28B - IV - 28G) SGC.

B Family of Outward Directed K^+ Currents from a P1 SGC

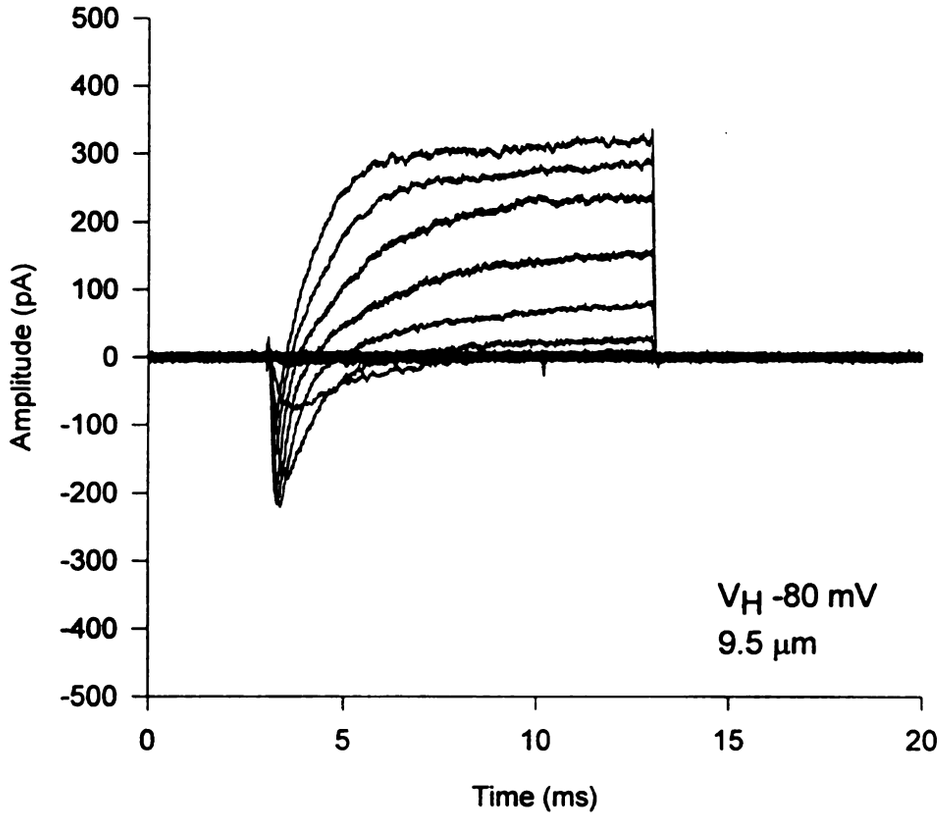

Figure IV-29

C Outward-Directed K^+ Current from a P3 SGC

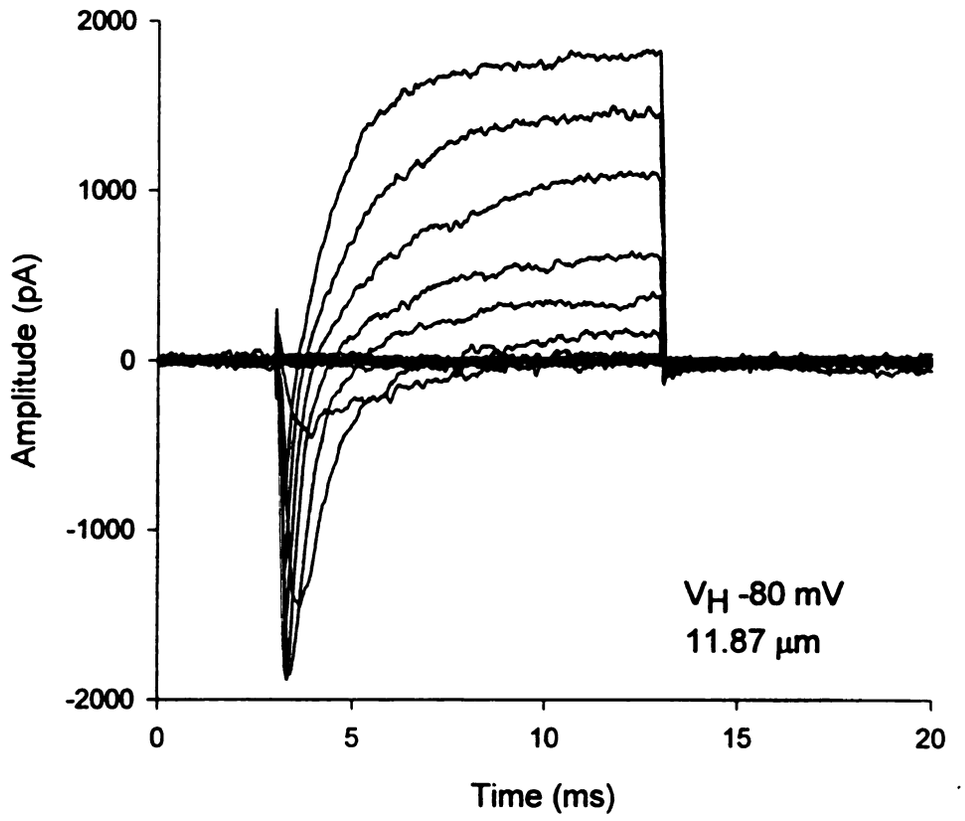

Figure IV-29

Outward-Directed K^+ Current from a P5 SGC

D

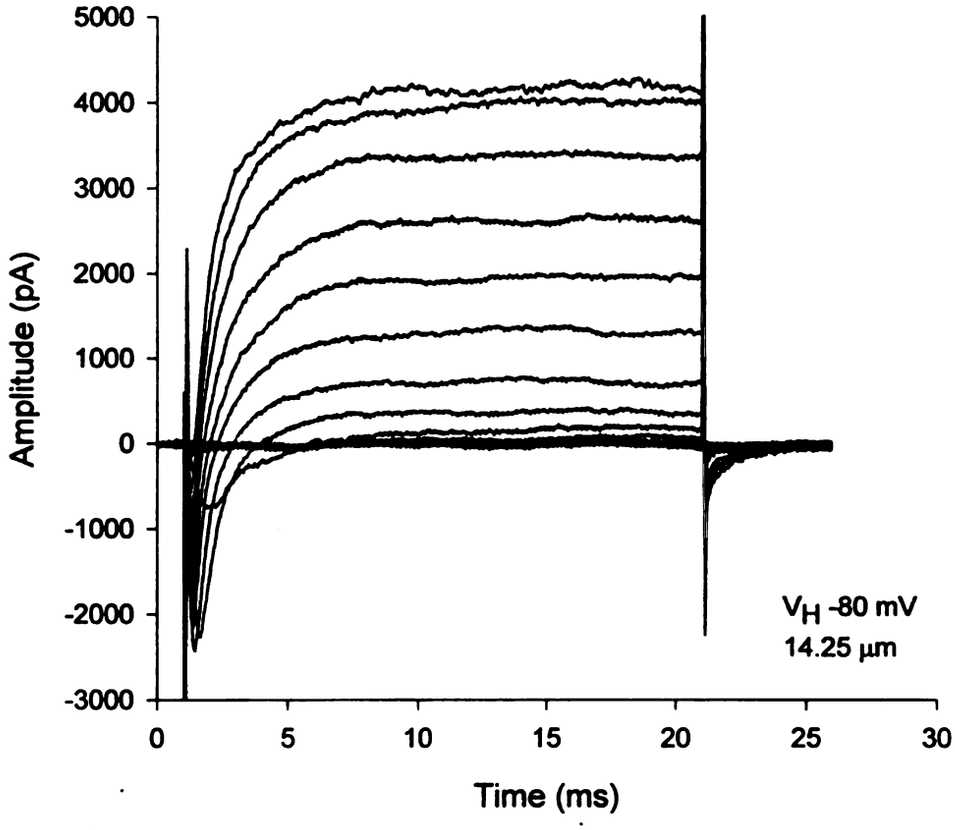

Figure IV-28

Outward-Directed K^+ Current From a P6 SGC

E

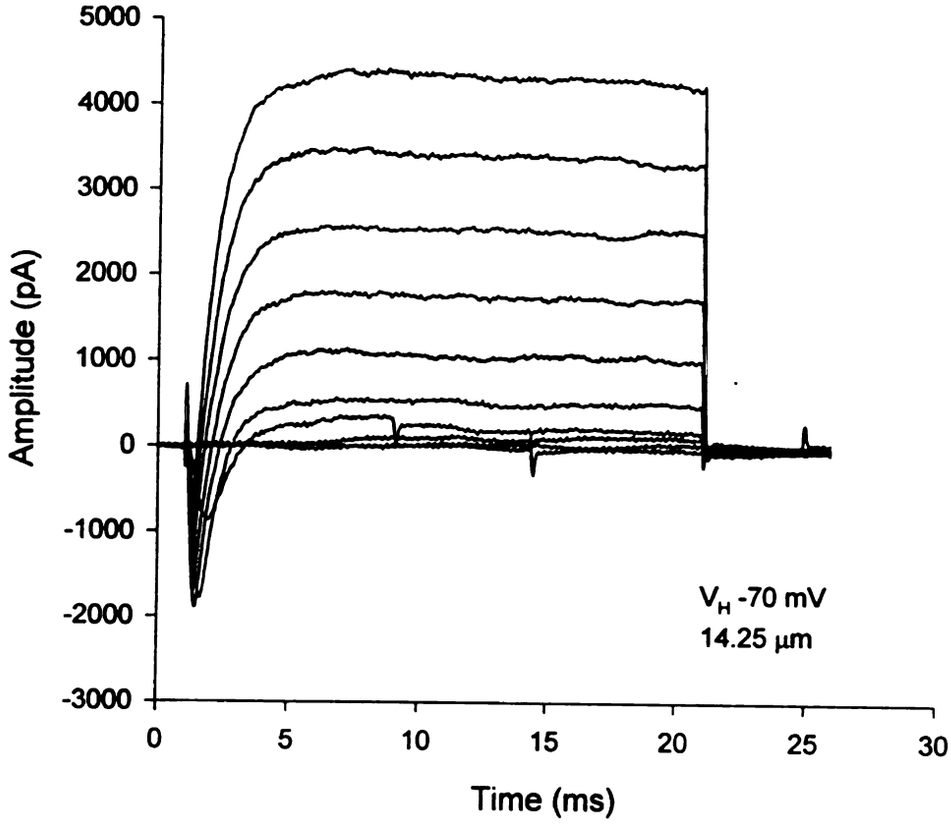

Figure IV-28

Outward-Directed K^+ Currents From a P7 SGC

F

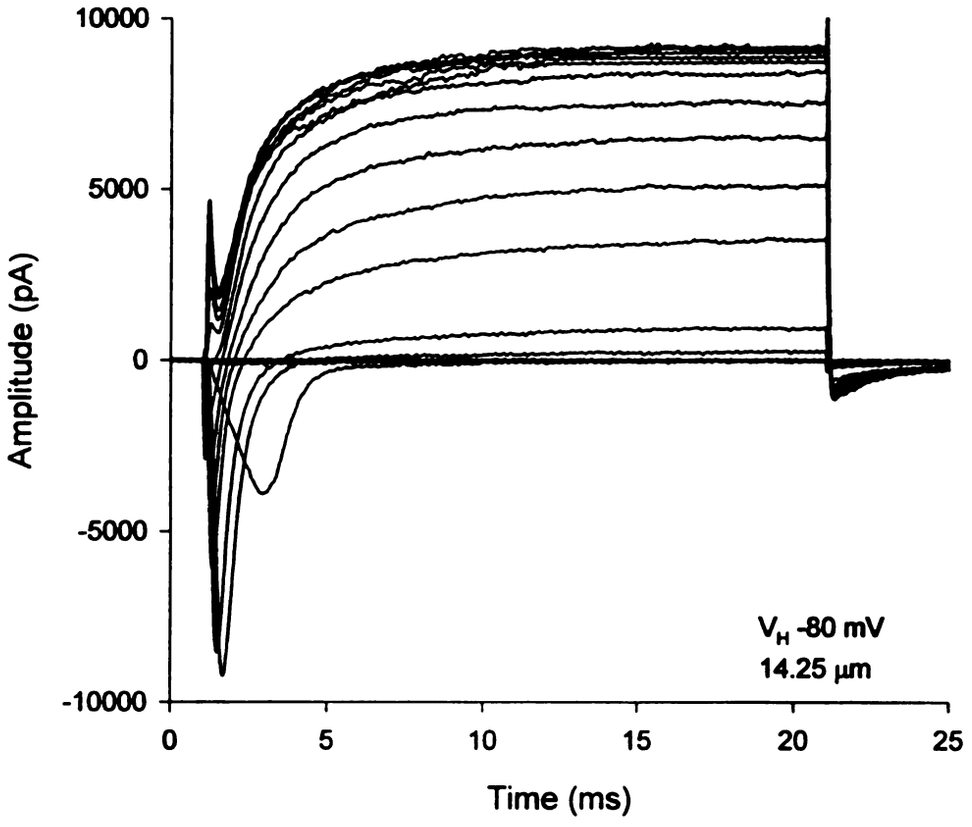

Figure IV-28

G

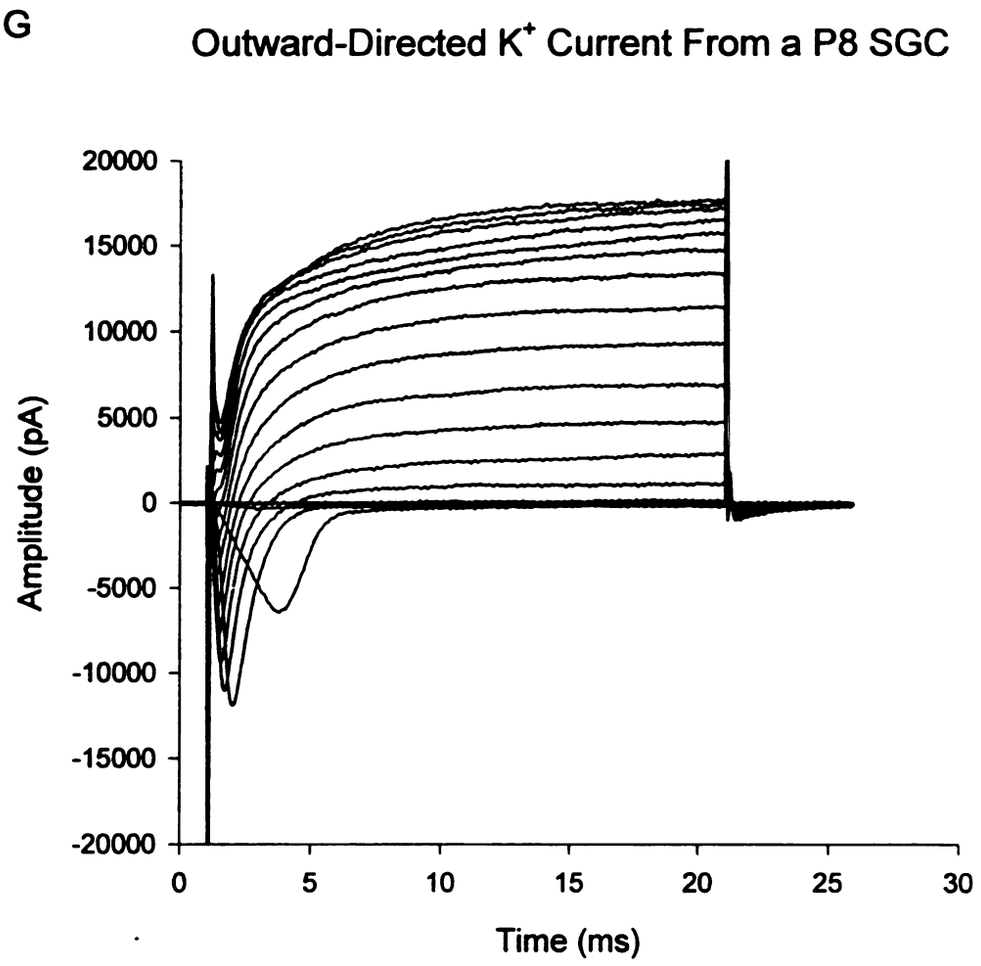

Figure IV-28

CHAPTER V

DISCUSSION

The human peripheral auditory system is described as precocious. This is supported in part by developmental studies that have described the ontogeny of the various organs, structures and fibers that comprise the auditory system. Until recently, however, only a few researchers have investigated basic underlying ionic mechanisms that act synergistically with anatomical structures in processing sound. Considering the significance attributed to the influence of normal hearing on early patterns of normal speech and language development, two questions are asked: First, "Is the auditory system truly precocious, or are only the anatomical structures which comprise the ear that are present prenatally?" In other words, are the underlying neurological mechanisms responsible for signal transduction such as voltage-gated ionic channels present prenatally? Secondly, are the development of ionic mechanisms coincident with the development of anatomical structures which seem to convey auditory information?

Unlike humans, rats are not capable of perceiving sound until after birth, usually between P9-P12 (Crowley and Heap-Raymond, 1966). They therefore serve as an ideal model for studying the development of voltage-gated membrane ionic currents. Since voltage-gated sodium current and potassium current are important to auditory nerve action potential generation, these currents were recorded from both embryonic and postnatal rat SGC as part of a developmental study. This was accomplished to (1) determine if endogenous ionic properties of SGCs are present at embryonic and postnatal

stages of development, and (2) to determine whether sodium and potassium kinetic properties change with maturation.

The auditory nerve transfers neural signals from the auditory sensory receptor hair cells to the cochlear nucleus complex located in the brain stem. The 8th cranial nerve is comprised partly of nerve fibers, which extend centrally from two specific populations of auditory ganglion, type I and type II SGCs. The ganglion cells are the cell bodies of the cochlear branch of the 8th cranial nerve. Numerous single unit fiber recordings have been made from auditory nerve fibers (Galambos and Davis, 1943, 1944; Tasaki, 1954; Javel, 1986, to name a few). The auditory nerve is perhaps one of the most thoroughly studied set of nerve fibers of the auditory system. However, the role of SGCs in the transfer of auditory cues along the length of the auditory nerve is uncertain. Santos-Sacchi (1993) suggested that SGCs serve as an internode inserted along the length of the auditory nerve, and as such, assist in conducting impulse trains along the length of the nerve. Mo and Davis (1997) and Lin (1997) who recorded spike activity from postnatal SGCs during current-clamp experiments recently supported his supposition. However, there is still some uncertainty as to the specific role of SGCs in the processing of auditory signals.

Although voltage-gated studies have been conducted using the mammalian auditory system, only one investigation has been reported in the literature that described developmental changes of voltage-gated membrane ionic currents. The avian auditory system was investigated using cochlear ganglion cells (albeit the chick cochlea does not spiral, hence cochlear ganglion rather than spiral ganglion) removed from chick embryos

at various developmental stages (Valverde et al., 1992). Thus, to date, there are no studies cited in the literature, which have investigated developmental patterns of membrane ionic currents of mammalian SGCs.

We now have data to support the presence of a truly prenatal auditory system using electrophysiologic methods. The data presented here indicate that embryonic SGCs possess functional sodium channels and potassium channels which produce inward-directed sodium currents and outward-directed potassium currents, respectively. The kinetics of the currents of these voltage-gated channels, however, appear to change appreciably with maturation. These changes, perhaps, contribute to improvement in auditory sensitivity as the auditory system matures.

Morphological Characteristics of SGCs and Auditory Nerve Fibers

The human auditory nerve bundle has approximately 30,000 - 35,000 spiral ganglion neurons, while the rat possesses only 15,000 - 20,000 (Schwartz, 1986). In the present investigation, both embryonic and postnatal rat cell cultures produced a high yield of dissociated SGCs from which to investigate. The cells appeared phase bright when viewed under an inverted microscope. Morphologically, they exhibited a spherical shape and showed early signs of neurite outgrowth, which extended at different rates. Neurites displayed by embryonic neurons appeared approximately four hours after an incubation period, while postnatal neurons displayed signs of neurite outgrowth within a five-hour period. Thus, neurite outgrowth appeared to occur at a faster rate during the embryonic stages of development than during postnatal stages of development.

On occasion the phenotype of the axons from postnatal SGCs could be identified when observed under an inverted microscope. The diameter of the presumed peripheral axon, which extended from the cell soma, appeared small in comparison to the diameter of the presumed central axon. This is a morphologic characteristic often cited in labeling studies of type I and type II SGCs (Brown, 1987; Brown et al., 1988). The larger outer diameter of central axons perhaps results from the layers of compact myelin which ensheathed the axon, a necessary conductor material for the propagation of fast signal transduction. This notion is further supported by the comparison of presumed type II SGCs. These ganglion cells have a smaller cross-sectional diameter and are often characterized as unmyelinated, or at least ensheathed by only a few layers of loose myelin.

Schwartz et al. (1983) categorized the development of rat postnatal SGCs into four developmental stages: Stage 1, newborn through P2; Stage 2, P4 - P6; Stage 3, P8 - P10 and Stage 4, P14 - P30. Embryonic SGCs were not investigated. Very few anatomical changes occurred within the first postnatal week. At birth, the SGCs appeared as a homogeneous population of cells. They were ensheathed by a single layer of Schwann cell processes. The process of myelination began at birth and continued throughout the first postnatal month. Our studies found myelin present in both embryonic and postnatal cell preparations. Enzymatic treatment during cell culture did not always eliminate unwanted myelin. Myelin was observed surrounding the peripheral edges of the cell soma several hours following an incubation period (e.g., four hours). The presence of myelin during embryonic stages offers further support, which suggest

that specific underlying anatomical mechanisms responsible for fast signal propagation are present during early stages of development.

While previous studies have used cell size diameter as a marker to differentiate type I SGCs from type II SGCs, cell size diameter in the present investigation was not always a valid measure to differentiate ganglion cell types. That is, embryonic SGCs showed considerable variability in somatic cell size. Cross-sectional diameter averaged 12.41 μm and ranged between 9.5 to 16.62 μm (n = 78). The cross-sectional diameter of postnatal SGCs, however, were also variable and averaged 14.83 μm (n =114), with a range of 11.87 - 23.75 μm. This noted overlap in cross-sectional diameter between the somatic measurements obtained for embryonic SGCs and those obtained for postnatal SGCs made questionable the use of cross-sectional diameter as a marker to differentiate ganglion cell types. Brown et al. (1988) made the same observations, indicating that the morphometric characteristics used to separate type I SGCs from type II SGCs in larger animals was less useful in predicting cell type of smaller animals.

There are several reasons that could account for the variability in cell size among embryonic rat pup SGCs. First, the most obvious reason for the variability is the differences in the size of the rat pups. Although the age was maintained constant for different populations, pups differed in size, based upon their body weight/fat and/or skeletal frame. Secondly, SGCs with larger cross-sectional diameters (e.g., 14.25 μm) may reflect those embryonic cells that have already reached their morphologic adult cell size. Zimmer et al. (1994) conducted a developmental study of the structural maturation of the rat's middle-ear system in which measurements were made of various middle ear

structures. Their state of maturation was based upon percentages for obtaining an adult state of development. For example, the arm of the incus achieved 90% of its adult size within 26 days while the arm of the malleus took 34 days to achieve 90% of its adult length. Thirdly, in keeping with the premise that the cochlea develops from base to apex, the larger SGCs may comprise basal ganglion cells which have reached their adult state of maturation prior to those ganglion cells originating from more apical regions. The final reason is derived from the concept of tonotopicity as frequency specificity is maintained throughout the auditory system. Sensory receptor cells most sensitive to high frequency stimuli are located towards the basal end of the basilar membrane, while the receptor cells most sensitive to low frequency stimuli are located towards the apical end of the basilar membrane. The larger SGCs may result from the cell bodies of auditory neurons which innervate a specific frequency region of the basilar membrane, and thus, maintain the tonotopic nature of the auditory system (Moore et al., 1996).

Voltage-gated Ionic Currents of Embryonic SGCs

Several investigators have identified membrane ionic properties of dissociated cultured CGNs of the avian auditory system (Yamaguchi, 1988; Yamaguchi and Ohmori, 1990; Nakagawa et al., 1991; Valverde et al., 1992; Sheppard et al., 1992; Yamaguchi and Ohmori, 1993). The first reports cited in the literature which discussed voltage-gated as well as ligand-gated membrane ionic properties in mammalian SGCs followed (Nakagawa et al., 1991; Santos-Sacchi, 1993; Moore et al., 1996; Davis, 1996; Mo and Davis, 1997; Lin, 1997). To date, there have been no reports of developmental changes that occur in voltage gated membrane ionic currents in mammalian SGCs.

Both inward-directed sodium currents and outward-directed potassium currents were present in embryonic SGCs following application of depolarizing test pulses. The presence of sodium currents and potassium currents in embryonic SGCs suggests that these neurons contain two of the essential ions necessary for cell excitability and the generation of action potentials. Although the underlying ionic properties necessary for the generation of APs are present and functioning, other areas within the auditory system, such as the middle ear mechanism and the cochlea, are underdeveloped and continue to undergo maturational changes.

The cochlea of the rat is immature at birth and development progresses very slowly during the first postnatal week (Crowley and Hepp-Reymond, 1966; Lenoir et al., 1980; Roth and Bruns, 1992). In fact, auditory brainstem response (ABR) measures suggest that rat pups are born with a mixed hearing loss resulting from the under-development of both the conductive and cochlear systems. With maturation, both systems show signs of improved sensitivity. Geal-Dor et al. (1993) performed ABR measures on 160 neonatal rat pups. Responses to stimuli presented via air conduction (AC) were not elicited until P11, while responses via bone conduction (BC) were obtained between P7-P8, but were obtained at the maximal output levels of the equipment. By P15, ABR responses to AC and BC stimuli had improved and approached adult thresholds. The air-bone gap obtained during the first two weeks diminished to 0 dB. Thus the maturation of the conductive apparatus was completed by P15, while sensorineural maturation continued to improve later than P15.

Lenoir et al. (1980) investigated the development of synaptogenesis in the rat. Inner hair cell (IHC) synaptogenesis appeared to be closely completed at birth. Nerve fibers were in place and were seen beneath both immature IHC and outer hair cells (OHC). Numerous well-developed afferent and efferent fibers were in place beneath IHCs, as well as pre-synaptic vesicles and post-synaptic thickenings. Only afferent fibers were in place beneath OHCs. Specific changes occurred in the afferent innervational patterns as the days progressed for both receptor cells. However, innervation patterns occurred first at the level of the IHC. OHC synapses were rather complex and did not mature until approximately P16.

Ontogenetic changes of the cochlea continued through P12. Although development of the middle ear system and cochlea continue to mature after birth, the adult appearance of the organ of Corti does not occur until P20. Specific structural changes within the cochlea continue to develop postnatally and are attributed to the improvement in hearing sensitivity (Roth and Bruns, 1992). The first electrophysiological measures of the cochlear microphonic (CM) can not be recorded from the round window of the rat until P8 - P9. The action potential follows the emergence of the CM and can not be recorded from the auditory nerve until P11 - P12. Therefore, sodium and potassium channels responsible for the generation of action potentials are present and capable of producing functioning membrane ionic currents during an early stage of development. However, the peripheral auditory structures, including the middle ear and inner ear mechanisms, are continuing to develop during the

first month of life. Thus, continued development of the middle and inner ear systems perhaps accounts for the improvement in auditory sensitivity over time.

Embryonic Sodium Current Peak Magnitude

Peak sodium currents exhibited by embryonic SGCs were small and did not exceed 1500 pA. The amplitude of the inward-directed current varied considerably between cells. The variability observed between cells was not a direct reflection of cell size, but would appear to be an indication of the number of functional channels that contribute to the whole-cell current. This was evident when comparing sodium current generated by a number of different cells removed from the same pup. It is not clear, however, how differences in the magnitude of sodium current amplitude influence neural coding among cells. However, it is conjectured that the variability is significant for coding frequency as well as temporal cues. The differences observed in current magnitude may result from the characteristics of tonotopic organization, as tonotopicity is maintained throughout the cochlea, auditory nerve, brain stem and auditory cortex. The receptor cells that align the length of the basilar membrane are tonotopically arranged. The auditory nerve trunk, which arises from type I and type II fibers, innervates the IHCs and OHCs, respectively, are coiled and organized tonotopically. Fibers innervating the basal regions of the cochlea are located towards the periphery of the nerve trunk while fibers innervating apical regions of the cochlea are located medially within the trunk. Tuning curves generated from single auditory nerve fibers also demonstrate the specificity to which single auditory nerve fibers are most sensitive. The differences in peak sodium current magnitude generated by the different isolated SGCs may reflect the

current properties specific for coding frequency information, and thus, maintain tonotopicity.

TTX-Sensitive vs. TTX-Resistive Sodium Channels

Sodium currents generated by postnatal SGCs from early, intermediate, and differentiated stages of development were readily blocked by 0.5 μM TTX. This effect was reversible as inward sodium currents almost returned to normal magnitude following a two-minute wash in a TTX-free external solution (140 mM NaCl). This response confirms the presence of TTX-sensitive sodium channels in postnatal (P1-P9) rat SGCs. TTX-R sodium currents were not observed in postnatal SGCs at any of the developmental stages. This does not suggest that rat SGCs do not possess TTX-R sodium channels. Rather, the absence of TTX-R sodium currents in SGCs may be due to the precocious development of TTX binding sites early on during prenatal stages of development. It is possible that the binding sites to which TTX molecules attach, develop prenatally and are functionally active during the early postnatal stages of development, thus, rendering a larger number of TTX-S sodium channels active.

The literature has consistently shown the presence of a larger proportion of TTX-R sodium channels in younger neuronal cells than in older neuronal cells, suggesting a developmental trend in the sensitivity to TTX. In a developmental study of dorsal root ganglion (DRG) neurons, Roy (1992) found a correlation between the age of rat pups and the expression of TTX-S and TTX-R sodium currents. Currents expressed by young (P3 - P4) acutely dissociated DRG neurons were predominantly TTX-R sodium currents, while currents recorded from older (P4 - P8) DRG neurons expressed a combination of

both TTX-R and TTX-S sodium currents. However, sodium currents recorded from (P8 - P12) rat pups and adult animals expressed predominantly TTX-S sodium currents. Weiss and Horn (1986) observed the same trend in developing skeletal muscle. A larger proportion of TTX-R sodium channels were present in developing myoblast cells, the embryological precursors to myotubes found in skeletal muscle. Comparatively, a higher proportion of TTX-S sodium channels was found in myotubes.

Differences exist in the times at which neuronal cells attain their binding sites. A number of studies found an increase in saxitoxin (STX) binding density with age (Baumgold et al., 1983; Cummins et al., 1994), while others have found the development of STX binding sites early on during embryonic development (Couraud et al., 1986). Baumgold et al. (1983) found a gradual increase in the binding of [^{3}H]STX, a known sodium channel blocker, in rat brain fragments of prenatal and postnatal Sprague-Dawley rat pups. At E19, binding of [^{3}H]STX was minimal (100 fmol/mg), however, by P15, the binding of [^{3}H]STX had increased by seven times more (700 fmol/mg). He compared the development of binding sites to the development of myelination and found that the development of [^{3}H]STX binding occurred sooner than the maturation of myelin. Myelination in rat brain occurs at a much later stage, between P15 and P21. Thus, these findings perhaps lend support to the precocious development of the auditory system. If the pattern of neuronal development were consistent within the peripheral nervous system, this finding would lend further support to the presence of active TTX binding sites during prenatal stages of development. This will perhaps explain the reduction in the number of TTX-R sodium channels.

Unknown Inward-Directed Current

The presence of an unknown voltage-gated inward current appeared following the application of a depolarizing test protocol. While the cell was held at a holding potential of -80 mV, 10 mV step commands lasting 10 ms were stepped from –80 to +80 mV. A family of inward-directed non-inactivating currents emerged at potentials more positive than –40 mV. The current was initially believed to be either a calcium current (Trombley and Westbrook, 1991; Santos-Sacchi, 1993; Roth and Grantyn, 1994; Lin, 1997) or a TTX-R current (Roy, 1992). However, in the presence of 0.5 μM TTX, the rapidly activating and slowly-non-inactivating inward currents were abolished. These inward-directed currents returned to one-third of its initial peak amplitude following a wash with normal (140 mM NaCl) external solution. Similar non-inactivating inward currents were observed by Santos-Sacchi (1993) in mature SGCs of adult guinea pigs. These sustained inward currents were reduced in the presence of 50 μM Gd^{3+}. Cobalt also blocked the inward current in the absence of extracellular Ca^{2+}. Santos-Sacchi (1993) indicated that the non-inactivating inward currents consisted partially of a Ca^{2+} component.

Santos-Sacchi (1993) compared further the slow inward current to the currents generated by the bag neurons of Aplysia, pointing out similarities to TTX sensitivity, activation potential and reversal potentials which were similar in both current types. Despite the evidence presented, however, he did not identify the specific current type and encouraged further studies in order to characterize the slow non-inactivating inward current using more aggressive current isolation techniques. The two currents may or may not originate from the same type of voltage-gated channel. Therefore, further studies are

necessary also in order to identify the specific kinetic properties of the inward non-inactivating currents observed. The fact that the currents were sensitive to TTX does not therefore rule out a sodium component.

Differences between Embryonic and Postnatal Sodium Currents

For the purposes of studying the inward-directed sodium current, postnatal SGCs were categorized into three developmental groups: early (P1 - P4); intermediate (P5 - P7) and differentiated (P8 and older). One of the most obvious developmental changes observed in the kinetics of inward-directed sodium current was an increase in peak sodium current magnitude. Similar to the embryonic findings, however, peak sodium current amplitude for the postnatal groups varied between cells. Under the same testing conditions, the overall magnitude of peak sodium current exhibited by postnatal SGCs increased as a function of maturity in comparison to embryonic peak sodium currents. Some currents, however, remained small despite continued maturational changes and an increase in cell size. The increase in peak sodium current amplitude reflects perhaps the maturational changes resulting from an increase in the number of active sodium channels, which contribute to the whole-cell current. Voltage-gated data involving sodium currents from other neuronal cells have reported similar findings. Valverde et al. (1992) recorded fast transient inward currents from an E8 CGN. The amplitude of the inward-directed sodium current increased in magnitude through P17. Cummins et al. (1994) noted an increase in peak sodium current amplitude as a function of maturational changes in rat pyramidal neocortical cells. All neurons, however, did not follow the same developmental pattern. There were some cells that developed adult-like characteristics

early on and did not show significant changes in peak current magnitude with age. Furthermore, changes in sodium current amplitude remained consistent throughout development among three sodium current types of P1 - P8 DRG neurons (Schwartz et al., 1990). However, a change was observed in the relative frequency-of-occurrence among three different types of sodium currents, fast adult (FA), fast newborn (FN), and slow (S), present in DRG neurons.

Current-voltage curves for embryonic (E18) SGCs showed sodium currents, which activated at potentials more positive than -30 mV and peaked at -20 mV. Mature postnatal SGCs activated at potentials more positive than -40 mV and peaked as well at -20 mV. The 10-mV shift in membrane activation to the left in a more hyperpolarized direction for postnatal SGCs was also observed in rat pyramidal neocortical neurons (Cummins et al., 1994). This would suggest a more sensitive threshold of –10 mV.

Sodium currents generated by adult SGCs isolated from the guinea pig (Santos-Sacchi, 1993) exhibited thresholds of activation which were similar to measures obtained for rat postnatal SGCs, and occurred at potentials more positive than -40 mV. Comparatively, Lin (1997) reported activation thresholds of -60 mV in P0 - P1 gerbil SGCs. When comparing the kinetic properties of rat neurons to the avian auditory system, fast transient inward currents generated by E16 CGNs activated at thresholds of -40 mV (Valverde et al., 1992). The -40 mV threshold of activation was obtained for both young (E8.5) and mature (E16) CGNs.

The rate-of-activation is another kinetic parameter that is used to characterize membrane ionic currents. It is the amount of time required for the current to reach peak

magnitude. The rates were calculated from stimulus onset to peak current magnitude. The present findings found that the rates of sodium peak current activation decreased with maturation (See Table IV-I). Time-of-activation for peak sodium currents were greater for embryonic SGCs than for postnatal rates of activation. These findings suggest that developmental changes are continuing to occur postnatally in the underlying ionic mechanisms responsible for the generation of APs. The continued developmental refinements of channels in addition to anatomical maturation of the cochlea and auditory nerve are probably what accounts for the improved auditory sensitivity observed postnatally.

Effects of Pb^{2+} on the Sodium Current

Lead (Pb^{2+}) is a potent environmental toxin. It has been shown clinically to have adverse effects on auditory function, but the results of the literature are not definitive. Low levels (10 - 20 μg/dl) to moderate levels (21 - 60 μg/dl) of Pb^{2+} exposure have been reported to cause elevated hearing thresholds (Schwartz and Otto, 1987, 1991; Otto and Fox, 1993) and delayed latencies of ABRs (Otto et al., 1985; Holdstein et al., 1986; Lille et al., 1988). However, Counter et al. (1997) report normal auditory thresholds for pure tone frequencies between 0.25 – 8 KHz, as well as normal absolute and interpeak latencies for ABR measures in a group of children exposed to moderate levels of Pb^{2+} (52.6 μg/dl). High doses (> 60 μg/dl) of Pb^{2+} exposure has been shown to cause an increase in AP thresholds, as well as axonal segmental demyelination and subsequent auditory nerve degeneration (Otto and Fox, 1993). The cochlear nerve and sensory ganglia (cochlear and vestibular) remained intact (Otto and Fox, 1993). It is uncertain,

however, as to underlying mechanisms of Pb^{2+} responsible for these actions within the auditory system. Pharmacologically, it has been found that toxicity exerted by heavy metals such as Pb^{2+}, Hg^{+}, As^{3+} and Cd^{2+} occurs when the metal combines with one or more reactive groups (ligands), forming a complex which disrupts normal enzymatic function (Klaassen, 1996).

Sub-acute and chronic exposure to Pb^{2+} is known to produce neurological symptoms in both the periphery and the central nervous system of humans and laboratory animals (Atchison and Narahashi, 1984) . Lead palsy is one of several disorders which has been attributed to exposure to Pb^{2+}, causing a peripheral neuromuscular weakness. The mechanisms responsible for this effect are not completely understood. Studies conducted at the neuromuscular junction of various animal preparations have shown that Pb^{2+} blocks the end-plate potential and the subsequent release of acetylcholine (ACh). The same effect was shown in the cat superior cervical ganglion (Kostial and Vouk, 1957), at the frog neuromuscular junction (Manalis and Cooper, 1973; Cooper et al., 1984) and in the phrenic nerve of rat (Atchison and Narahashi, 1984). The effects of Pb^{2+} are most prominent presynaptically. At the post-synaptic site, Pb^{2+} increases the spontaneous quantal release of ACh and thus increases the miniature end-plate potential. While the specific mechanism of action is unknown, it is believed that Pb^{2+} acts at the nerve terminal to increase the concentration of intracellular Ca^{2+} (Atchison and Narahashi, 1984).

Pb^{2+} is a potent inhibitor of voltage-gated calcium channels (Audesirk and Audesirk, 1993). It has been shown to decrease the number of active voltage gated Ca^{2+}

currents in mouse neuroblastoma cells (Oortgiesen et al., 1990a), in human neuroblastoma cells (Reuveny and Narahashi, 1991), and in E18 rat hippocampal cells (Audesirk and Audesirk, 1993), in a concentration-dependent manner. Various subtypes of calcium channels (e.g., T-type, L-type, and N-type) can be blocked by the presence of Pb^{2+}. The L-type Ca^{2+} channel has the greatest affinity for binding with Pb^{2+}. Reportedly, sodium channels are not affected by the presence of lead. Patch-clamp studies using concentrations of 10 μM Pb^{2+} (Reuveny and Narahashi, 1991) and 100 μM Pb^{2+} (Oortgiesen et al., 1990a), have revealed sodium channels which were not affected by the presence of Pb^{2+}.

Various concentrations of Pb^{2+} (0.1 μM, 3.0 μM, 3.0μM and 10.0μM) were used to study its effects on the inward-directed sodium current of rat SGCs. However, bath applications of Pb^{2+} did not potentiate nor completely block the inward-directed sodium current. Results obtained from embryonic animals were inconclusive and showed signs of a possible effect of Pb^{2+}. Results obtained with postnatal SGCs, however, showed a slowing effect on sodium current inactivation rather than a reduction of peak current. Slowing of the inactivation would cause the AP to be prolonged beyond its nominal duration.

Inward-directed sodium currents were produced by an embryonic (E18) SGCs, which produced a peak current measuring 1600 pA. In the presence of 3.0 μM Pb^{2+}, peak sodium current amplitude was reduced by approximately 22% (350 pA) of its initial value after the cell was exposed for two minutes to Pb^{2+}. The effect remained and was not reversed following a two-minute wash with normal external solution (140 mM NaCl).

An additional decrement of 100 pA was noted in peak sodium current following an additional two-minute wash. The reduction in the peak sodium current following the wash was close to three times less than the effect noted in the presence of Pb^{2+}. Thus, the reduction in peak sodium current noticed following the wash was believed to be the effects of run down. However, the effects observed after the application of 3.0 μM Pb^{2+} was believed to be the result of the presence of Pb^{2+}. Unfortunately, these observations could not be repeated due to rapid cell death. Unlike DRG neurons, SGCs do not survive the patch-clamp process for long periods of time as they tend to deteriorate only minutes after securing a gigaohm seal. Further studies are needed to confirm an effect on the embryonic sodium peak current in the presence of 3.0 μM Pb^{2+}.

The effects of Pb^{2+} was investigated also on postnatal sodium currents produced by SGCs from two developmental stages, intermediate (P5 – P7) and differentiated (P8 and older). When 1.0 μM Pb^{2+} was externally applied to a P5 SGC, the amplitude of the inward current remained virtually unchanged as the Pb^{2+} did not block nor enhance the sodium current. Similar to the effects exhibited by embryonic cells, only a minimal reduction in peak sodium current was noted. Once the holding potential was changed from -60 mV to -80 mV, however, the magnitude of the inward peak sodium current was restored. The increase in peak sodium current in the presence of a more negative holding potential may be indicative of a larger number of active sodium channels which were not blocked by the presence of 1.0 μM Pb^{2+}, or were not in an inactivated state. This behavior is best explained by the inactivation curve that illustrates how a larger number of sodium channels are active at more negative holding potentials. This does not negate

the possible blocking effect of Pb^{2+} on the inward-directed sodium current. The increase in peak sodium current following the introduction of a more negative holding potential may provide further evidence which suggests Pb^{2+} does in fact have a partial blocking effect on the sodium current, therefore, rejecting the idea of cell run down.

Increasing the concentration of Pb^{2+} tenfold to 10 μM, the sodium current generated by mature P9 SGCs showed slowing of inactivation. No significant changes were noted in peak sodium current magnitude. However, rates of activation increased in the presence of 10 μM Pb^{2+}. Following a four-minute rinse in Pb^{2+} free solution, the effect of Pb^{2+} on rates of activation and inactivation disappeared and currents were returned to normal.

Based on the data obtained during this study, it is concluded that levels of Pb^{2+} as low as 0.1 μM - 3.0 μM produce negligible effects on the rates of activation, inactivation and amplitude of peak sodium currents. However, 10 μM of Pb^{2+} delays the rate of activation and inactivation of the sodium current of mature differentiated type I SGCs. There is no effect on inward-directed peak sodium current magnitude.

The action of Pb^{2+} on embryonic SGCs requires further investigation. The possible effect on peak sodium current remains to be demonstrated. If the shift in peak sodium current were a true reaction to the presence of Pb^{2+}, it would appear that immature SGCs are more susceptible to the influence of Pb^{2+} than postnatal SGCs. This would support the reports in the literature which suggest that the young developing nervous system is more vulnerable to the effects of Pb^{2+} than the more mature nervous system.

Potassium Current

According to Hille (1996), the participation of potassium conductance within the cell membrane plays a vital role in the process of cellular physiology. The complexity of neuronal coding rests in the diversity of potassium channels found in neuronal cells. Potassium channels serve a variety of functions: (1) set the resting membrane potential, (2) keep fast action potentials short, (3) terminate periods of intense activity, (4) time the interspike intervals during repetitive firing, and (5) lower the effectiveness of excitatory inputs on a cell when channels are open (Hille, 1992). Valverde et al. (1992) studied the developmental pattern of sodium and potassium channels of CGNs of embryonic chicks. Outwardly rectifying potassium currents appeared as early as E6, while sodium currents appeared several days (E8) later. Similar to the findings reported for sodium currents, activation of the potassium current shifted towards the left to a more hyperpolarized state with maturation.

In this investigation, outwardly directed non-inactivating potassium currents were recorded in embryonic rat SGCs (E17). Embryonic potassium peak current was considered small when compared to the amplitude of outward-directed potassium currents generated by postnatal SGCs. The magnitude of peak potassium current, however, was always characteristically larger than peak sodium current amplitude for both embryonic and postnatal cells. In most instances, potassium current amplitude demonstrated currents that were twice the size of their accompanying sodium current magnitudes. The delayed rectifying potassium current functions partly to repolarize the cell membrane following a short duration (1 - 10 ms) action potential. Due to the rapid

rates which are required to code auditory information, perhaps the 1:2 sodium/potassium ratio observed in the present SGCs is necessary for the rapid repolarization following a rapid AP. Santos-Sacchi (1993) reported that adult SGCs possessed the rapid conductances and kinetic activity to account for faithfully transmitting receptor potential information required to code frequency and intensity information. Perhaps this is one of the reasons why responses in the auditory system can occur so rapidly.

The growth in postnatal peak current potassium amplitude, however, reflects the process of maturation and the subsequent participation of perhaps a larger number of functional potassium channels or channels whose conductances are considerably larger. The currents observed in embryonic and postnatal SGCs exhibited characteristics that mimicked the delayed rectifying potassium channel. This was further substantiated by the blocking action of TEA-Cl, a well-known potassium channel blocker. In the presence of 20 mM TEA-Cl, these outward-directed non-inactivating currents were selectively blocked suggesting that the currents recorded from rat SGCs were of the delayed rectifying potassium channel type (Moore et al., 1996).

Apoptosis or Programmed Cell Death

It was of interest as to why so many of our SGCs deteriorated or failed to exhibit currents during many patch clamp-recording sessions. There may be perhaps a relationship between these observations and apoptosis. Apoptosis is a subject of biological interest that has recently received a significant amount of attention in the literature. Apoptosis has been defined as programmed cell death and is believed to be a normal biological process which reportedly occurs in most animal tissue (Raff, 1992). It

is considered a mechanism for eliminating the body of unwanted cells. Apoptosis differs from that of necrosis or the removal of injured cells. Under circumstances of pathological cell death resulting from cell injury, cells tend to swell and cell contents accumulate into the extracellular space. This swelling is perceived as inflammation.

The process of apoptosis, on the other hand, eliminates unwanted cells of the body in a completely different manner. The nucleus and cytoplasm of the cell shrinks and in some cases, fragments. The shrunken cells or fragments are subsequently phagocytosed by neighboring cells. The process of phagocytosis involves the uptake of particulate material or cell fragments by invagination into phagosomes - membrane bound vesicles, by plasma membrane. Thus, the process of apoptosis involves the removal of otherwise normal cells that are no longer required by the body. There are several reasons why the body would rid itself of unwanted cells: (1) removal of cells which initially served a specific function during development and are no longer required, (2) cells which are gender specific-cells which are specific for males while others are specific for females, (3) cells which are sacrificed in the process of sculpting the body and (5) removal of cells which migrate to abnormal locations (Raff, 1992).

The specific mechanism by which apoptosis occurs is still unknown. There are several theories, one of which involves programmed cell death or cell suicide. Just as cells receive signals from other cells in order to proliferate, proponents of this theory believe the deliberate absence of a chemical signal from neighboring cells causes a cell to kill itself by activating an intrinsic suicide program (Raff, 1992). By the same token, cells are dependent upon the presence of chemical signals for survival. The development

and survival of many vertebrate cells is dependent upon neurotrophic factors secreted by the target cells which they innervate (Raff, 1992). Those cells that fail to receive enough of the signal (i.e., neurotrophins, hormones, etc.) tend to die. The evidence to support the process of programmed cell death is derived from several compelling findings identified through genetic analyses, cytological studies and biochemical analyses.

The auditory and vestibular systems have not been excluded from the concept of apoptosis. Li et al. (1995) investigated the pattern of cell death in vestibular sensory hair cells following treatment with an ototoxic aminoglycoside, gentamicin. Two distinct modes of hair cell loss were noted, degeneration and extrusion. The cells which deteriorated following exposure to gentamicin presented morphological features consistent with those described for apoptosis including fragmentation, cytoplasmic blebbing and absence of inflammation, just to name a few effects.

The role of apoptosis in cell maturation and cell survival has been investigated within the cochlea as well. An array of neurotrophic factors, i.e., nerve growth factor (NGF), brain-derived neurotrophic factor (BDNF), neurotrophins 3, 4/5 and 6, have been identified in the cochlea, and are believed to have an effect on both development and cell survival.

Staecker et al.(1996) used immunohistochemical techniques and antisense oligonucleotide treatments to investigate neuronal survival and axonal morphology of auditory neurons. He found that the survival of spiral ganglion neurons was dependent upon the expression of specific neurotrophins that were most effective during specific periods of development and less effective beyond certain specified periods. For example,

BDNF functioned most effectively as a survival factor immediately after birth and failed to provide the same survival responses during later stages of development. NT-3 had almost the opposite effect. NT-3 provided minimal survival factor during early postnatal stages of development, but rapidly became a survival factor as the cochlea matured. Thus, there appeared to be a relationship between specific neurotrophins and cell survival. Therefore, Staecker et al. (1996) concluded that the changes in the expression of neurotrophins controlled the processes of neuronal apoptosis in SGCs and the maturational pattern of sensory hair cell innervation.

The information describing the concept of apoptosis was presented in order to offer a possible explanation for the rapid deterioration of SGCs observed during patch-clamp recordings. The viability of SGCs was very limited, lasting for only a few minutes in some instances once a gigaohm seal had been secured. In addition, the life span of both embryonic and postnatal SGCs within the incubator typically did not last more than 24 hours. The reason(s) for this rapid cell death is unknown. There may be several reasons contributing to this rapid deterioration, however, the concept of apoptosis offers a reasonable explanation. Some of the same morphological characteristics described in apoptotic cells were observed in deteriorating SGCs. If SGCs are indeed programmed to receive chemical signals from neighboring cells or target cells for the purposes of maturation and innervation, the morphological organization between cells is disrupted by the isolation of SGCs during tissue culturing techniques.

SGCs extend two processes, one of which innervates the sensory hair cell receptor and the other which innervate the neurons of the cochlear nucleus. The isolation of SGCs

during cell culture techniques disrupts the normal connection between cells and thus the ganglion, as well as innervational patterns which exist between sensory receptor cells and centrally located neurons no longer exist. Thus, the isolation of SGCs and the detachment of neurons from their target cells compromise the natural environment in which they would normally receive signals from neighboring or target cells. The lack of apposition between such cells perhaps prevents the reception of specific neurotrophic chemical signals necessary for the survival of SGCs. Based on findings reported by Staecker et al. (1996), it is plausible that the rapid deterioration of SGCs in this study is a consequence of apoptosis during the early stages of development.

Conclusions

Underlying ionic mechanisms responsible for signal transduction such as voltage-gated ionic channels are present within embryonic SGCs. Although maturation of anatomical structures within the middle ear and inner ear are continuing to mature postnatally, the development of membrane-bound ionic channels in SGCs is coincident with the innervation patterns and the development of structures within the cochlea. The presence of functional voltage-gated sodium channels and potassium channels early on suggest that these young cells are capable of generating action potentials.

At E16, cross-sectional diameters of SGCs are highly variable and change in cell size. Current amplitude continued to increase through postnatal stages of development. The high variability in cross-sectional diameter may either reflect the mixture of neurons that have attained their adult cell size with neurons that continue to grow and develop. It may reflect also neurons which are tonotopically specific, representative of a frequency

place along the length of the basilar membrane (e.g., basal vs. apical regions). From a developmental point of view, the first suggestion is more feasible in that the high variability in cross-sectional diameter disappears in older embryonic and postnatal neurons, suggesting that maturation is nearing its end and cells are approaching adult sizes.

Embryonic (E17- E18) SGCs displayed both inward-directed sodium current and outward-directed potassium currents in response to depolarizing voltage commands. Amplitude for both current types were small when compared to the amplitude of currents generated by postnatal SGCs. These findings suggest that sodium current and potassium current generated by embryonic SGCs are not mature and are continuing to develop postnatally. These findings were supported by the changes observed in the amplitude of both sodium currents and potassium current, as well as the change in the threshold of activation for sodium currents. The threshold of activation in embryonic SGCs (- 40 mV) shifted in postnatal SGCs to the left (-50 mV) to a more hyperpolarized state. This observed shift in potential is closer perhaps to the resting membrane potential of mature SGCs.

Postnatal SGCs from all three stages of development produced sodium currents that were reversibly blocked by the presence of 0.5 μM TTX. The blocking classified the cells as exhibiting TTX-S sodium currents. Thus, cells from all three stages of development possess sodium channels that are pharmacologically active. TTX-R sodium channels were not observed. These findings lend support to the notion of highly

precocious development of SGCs, and emphasize the presence of active binding sites for TTX at early stages of development.

Although behavioral and objective measures have demonstrated that Pb^{2+} influences cognitive function, ABR latencies, and hearing thresholds, the mechanisms of this action remain unclear. Pb^{2+} has been found to have no effect on peak sodium current in previous studies (e.g., see Reuveny and Narahashi, 1991). The present findings, although inconclusive, do not rule out negligible effects of Pb^{2+} on either embryonic or postnatal SGCs sodium current peak magnitude. From the results obtained using both embryonic and postnatal SGCs, it is concluded that Pb^{2+} does change sodium currents by prolonging inactivation. Further studies are needed using larger concentrations of Pb^{2+}, however, before more definitive conclusions can be made about its effect on peak sodium current.

Suggestions for Future Research

The ability to record from a SGC for an extended period of time was very challenging, to say the least. This limitation made it difficult to obtain a more complete set of data for certain of the experiments. This area of investigation provides an opportunity to explore several other facets of ionic channels of SGCs. The following research studies seem appropriate:

- Determine the initial emergence of sodium and/or potassium currents within embryonic SGCs, i.e., less than P16.
- Continue the search for TTX-R sodium channels in both embryonic and postnatal SGCs.

- Conduct additional Pb^{2+} studies for both sodium and calcium channels (embryonic and postnatal) to include higher concentrations of Pb^{2+} of up to 100 μM.
- Generate a dose-response curve for the sodium current using TTX .
- Characterize the unknown current through the use of more specific voltage-gated channel blockers.
- Conduct current-clamp studies to investigate excitability during control and in the presence of Pb^{2+}.
- Develop a co-culture of SGCs and hair cells, stimulate the hair cells and record from SGCs.
- Generate steady-state inactivation as well as recovery from inactivation data using TTX and Pb^{2+}.
- Determine whether use-dependency is present to various concentrations of Pb^{2+}.
- Develop a co-culture of SGCs and hair cells, stimulate the hair cells and record from SGCs.
- Isolate and record from SGC from different turns of the cochlea in order to investigate tonotopicity.

LIST OF REFERENCES

Atchison, W. D., and Narahashi, T. (1984). Mechansim of action of lead on neuromuscular junctions. NeuroToxicology, 5(3), 267-282.

Audesirk, G. and Audesirk, T. (1993). The effects of inorganic lead on voltage-sensitive calcium channels differ among cell types and among channel subtypes. NeuroToxicology, 14, 259-266.

Baumgold, J., Zimmerman, I., and Bambrick, L. (1983). Appearance of [^{3}H}saxitoxin binding sites in developing rat brain. Developmental Brain Research, 9, 405-407.

Bellinger, D., Leviton, A., Waternaux, C., Needleman, H., and Rabinowitz, M. (1987). Longitudinal analyses of prenatal and postnatal lead exposure and early cognitive development. The New England Journal of Medicine, 316 (17), 1037-1043.

Bezanilla, F., and Armstrong, C. M. (1977). Inactivation of the sodium channel. I. sodium current experiments. Journal of General Physiology, 70, 549-566.

Brown, M. C. (1987). Morphology of labeled afferent fibres in the guinea pig cochlea. The Journal of Comparative Neurology, 260, 591-604.

Brown, M. C., Berglund, A M. Kiang, N. Y. and Ryugo, D. K. (1988). Central trajectories of type II spiral ganglion neurons. The Journal of Comparative Neurology, 278, 581-590.

Cooper, G. P., Suszkiw, J. B. and Manalis, R. S. (1984). Heavy metals: effects on synaptic transmission. Neurotoxicology, 5, 247-266.

Counter, S. A., Vahter, M., Laurell, G., Buchanan, l. H., Ortega, F., and Skerfving, S. (1997). High lead exposure and auditory sensory-neural function in Andean children. Environmental Health Perspective, 105, (5), 522-526.

Couraud, F., Moutot-Martin, N., Koulakoff, A., and Berwald-Netter, Y. (1986). Neurotoxin-sensitive sodium channels in neurons developing in vivo and in vitro. The Journal of Neuroscience, 6, 192-198.

Crowley, D. E., and Hepp-Reymond, M. (1966). Development of cochlear function in the ear of the infant rat. Journal of Comparative and Physiological Psychology, 62, 427-432.

Cullen, M. R., Robins, J. M., and Eskenazi, B. (1983). Adult inorganic lead intoxication: presentation of 31 new cases and a review of recent advances in the literature. Medicine, 62, 221-247.

Cummins, T. R., Xia, Y., and Haddad, G. G. (1994). Functional properties of rat and human neocortical voltage-sensitive sodium currents. Journal of Neurophysiology, 71, 1052-1064.

Davis, J. M., and Svendsgaard, D. J. (1987). Lead and child development. Nature, 329, 297-300.

Davis, R. L. (1993). Complex firing patterns of mouse VIII cranial nerve cell *in vitro*. Association for Research in Otolaryngology. Abstract 17, 33.

Davis, R. L. (1996). Differential distribution of potassium channels in acutely demyelinated, primary-auditory neurons in vitro. Journal of Neurophysiology, 76, 438-447.

Dietrich, K., Succop, P., Berger, O., and Keith, R. (1992). Lead exposure and the central auditory processing abilities and cognitive development of urban children: the Cincinnati lead study cohort at age 5 years. Neurotoxicology and Teratology, 14, 51-56.

Galambos, R., and Davis, H. (1943). The response of single auditory-nerve fibers to acoustic stimulation. Journal of Neurophysiology, 6, 39-57.

Galambos, R., and Davis, H. (1944). Inhibition of activity in single auditory nerve fibers by acoustic stimulation. Journal of Neurophysiology, 7, 287-303.

Geal-Dor, M., Freeman, S., Li, G., and Sohmer, H. (1993). Development of hearing in neonatal rats: air and bone conducted ABR thresholds. Hearing Research, 69, 236-242.

Hafidi, A., Despres, G. and Romand, R. (1993). Ontogenesis of type II spiral ganglion neurons during development: peripherin immunohistochemistry. International Journal of Developmental Neuroscience, 11, (4) 507-512.

Hamill, O. P., Marty, A., Neher, E, Sakmann, B., and Sigworth, F. J. (1981). Improved patch-clamp techniques for high-resolution current recording from cells and cell-free membrane patches. European Journal of Physiology, 391, 85-100.

Hille, B. (1992). Ionic Channels of Excitable Membranes. Sunderland: Sinauer Associates Inc.

Holdstein, Y., Pratt, H., Goldsher, M., Rosen, G., Shenhav, R., Linn, S., Mor, A., and Barkai, A. (1986). Auditory brainstem evoked potentials in asymptomatic lead-exposed subjects. The Journal of Laryngology and Otology, 100, 1031-1036.

Javel, E. (1986). Basic response properties of auditory nerve fibers. In: R. A. Altschuler, D. W. Hoffman and R. P. Bobbin (Eds.), Neurobiology of Hearing: the Cochlea. (pp. 213-245) New York: Raven Press,.

Kandel, E. R., Schwartz, J. H., and Jessell, T. M. (1991). Principles of Neural Science (3rd ed.). Norwalk: Appleton and Lange.

Klaassen, C., (1996). Heavy Metals and Heavy-Metal Antagonists. In: J. G. Hardman, L. E. Limbird, P. B. Molinoff, R. W. Ruddon, and Gilman, A. G. (Eds.), Goodman and Gilman's The Pharmacological Basis of Therapeutics. (pp. 1649-1671) New York: McGraw Hill.

Koester, J. (1991). Voltage-gated ion channels and the generation of the action potential. In: E. R. Kandel, and J. H. Schwartz, (Eds.), Principles of neural science. (pp. 104-118) New York: Elsevier..

Kostial, K. and Vouk, V. B. (1957). Lead ions and synaptic transmission in the superior cervical ganglion of the cat. British Journal of Pharmacology, 12, 219-222.

Kostyuk, P. G., Veselovsky, N. S., and Tsyndrenko, A. Y. (1981). Ionic currents in the somatic membrane of rat dorsal root ganglion neurons-I sodium currents. Neuroscience, 6 (12), 2423-2430.

Lenoir, M., Shrerson, A., and Pujol, R. (1980). Cochlear receptor development in the rat with emphasis on synaptogenesis. Anatomy and Embryology, 160, 253-262.

Li, L., Nevill, G., and Forge, A. (1995). Two modes of hair cell loss from the vestibular sensory epithelia of the guinea pig inner ear. The Journal of Comparative Neurology, 355, 405-417.

Lin, X. (1996). Single channel recording differentiates two types of potassium channels in the cultured spiral ganglion neuron of postnatal gerbil. Association for Research in Otolaryngology. Abstract 345, 87.

Lin, X. (1997). Action potentials and underlying voltage-dependent currents studied in cultured spiral ganglion neurons of the postnatal gerbil. Hearing Research, 108, 157-179.

Lille, F., Hazemann, P., Garnier, R., and Dally, S. (1988). Effects of lead and mercury intoxications on evoked potentials. Clinical Toxicology, 26, 103-116.

Manalis, R. S., and Cooper, G. P. (1973). Presynaptic and postsynaptic effects of lead at the frog neuromuscular junction. Nature, 243, 354- 356.

Mo, Z. and Davis, R. L. (1997). Endogenous firing patterns of murine spiral ganglion neurons. Journal of Neurophysiology. 77, 1294-1305.

Moore, E. J., Hall, D. B., and Narahashi, T. (1996). Sodium and potassium currents of type I spiral ganglion cells from rat. Acta Otolaryngol (Stockh), 116 552-560.

Nagata, K., Huang, C., Song, J. Narahashi, T. (1997). Lead modulated of the neuronal nicotinic acetylcholine receptor in PC12 cells. Brain Research, 754, 21-27.

Nakagawa, T., Komune, S., Uemura, T., and Akaike, N. (1991). Excitatory amino acid response in isolated spiral ganglion cells of guinea pig cochlea. Journal of Neurophysiology, 65 (3), 715-723.

Needleman, H. L., Gunnoe, C., Leviton, A., Reed, R., Peresie, H., Maher, C., and Barret, P. (1979) Deficits in psychologic and classroom performance of children with elevated dentine lead levels. The New England Journal of Medicine, 300 (13), 689-695.

Northern, J. L., and Downs, M. P. (1991). Hearing in children. Baltimore: Williams and Wilkins.

Oortgiesen, M., Van Kleef, R. G. D. M., Bajnath, R. B. and Vijverberg, H. P. M. (1990a). Nanomolar concentrations of lead selectively block neuronal nicotinic acetylcholine responses in mouse neuroblastoma cells. Toxicology and Applied Pharmacology, 103, 165-174.

Oortgiesen, M., Van Kleef, R.G.D.M. and Vijverberg, H.P.M. (1990b). Novel type of ion channel activated by Pb^{2+}, Cd^{2+}, and Al^{3+} in cultured mouse neuroblastoma cells. Journal of Membrane Biology, 113, 261-268.

Otto, D. A., and Fox, D. A. (1993). Auditory and visual dysfunction following lead exposure. Neurotoxicology, 14, 191-208.

Otto, D., Robinson, G., Baumann, S., Schroeder, S., Mushak, P., Kleinbaum, D., and Boone, L. (1985). 5-year follow-up study of children with low-to-moderate lead absorption: electrophysiological evaluation. Environmental Research, 38, 168-186.

Pickles, J. O. (1988). An Introduction to the Physiology of Hearing (2nd ed.). New York: Academic Press.

Raff, M. C. (1992). Social controls on cell survival and cell death. Nature, 356, 397-399.

Reuveny, E., and Narahashi, T. (1991). Potent blocking action of lead on voltage-activated calcium channels in human neuroblastoma cells SH-SY5Y. Brain Research, 545, 312-314.

Roth, B., and Bruns, V. (1992). Postnatal development of the rat organ of Corti. Anatomy and Embryology, 185, 559-569.

Rothe, T. and Grantyn, R. (1994). Retinal ganglion neurons express a toxin-resistant developmental regulated novel type of high-voltage-activated calcium channel. Journal of Neurophysiology, 72, 2542-2546.

Roy, M. L., and Narahashi, T. (1992) Differential properties of tetrodotoxin-sensitive and tetrodotoxin-resistant sodium channels in rat dorsal root ganglion neurons. Journal of Neuroscience, 12, 2104-2111.

Roy, M. L. (1992). The physiology and pharmacology of tetrodotoxin-sensitive and tetrodotoxin-resistant sodium channels in rat dorsal root ganglion neurons. Doctoral Dissertation, Northwestern University, Chicago, IL.

Santos-Sacchi, J. (1990). Studies on the fast inward Na^+ currents in isolated type I spiral ganglion cells. Association for Research for Otolaryngology. Abstract.

Santos-Sacchi, J. (1993). Voltage-dependent ionic conductances of type I spiral ganglion cells from the guinea pig inner ear. The Journal of Neuroscience, 13 (8), 3599-3611.

Schwartz, A. M., Parakkal, M. and Gulley, R. L. (1983). Postnatal development of spiral ganglion cells in the rat The American Journal of Anatomy, 167, 33-41.

Schwartz, A. M., (1986). Auditory nerve and spiral ganglion cells: morphology and organization. In: R. A. Altschuler, D.W. Hoffman, and R. P. Bobbin, (Eds.). Neurobiology of Hearing: The Cochlea. New York: Raven Press.

Schwartz, A., Palti, Y., and Meiri, H. (1990). Structural and developmental differences between three types of Na channels in dorsal root ganglion cells of newborn rats. Journal of Membrane Biology, 116, 117-128.

Schwartz, J. and Otto, D., (1991). Lead and minor hearing impairment. Archives of Environmental Health, 46 (5), 300-304.

Sheppard, D. N., Valverde, M. A., Represa, J., and Giraldez, F. (1992). Transient outward currents in cochlear ganglion neurons of the chick embryo. Neuroscience, 51 (3), 631-639.

Silbergeld, E. (1992). Mechanisms of lead neurotoxicity or looking beyond the lamppost. FASEB Journal, 6 (13), 3201-3206.

Singh, A. K. (1993). Age-dependent neurotoxicity in rats chronically exposed to low levels of lead: calcium homeostasis in central neurons. Neurotoxicology, 14 (4), 417-428.

Staecker, H., Galinovic-Schwartz, V., Liu, W., Lefebvre, P., Kopke, R., Malgrange, B., Moonen, G., and Van De Water, T. (1996). The role of the neurotrophins in maturation and maintenance of postnatal auditory innervation. The American Journal of Otology, 17, 486-492.

Tasaki, I. (1954). Nerve impulses in individual auditory nerve fibers of guinea pig. Journal of Neurophysiology, 17, 97-122.

Trombley, P. Q. and Westbrook, G. L. (1991). Voltage-gated currents in identified rat olfactory receptor neurons. Journal of Neuroscience, 11, 435-444.

Ujihara, H. and Albuquerque, E. X. (1992). Developmental change of the inhibition by lead of NMDA-activated currents in cultured hipppocampal neurons. The Journal of Pharmacology and Experimental Therapeutics, 263 (2), 868-875.

Uziel, A., Romand, R. and Marot, M. (1981). Development of cochlear potentials in rats. Audiology, 20, 89-100.

Valverde, M. A., Sheppard, D. N., Represa, J., and Giraldez, F. (1992). Development of Na^+ and K^+ currents in the cochlear ganglion of the chick embryo. Neuroscience, 51 (3), 621-630.

Vander, A. J., Sherman, J. H., and Luciano, D. S. (1990). Human physiology. New York: McGraw-Hill.

Weiss, R. E., and Horn, R. (1986). Functional differences between two classes of sodium channels in developing rat skeletal muscle. Science, 233, 361-364.

Wong, V. C. N., Ng, T. H. K., and Yeung, C. Y. (1990). Electrophysiologic study in acute lead poisoning. Pediatric Neurology, 7 (2), 133-136.

Yamaguchi, K. (1988). Dissociated cell culture of the cochlear ganglion neuron from the chick embryo and its membrane properties. Biomedical Research, 9 (Supp 2), 79-82.

Yamaguchi, K., and Ohmori, H. (1990). Voltage-gated and chemically gated ionic channels in the cultured cochlear ganglion neuron of the chick. Journal of Physiology, 420, 185-206.

Yamaguchi, K., and Ohmori, H. (1993). Suppression of the slow K^+ current by cholinergic agonists in cultured chick cochlear ganglion neurons. Journal of Physiology, 464, 213-228.

Zimmer, W. M., Rosin, D. F. and Saunders, J. C. (1994). Middle-ear development VI: Structural maturation of the rat conducting apparatus. The Anatomical Record, 239, 475-484.

Zun-Li, M. and Davis, R. L. (1997). Endogenous firing patterns of murine spiral ganglion neurons. Journal of Neurophysiology, 77, 3, 1294-1305.